ELECTROCHEMICAL REMOVAL OF MERCURY FROM AQUEOUS SOLUTION USING TASK-SPECIFIC IONIC LIQUID IMMOBILISED ON PALM SHELL ACTIVATED CARBON

HAWAIAH IMAM MAAROF

FACULTY OF ENGINEERING
UNIVERSITY OF MALAYA
KUALA LUMPUR

2022

ELECTROCHEMICAL REMOVAL OF MERCURY FROM AQUEOUS SOLUTION USING TASK-SPECIFIC IONIC LIQUID IMMOBILISED ON PALM SHELL ACTIVATED CARBON

HAWAIAH IMAM MAAROF

THESIS SUBMITTED IN FULFILMENT OF THE REQUIREMENTS FOR THE DEGREE OF DOCTOR OF PHILOSOPHY

FACULTY OF ENGINEERING
UNIVERSITY OF MALAYA
KUALA LUMPUR

2022

UNIVERSITY OF MALAYA

ORIGINAL LITERARY WORK DECLARATION

Name of Candidate: Hawaiah Binti Imam Maarof

Registration/Matric No: 17020103/1 or KHA140058

Name of Degree: Doctor of Philosophy (PhD)

Title of Project Paper/Research Report/Dissertation/Thesis ("this Work"):

Electrochemical removal of mercury from aqueous solution using task-specific ionic liquid immobilised on palm shell activated carbon

Field of Study: Purification and Separation Processes (Chemical Process)

I do solemnly and sincerely declare that:

(1) I am the sole author/writer of this Work;
(2) This Work is original;
(3) Any use of any work in which copyright exists was done by way of fair dealing and for permitted purposes and any excerpt or extract from, or reference to or reproduction of any copyright work has been disclosed expressly and sufficiently and the title of the Work and its authorship have been acknowledged in this Work;
(4) I do not have any actual knowledge nor do I ought reasonably to know that the making of this work constitutes an infringement of any copyright work;
(5) I hereby assign all and every rights in the copyright to this Work to the University of Malaya ("UM"), who henceforth shall be owner of the copyright in this Work and that any reproduction or use in any form or by any means whatsoever is prohibited without the written consent of UM having been first had and obtained;
(6) I am fully aware that if in the course of making this Work I have infringed any copyright whether intentionally or otherwise, I may be subject to legal action or any other action as may be determined by UM.

Candidate's Signature Date: 17/5/2022

Subscribed and solemnly declared

Witness's Signature Date: 17/05/2022

Designation:

ELECTROCHEMICAL REMOVAL OF MERCURY FROM AQUEOUS SOLUTION USING TASK-SPECIFIC IONIC LIQUID IMMOBILISED ON PALM SHELL ACTIVATED CARBON

ABSTRACT

Electrode design is one of the most important criteria in providing a satisfactory performance of an electrochemical process. The conventional two-dimensional (2D) electrode provides low current efficiency despite high percentage removal and recovery of metal ions from dilute concentrations. Meanwhile, emerging advanced materials, such as task-specific ionic liquids (TSIL), have presented prominently to electrode modifications' technological advancement. In this present work, two types of three-dimensional (3D) electrodes were developed. The precursor is an activated carbon derived from solid waste, namely palm shell. The performance of palm shell activated carbon (PSAC) and trioctylmethylammonium thiosalicylate immobilised on PSAC (PSAC-TOMATS) electrodes were evaluated. The prepared electrodes were electrochemically characterized by voltammetric techniques and potentio electrochemical impedance spectroscopy (PEIS). Next, the prepared electrodes were employed as the cathode in a batch-mode electrochemical process system to remove Hg from synthetic wastewater. In the preparation steps and electrochemical characterization of the PSAC electrode, 20% carbon black (CB) was found to give low electron charge resistance and the maximum current peak for the redox reaction of ferrocyanide/ferricyanide. Meanwhile, by increasing the amount of binder from 10% to 20%, the electrochemical active surface area was decreased by 42%. The most suitable supporting electrolyte for the electro characterisation of the prepared electrode was NaCl because it provides the lowest double-layer capacitance effect compared to HCl and NaOH. Cyclic voltammetry data suggest that the PSAC electrode is undergoing a quasi-reversible process for which the equivalent effect, both that of the electron transfer rate and mass transfer rate, has

been taking place. The presence of interfacial interaction, such as adsorption, was also observed from the chronocoulometry analysis. The removal of Hg in a batch-mode electrochemical system was very rapid using the PSAC-TOMATS electrode. However, the modified electrode required an adequate amount of TOMATS to grant a higher percentage of Hg removal. By immobilising 0.2 g TOMATS on the PSAC, a removal of 97.1% of Hg (from an initial Hg concentration of 100 ppm) was achieved within 1.5 hours of electrochemical treatment time, while the PSAC electrode required a longer treatment time (6 hours). Additionally, the PSAC-TOMATS electrode provides higher current efficiency, higher percentage removal and lower energy consumption than the PSAC electrode. Under the electrode reusability studies, the PSAC-TOMATS electrode's efficiency was found to undergo a 15% reduction after the second cycle. However, only a slight reduction (2%) was observed for the third cycle. In conclusion, an electrochemical process using the PSAC-TOMATS electrode offers a promising approach to facilitate an effective removal of Hg from an aqueous solution.

Keywords: cyclic voltammetry, electrodeposition, electrosorption, mercury, trioctylmethylammonium thiosalicylate

PENYINGKIRAN MERKURI DARI LARUTAN BERAIR SECARA ELEKTROKIMIA MENGGUNAKAN CECAIR BERION TUGAS-TENTU YANG TERLETAK PADA KARBON TERAKTIF

ABSTRAK

Reka bentuk elektrod merupakan salah satu kriteria paling penting bagi memberikan prestasi yang memuaskan bagi sesuatu proses elektrokimia. Elektrod dua-dimensi (2D) merupakan elektrod konvensional yang menyediakan kecekapan arus yang rendah walaupun mampu memberi peratusan penyingkiran dan perolehan ion logam yang tinggi daripada sumber ion logam yang berkepekatan rendah. Selain itu, kemunculan bahan termaju seperti cecair berion tugas-tentu (TSIL) didapati dapat membantu kepada kemajuan teknologi pengubahsuaian elektrod. Dalam kajian ini, dua jenis elektrod tiga-dimensi (3D) dihasilkan. Elekrod ini diperbuat daripada karbon teraktif yang dihasilkan daripada sisa pepejal iaitu tempurung kelapa sawit. Prestasi elektrod karbon teraktif tempurung kelapa sawit (PSAC) dan PSAC yang digabungkan dengan trioktilmetilammonium thiosalisilat (PSAC-TOMATS) telah dikaji. Elektrod yang telah dihasilkan dicirikan dengan kaedah elektrokimia menggunakan teknik meter volt yang umum dan spektroskopi galangan elektrokimia potentio (PEIS). Seterusnya, elektrod yang telah dihasilkan digunakan sebagai katod dalam sistem elektrokimia secara mod-kelompok untuk penyingkiran Hg daripada air sisa sintetik. Dalam kerja-kerja menghasilkan elektrod dan mencirikan elektrod secara elektrokimia, 20% karbon hitam (CB) didapati memberikan rintangan caj elektron dan yang rendah dan menghasilkan puncak arus yang maksimum bagi tindak balas redoks ferrosianida/ferrisianida. Sementara itu, dengan meningkatkan jumlah pengikat daripada 10% kepada 20%, kawasan permukaan aktif elektrokimia menurun sebanyak 42%. Hasil kajian mendapati elektrolit penyokong yang paling sesuai dalam mencirikan electrode yang dihasilkan adalah NaCl kerana ianya memberi kesan dua lapisan kemuatan yang paling rendah

dibandingkan dengan HCl dan NaOH. Data daripada meter volt berkitar menunjukkan elektrod PSAC mempunyai proses mirip-boleh balik, yang mana kedua-dua kadar pemindahan elektron dan kadar pemindahan jisim telah mengambil bahagian dengan kesan yang setara. Kehadiran interaksi antara muka seperti penjerapan turut dapat dilihat melalui analisis chronocoulometri yang telah dijalankan. Proses penyingkiran Hg secara mod-kelompok adalah sangat cepat menggunakan elektrod PSAC-TOMATS. Walaubagaimanapun, elektrod yang diubahsuai memerlukan jumlah TOMATS yang mencukupi untuk memberikan penyingkiran Hg dengan peratusan yang lebih tinggi. Dengan menggabungkan 0.2 TOMATS, sebanyak 97% Hg (daripada kepekatan awal 100 ppm) dapat disingkirkan dalam masa 1.5 jam menggunakan rawatan elektrokimia, manakala masa yang lebih lama diperlukan oleh elektrod PSAC. Selain itu, elektrod PSAC-TOMATS menyediakan kecekapan arus yang lebih tinggi, peratus penyingkiran yang lebih tinggi dan penggunaan tenaga yang lebih rendah berbanding dengan elektrod PSAC (6 jam). Melalui kajian penggunaan semula elektrod, kecekapan elektrod PSAC-TOMATS didapati berkurangkan sebanyak 15% selepas kitaran kedua, tetapi hanya sedikit pengurangannya (2%) diperhatikan untuk kitaran ketiga. Kesimpulannya, proses elektrokimia menggunakan PSAC-TOMATS didapati menjanjikan satu kaedah yang berkesan untuk penyingkiran Hg daripada larutan akueus.

Kata kunci: voltammetri berkitar, elektroenapan, elektroerapan, merkuri, trioktilmetilammonium thiosalisilat

ACKNOWLEDGEMENTS

Firstly, I would like to express my gratefulness to Allah SWT for the completion of this thesis. Next, sincere thanks to my respective supervisors, Prof. Dr Mohamed Kheireddine Aroua and Prof. Ir. Dr Wan Mohd Asri Bin Wan Daud for their guidance, supervision, and not to mention his continuous support throughout the years. Their assistance, valuable comments and suggestions have contributed to the success of this research work. I wish to express my appreciation to all staff at the Department of Chemical Engineering, University of Malaya, who gave their kind assistance while doing the research work. Endless support from Ms Fazizah and all staff at the workshop is respected.

I also acknowledge the financial support from the Ministry of Education (MOE), Malaysia for High Impact Research Grant (UM.C/HIR/MOHE/ENG/43), the University of Malaya for the Post Graduate Research Grant (PPP) (PG149-2016A) and the facilities provided at the Centre for Separation Science and Technology (CSST). Sincere gratitude also goes to the Ministry of Higher Education (MOHE) and Universiti Teknologi MARA for funding my studies under Skim Latihan Akademik IPTA (SLAI).

Thank you very much to all my family members, especially my beloved husband (Mozaid Bin Tajuddin), my dearest family members (Derma Ibrahim, Hamrah Adnan, Tajuddin Ibrahim) and my lovely daughter (Mardhiah Husna) for their endless support and prays. Finally, thanks to all my friends for your help and support, particularly Dr Mohammed Ajeel, Dr Fariha, Dr Pei San, Dr Nurul Ain, Dr Mook, and Dr Norhaslinda. Thank you very much.

TABLE OF CONTENTS

LIST OF FIGURES

LIST OF TABLES

LIST OF SYMBOLS

$E°$	:	standard reduction potential, V
ΔE_p	:	peak potential separation, V
I	:	current, A
i	:	current density, A/m^2
i_{pa}	:	anodic peak current
i_{pc}	:	cathodic peak current
M	:	molecular mass, g/mol
m	:	mass of product, kg
Δm	:	mass of reduced metal in an interval time, Δt
n	:	number of electrons transferred in the redox reaction
T	:	temperature, K
t	:	electrolysis time, h
Δt	:	an interval time, s
V	:	voltage, V
ν	:	scan rate, V/s
z	:	charge number

LIST OF ABBREVIATIONS

2D	:	Two-dimensional
3D	:	Three-dimensional
AC	:	Alternating current
BJH	:	Burnett, Jeyner, Halenda
BET	:	Brunauer-Emmett-Teller
CB	:	Carbon black
CPE	:	Constant phase element
CV	:	Cyclic voltammetry
DFT	:	Density functional theory
DMAc	:	Dimethylacetamide
DMSO	:	Dimethyl sulfoxide
DSA	:	Dimensionally-stable anode
EDX	:	Energy dispersive x-ray
FESEM	:	Field emission scanning electron microscopy
FTIR	:	Fourier Transform-Infrared Spectroscopy
ICP-MS	:	Inductively coupled plasma-mass spectroscopy
ICP-OES	:	Inductively couple plasma-optical emission spectroscopy
IUPAC	:	International Union of Pure and Applied Chemistry
PEIS	:	Potentio electrochemical impedance spectroscopy
PES	:	Polyethersulfone
PIM	:	Polymer inclusion membrane
PSAC	:	Palm shell activated carbon
PSAC-TOMATS	:	Trioctylmethylammonium thiosalicylate immobilised on PSAC
PSAC-TSIL	:	Task-specific ionic liquid immobilised on PSAC

PTFE	:	Polytetrafluoroethylene
PVDF	:	Polyvinylidene fluoride
RVC	:	Reticulated vitreous carbon
THF	:	Tetrahydrofuran
TSIL	:	Task-specific ionic liquid

LIST OF APPENDICES

Appendix A

Appendix B

CHAPTER 1: INTRODUCTION

1.1 Research background

The toxicity of several heavy metals such as cadmium, lead, chromium(IV), and mercury to humans is well reported in various literature. Moreover, these four heavy metals are listed as one of the ten restricted substances under Restriction of Hazardous Substances (RoHS) compliance, originated in the European Union 2002. Thus, all the products in the European Union market must comply to meet a composition of heavy metals below the maximum allowable concentration. For instance, the maximum permissible amount of mercury and cadmium in a component should be lower than 100 ppm. While for lead and chromium(IV), it should be less than 1000 ppm. Nevertheless, heavy metals are used to manufacture a broad range of products. Metals play an essential role in manufacturing processes, namely semiconductors, electrical appliances, constructions and jewellery. Metals play an essential role in manufacturing processes, namely semiconductors, electrical appliances, constructions and jewellery. Although metals are beneficial to the manufacturing industries, in the meantime, a certain proportion of these metal ions is dragged out from the process line and accounts for a large volume of metal-laden wastewater. For instance, in a tin or nickel-plating process line, a large volume of water containing metal ions is present in a rinsing station. An overflow of demineralised water is allowed in the rinsing tank to clean the plated product from the remaining plating bath solution. Finally, the metal-laden wastewater from the rinsing station is channelled and accumulated in the wastewater pond. Besides metal plating, several other primary sources of heavy metals in the environment are industrial discharge by mining, batteries, fertilizer industries and tanneries (Kumar & Dwivedi, 2021). These industrial wastewaters contain poisonous heavy chemicals, for example, mercury, cadmium, lead, zinc, copper, nickel and chromium (Li et al., 2022). Heavy metals are non-biodegradable and tend to accumulate in living organisms (Gu et al., 2018;

Raffa et al., 2021). Therefore, it is crucial to treat them efficiently before the wastewater can be discharged into the environment.

Heavy metals are eliminated from wastewater streams by several conventional chemical-physical treatment methods such as chemical precipitation (Kim et al., 2022; Zhang & Duan, 2020), adsorption (Foroutan et al., 2021; Hu et al., 2021; Li et al., 2021; Wang et al., 2021), ion exchange (Czuprynski et al., 2022; Hussain & Ali, 2021), coagulation-flocculation (Jaradat et al., 2021; Nguyen et al., 2021) and flotation (Jia et al., 2022; Pooja et al., 2022). Modern technology such as membrane filtration (e.g., ultrafiltration, reverse osmosis, nanofiltration) has also received considerable attention for the removal of heavy metals (Ahmad et al., 2022; Kavitha et al., 2022; Teng et al., 2022). On the other hand, several studies utilized an environmental and eco-friendly biological method such as phytoremediation to achieve a similar goal (Chan et al., 2022; Masinire et al., 2021; Nugroho et al., 2021). Conventional chemical-physical treatment methods are reportedly effective for the removal of metals from wastewater (Barakat, 2011; Fu & Wang, 2011), but they suffer from several drawbacks such as high operational costs, incomplete removal, the consumption of a significant amount of energy or the requirement for large quantities of chemicals (Yang et al., 2021). In addition, conventional chemical-physical treatment technologies merely convert the dissolved heavy metals to solid sludge, which requires the allocation of a huge area for landfill disposal. Eventually, metal-laden wastewater streams are rich in numerous valuable constituents such as gold, silver, platinum and palladium. Electrochemical technology provides solutions for the removal and recovery of metals from wastewater in their most valuable state (Bebelis et al., 2013; Yang et al., 2021). The recovery and recycle approaches in industries are mainly driven by economic motivation. The increasing cost of industrial metals makes these efforts economically attractive. In addition, electrochemical processes offer a minimum generation of solid waste, simultaneously

reducing the processing cost for solid waste disposal (Hu et al., 2015; Liu et al., 2013b). As such, electrochemical technologies can potentially offer the best solution for the treatment of waste and wastewater laden with heavy metals. Additionally, according to Zheng et al. (2015)'s bibliometric report, the number of published articles related to electrochemical technology for water and wastewater treatment has increased dramatically over the last two decades (from 1994 to 2013). The exponential increase in the number of published articles per year began from 461 articles in 1993 and 3160 in 2013. The average number of articles that have been published increased by 150 each year. Recently, Yang et al. (2021) reported an escalating trend in electrochemical studies for metal removal and recovery between 2000 and 2020. It was reported that the number of articles published in 2018 (106) increased by over three times as compared to 2013 (34).

Several electrochemical approaches have been applied to remove and recover metal ions from an aqueous solution, namely electrodeposition, electrocoagulation, electroflotation, electrosorption, electrodialysis, electrodeionization and electrowinning (Punia et al., 2022). The advantages of electrochemical technologies are well reported because of their environmental compatibility and versatility (Basha et al., 2011; Yasri & Gunasekaran, 2017). Beyond the remarkable number of works that have been carried out, researchers have reported several problems in electrochemical processes, such as high energy consumption (Chellammal et al., 2010; Yao et al., 2022), low conductivity of electrodes (Du et al., 2021; Rasines et al., 2015), low removal or recovery of heavy metals especially for dilute metal ions (Peng et al., 2014), undesirable reactions (Aoudj et al., 2015; Wang et al., 2022) and poor electrode reliability (Vasudevan et al., 2011). Therefore, further research is being undertaken to minimize the shortcomings of the existing processes.

In 2022, Malaysia celebrated the 105th anniversary of the first commercial oil palm venture. There were 5.74 million hectares of oil palm planted in 2016 (after 100 years of the first commercial oil palm venture), and the site was increased by 1.28% (73160 hectares) in 2017, as reported by the Malaysian Palm Oil Council (MPOC, 2017). Additionally, the palm oil milling industries generate a huge amount of palm shells as a by-product. In 2014, it was reported that a total amount of 4.46 million tonnes of palm shells was generated nationally, which accounted for 95.38 million tonnes of processed fresh fruit bunches (Loh, 2017). Although burning the waste to fuel the boiler at the oil milling factory is one of the undemanding options for disposal, the burning consequence may lead to an air quality issue. However, there is a gradual interest in converting palm shells into valuable material. The works that explored the feasibility of palm shell as a prominent precursor of activated carbon commenced in the 1980s. Since then, numerous works have focused on palm shell carbonization and activation (Adebisi et al., 2017; Yek et al., 2019). To date, palm shell activated carbon (PSAC) is commercially produced while continuous effort remains in place to improve its performance. Nevertheless, several novel paradigms work to utilize the surplus value of PSAC as the raw material of porous electrodes (Chong et al., 2018; Ghafari et al., 2009; Ismaiel, 2013; Issabayeva et al., 2006). Porous, three-dimensional (3D) cathodes provide a high electrode surface area per unit volume of electrode and a high transfer coefficient compared to two-dimensional (2D) electrodes.

Ionic liquids exhibit several well-accepted unique properties such as negligible vapour pressure (non-volatility), high thermal stability, non-flammability and lower reactivity. A specific design of ionic liquid developed to achieve an explicit purpose is generally known as task-specific ionic liquid (TSIL). For instance, trioctylmethylammonium thiosalicylate (TOMATS) is designed to have a strong ability to extract heavy metals, namely lead, mercury, copper, and cadmium. Indeed, due to the uneconomically

profitable cost to recycle waste like mercury and cadmium, less effort has been made to recover these metals from the wastewater stream. However, it is crucial to treat the wastewater before it can be discharged into the environment due to environmental concerns.

Activated carbon offers a high surface area and has been proven as a superior electrode for capacitive deionization of brackish water. At the same time, TSIL demonstrates a high selectivity of heavy metal removal. Therefore, the present work is to develop the hybrid function of activated carbon and TSIL-based electrode from PSAC for the removal of Hg from synthetic wastewater. This approach mainly combines the exclusive characteristic of TSIL in extracting the metal ion and PSAC that is locally available at a low cost, high surface area with high adsorptive quality. This study may provide new insight and perspective in developing a better performance of the electrochemical process in terms of its effectiveness and economic values.

1.2 Problem statement

Mercury and its compound are toxins. It enters water or soil from the weathering of rocks that contain inorganic mercury salts and from point sources (factories or water treatment facilities) that release water contaminated with mercury. Several manufacturing lines associated with the use of mercury and its derivatives are the production of fluorescent lamps, button cell battery, whitening soap and colour paints. Once mercury enters the ecosystem, a significant amount of mercury may accumulate in the human body. Further, it harms the brain, heart, kidneys, lungs, and immune system. Therefore, without proper wastewater treatment methods, it causes great damage to humans and animals.

Conventional methods for the removal of mercury, such as chemical precipitation, adsorption and ion exchange suffer from several limitations in their application. Their

limitations include one or a combination of the following shortcomings: high operational costs, incomplete removal, consumption of a significant amount of energy and requirement for a large quantity of chemicals. In addition, many technologies merely convert the dissolved heavy metals to solid sludge, which subsequently requires the allocation of a dumping site for solid disposal and possibly causes groundwater pollution. Hence, the electrochemical process provides an appropriate method for the removal and recovery of mercury, which offers excellent effectiveness and minimizes the drawbacks of conventional methods. However, the application of the electrochemical process for the removal of mercury, particularly on a large scale, is considered limited compared to the conventional wastewater treatment method.

Electrodeposition of heavy metals offers the possibility of metal recovery in its most valuable state. Recovery of metal using a 2D electrode provides uniform reaction rate distribution over the surface of the electrodes due to the homogenous electrode potential. However, it has a relatively low specific electrode-electrolyte interphase per cell volume compared to the 3D electrode. Consequently, the electrochemical treatment is less energy efficient and the specific electrical energy consumption increases. Although this technology is mature with various applications, considerable efforts are being made to increase the electrode performance in terms of its efficiency while minimising the energy consumption.

Palm shell activated carbon (PSAC) is derived from the carbonization and activation of palm shells. Palm shells are produced as solid waste during palm oil milling and are abundantly available in tropical countries such as Malaysia, Indonesia, and Thailand. The work to investigate the performance of PSAC as the raw material of an electrode appears to provide a value-added product that is derived from local industrial solid waste. To date, there has only been a little work that studied the PSAC as an electrode for water and

wastewater treatment. Additionally, the electrochemical properties of PSAC as a prominent porous carbon-based electrode for this specific goal have not yet been addressed in detail.

1.3 Research objective

The objectives of this research are:

a) To investigate the electrochemical properties of palm shell activated carbon (PSAC) electrode using voltammetric techniques and potentio electrochemical impedance spectroscopy (PEIS).
b) To investigate the electrochemical properties and electrode reversibility studies of PSAC and task-specific ionic liquid immobilised on palm shell activated carbon (PSAC-TSIL).
c) To evaluate the performance of PSAC-TSIL electrodes for the removal of mercury from an aqueous solution.

1.4 Scope of work

This study focuses on preparing virgin PSAC and PSAC-TSIL electrodes, comparing the electrochemical properties of PSAC and PSAC-TSIL and applying the prepared electrodes for the removal of Hg. The preparation of the PSAC-TSIL electrode involves the development of PSAC immobilised with a task-specific ionic liquid (TSIL), namely, trioctylmethylammonium thiosalicylate (TOMATS).

In preparing the virgin PSAC electrode, the effect of the amount of binder was evaluated by varying the polytetrafluoroethylene (PTFE) composition (10, 20, 30 & 40%) and varying the carbon black composition (10, 20 & 30%). For the electrochemical characterization, the effect of the supporting electrolyte was tested for acidic (0.5 M HCl) , neutral (0.5 M NaCl) and and basic (0.5 M NaOH) conditions. The best supporting electrolyte (0.5 NaCl) is used to study the performance of PSAC electrode for electrochemical reversibility of common redox probe (5 mM potassium ferrocyanide) and

the electroreduction of mercury (5 mM Hg^{2+}). The electrochemical properties of the electrodes will be determined using cyclic voltammetry, chronoamperometry and PEIS analysis.

Next, the TSIL was immobilised on PSAC electrode surface to enhance the electrochemical activity. The prepared PSAC-TSIL electrodes were then be employed in an undivided batch electrolytic cell for the removal of Hg from artificial wastewater. The concentration of Hg was determined using Inductively Couple Plasma-Optical Emission Spectroscopy (ICP-OES) or Inductively Coupled Plasma-Mass Spectroscopy (ICP-MS) for lower initial Hg concentration (25 ppm) studies. The performance of PSAC-TSIL was studied under several operating parameters namely, amount of TSIL loading (0.2, 0.1, 0.5 g), current density (2, 4 & 6 mA/cm^2), pH (acidic, neutral & basic) and initial concentration of Hg (5, 20 & 100 ppm). The physical and chemical properties of the prepared electrode were studied using surface area and porosity analyser, Fourier Transform-Infrared Spectroscopy (FTIR) and Field Emission Scanning Electron Microscope with Energy Dispersive X-Ray (FESEM-EDX). Finally, this work carried out the electrode reusability study.

1.5 Significance of the study

The findings of this study redound to the benefit of society and industries, considering that having a better understanding of the characteristic of a composite porous activated carbon-ionic liquid as an electrode may lead to economics and an effective electrochemical process for wastewater treatment. Exploring the possibility of activated carbon-ionic liquid may give an insight into a value-added property of the existing application of activated carbon. This finding may give an intuition for future research in tailoring the properties of porous electrodes for the purpose of wastewater treatment via electrochemical technology. Additionally, this work is in line with the A National Key

Priority Area on Water (2015), which addresses the recovery of resource such as metal from wastewater. Consequently, this approach will reduce the amount of pollutant discharge into the environment. The research also supports the Eleventh Malaysian Plan in pursuing green growth for sustainability and resilience by managing waste holistically, referring to Chapter 6: Strategy B5-Focus area B.

1.6 Thesis outline

This thesis consists of five chapters as outlined below:

Chapter 1: Introduction

This chapter provides a general overview of the electrochemical process and electrode's role in removing and recovering heavy metals from wastewater. The problem statement, research objectives, scope of the study, and the research's significance are also outlined.

Chapter 2: Literature review

This chapter reviews the existing electrochemical approaches for the removal and recovery of metal ions. Various current works involving cell design and electrode development were addressed in distinguished electrochemical processes, namely, electrodeposition, electrocoagulation, electroflotation, and electrosorption. Some other topics, such as the current approach to remove Hg from wastewater, the advantages of TSIL and several findings on the electrochemical properties of the porous electrode are also highlighted.

Chapter 3: Methodology

Chapter three lists the chemicals and materials that were used in this work. It describes the electrode preparation method for the palm shell activated carbon (PSAC) and the palm shell activated carbon immobilised with TOMAT (PSAC-TOMATS). The process flow of the batch electrochemical process steps is also described in detail.

Chapter 4: Results and discussion

This chapter is divided into three parts, mainly to address three objectives. The first part describes the PSAC electrode preparation and characterization and discusses the effect of the amount of binder on the electrochemical activity in the cell. The second part of the chapter compares the electrochemical activity of PSAC and PSAC-TOMATS electrodes. Lastly, Part Three discusses the result and finding for the electrochemical removal of Hg from an aqueous solution using virgin PSAC and PSAC-TOMATS electrodes.

Chapter 5: Conclusion & Recommendation

This chapter concludes the main findings of this research. Several recommendations for future studies are also proposed.

CHAPTER 2: LITERATURE REVIEW

2.1 Mercury polluted wastewater

Mercury (Hg) is a naturally occurring element found in air, water, and soil. It exists in various forms either in metallic (liquid and gaseous states), inorganic (e.g., mercuric chloride, mercurous chloride, mercuric acetate), or organic (e.g., methylmercury, ethylmercury). It can be accumulated in living organisms. Mercury exists in three valence states (0, I and II). In wastewater, mercury occurs in the form of metallic, undissociated molecules (Hg^{2+}) and ions (Hg_2^{2+}) as well as complex ions. Methylmercury (MeHg) is the most toxic form of mercury, among others. Inorganic Hg in water is converted to methylmercury by the bacterial organism.

The evidence of Minamata disease was a vital outcome in history as the presence of Hg in the food chain leads to mercury poisoning among the residents of Minamata, Japan. The pollution originated by a chemical plant whose dumped their waste that contains Hg derivatives into the bay. It contaminated the fish and shellfish living in the Minamata Bay, and ultimately ended up in the human body via the food chain. This neurogenically disease was first discovered in 1956 at Minamata, and the second outbreak occurred at Niigata prefecture in 1965. The affected people were suffered from brain damage with observed symptoms such as mental retardation, sensory and auditory disturbances, constriction of the visual field, and dysarthria (Harada, 1995). Although the usage of Hg in product has been declined, several other industries are still using Hg because of their superior functionality. For this reason, those industries are likely to generate Hg-polluted solid waste and/or wastewater. Several common mercury compounds and their application include:

a) Mercuric chloride ($HgCl_2$), which can be described as a highly poisonous salt which once used as a wound disinfectant,

b) Mercurous chloride (Hg_2Cl_2) or also known as calomel, which is used as an antiseptic to kill bacteria,
c) Mercuric sulfide (HgS) is used to make red paint pigment called vermilion
d) Mercuric oxide (HgO) is used to make mercury batteries

Stringent rules have been established by the authorities to control the concentration of mercury in surface water. The maximum allowable concentration of Hg in drinking water is set to 2 μg/L by the United States Environmental Protection Agency (US EPA). Meanwhile, World Health Organization (WHO) allow a maximum of 6 μg/L (WHO, 2005). In Malaysia, the maximum allowable of Hg that can be discharged from the industrial effluent at the catchment area for water supply intakes for the purpose of human consumption is 5 μg/L; regulated in Environmental Quality (Industrial Effluent) Regulation 2009. However, according to National Water Quality Standards for Malaysia, the interim standard of mercury for marine water quality (Hajeb et al., 2012) is similar to the appointed limit by WHO. Mercury levels in water are generally very low and do not exceed more than 1 g/L (Li et al., 2009). Zhou et al. (2018) reported that the discharge of wastewater from 872 wastewater treatment plants in China was between 0.04 to 0.001 mg/L of Hg. However, higher concentration was found in wastewater produced by specific industries. For instance, the wastewater produced by the chlor-alkali process, poly(vinyl chloride) synthesis and pharmaceutical manufacturing was reported to contain between 10 μg/L to 10 mg/L of Hg (Candeago et al., 2020; Cyr et al., 2002). In Malaysia, it was estimated that 19405 kg of mercury was released into the environment (air, water, land, or by-products) in 2014 (KASA, 2021).

Despite the extremely low permissible Hg concentration, waste or product containing Hg is still plenty on the market. Intentional use of Hg is found to associate with several known industries such as the production of electrical switches, wiring devices, measuring

devices such as thermometer and barometer, lighting, dental work (Gupta et al., 2014) and production of vinyl chloride monomer (Lin et al., 2016). Additionally, mercury may also get into the ocean from various sources, including air and water pollution, along with naturally available minerals. For instance, Obrist et al. (2018) reported that most of the Hg in the Pacific Ocean originated from air pollution due to the emission from coal-fired power plants in the Asia continent. In another study, Sunderland et al. (2009) estimated that the levels of mercury in the North Pacific could be double by 2050 if human-induced emissions continue at the current rate.

Various methods were studied to explore the effective removal of mercury from wastewater. Several researchers aim to reduce Hg(II)) to Hg(0) by bioremediation method for which bacteria or fungi were employed as the biomediator (Amin et al., 2021; Chang et al., 2021). Although Hg(0) is relatively toxic, it is not even close to the toxicity of Hg(I) or Hg(II) because both of them can form organomercurial compounds like methylmercury and dimethylmercury. On the other hand, one could even drink or inject Hg(0) without severe complications. Because Hg(0) is volatile, reducing Hg(I) or Hg(II) to Hg (0) promotes volatilization and removal from their immediate environment. Recently, Hua et al. (2020) discussed about five typical methods to remove Hg from aqueous solution, namely (1) precipitation, (2) adsorption, (3) membrane separation, (4) biological treatment, and (5) ion exchange. They suggested that future studies should consider the development of nanomaterials with a large specific surface area and synergistic effects, including high adsorption and ion exchange. This novel advanced nanomaterial was proposed to be loaded on a substrate with the aim to provide high removal capacity, fast removal rate, ability to meet low mercury limit, low cost of material, easy to synthesize, and the materials are easily retrieved from solution after use. Although they pointed out that adsorption and ion exchange are the most promising technologies for the removal of mercury, perhaps a novel nanomaterial could be applicable to be introduced in all the five

removal methods that have been discussed. A similar intention to explore nanomaterial for effective removal of Hg was also reported by Sharma et al. (2021). Other than the methods mentioned earlier, several other mercury removal techniques from aqueous solution had been explored by other researchers but have not been caught the attention by Hua et al. (2020), Sharma et al. (2021) and their co-workers. For instance, research has been conducted to employ liquid extraction (Abbasi et al., 2019; Sato et al., 2002), photocatalysis (Casasus et al., 2020; Zhang et al., 2021) and electrochemical (Candeago et al., 2020; Du et al., 2022) for the removal of Hg from aqueous solution.

Electrochemical technology provides solutions for the removal and recovery of metals from wastewater in their most valuable state (Bebelis et al., 2013). The recovery and recycle approaches in industries are mainly driven by economic motivation. The increasing cost of industrial metals makes these efforts economically attractive. In addition, electrochemical processes offer a minimum generation of solid waste, simultaneously reducing the processing cost for solid waste disposal (Hu et al., 2015; Liu et al., 2013b). As such, electrochemical technologies can potentially offer the best solution for the treatment of waste and wastewater laden with heavy metals. In fact, a bibliometric analysis by Yang et al. (2021) and Zheng et al. (2015) proved that the trend of employing electrochemical technology for water and wastewater treatment has increased considerably from 1994 until 2020.

2.2 Electrodeposition

The electrodeposition process utilizes an external source of electrical current passing through an electrochemical cell to reduce dissolved metal cations and form a metal element on an electrode. This process was invented by Luigi Brugnatelli in 1805 and is commonly known as electroplating. To date, electrolytic recovery, electrowinning, and cathodic reduction are the other common terms used, which are also associated with the

electrodeposition process. In the water and wastewater treatment process, electrodeposition technology is employed for several purposes, such as the recovery of precious metals (e.g., silver, gold, platinum) (Padamata et al., 2020; Yi et al., 2019), the recovery of non-precious metals (e.g., Pb, Cu, Cd) (Kim et al., 2021; Song et al., 2021), the removal of metal ions from wastewater (Ghalehkhondabi et al., 2021) and the remediation of metal ions from groundwater (Zhang et al., 2018). Electrodeposition offers several advantages in that no chemical reagent is required, it forms a stable sludge (non-toxic and easily removable), has high selectivity and has a low operating cost (Qasem et al., 2021). However, in some particular designs of electrodeposition reactors, the process results in the production of dendrites, loose or spongy deposits and involves some gas evolution reactions, which may give rise to safety concerns (Chen, 2012). Therefore, improvements to the existing electrodeposition process are very much needed to minimize and eliminate these drawbacks.

The electrodeposition mechanism mainly refers to oxidation and reduction at the anode and cathode, respectively, when a current is introduced to the electrodes. Heavy metal ions in the electrolyte will be reduced to their elemental forms and deposited on the cathode's surface due to the chemical reaction. This mechanism is classified as a direct approach and is more suitable for high concentrations of metal ions (Chen, 2012). However, electrodeposition has also been reported to deal with dilute metal solutions with proper electrode designs (Martins et al., 2012; Recéndiz et al., 2011). A typical chemical reaction at the cathode is represented by Equation 2.1, where M is the metal and n is the metal's valence.

$$M^{n+}\ (aq) + ne^- \rightarrow M\ (s) \qquad \text{Equation 2.1}$$

It promises to recover high purity metal deposits at the cathode. However, some other competing reactions might occur at the cathode as the industrial wastewater also contains

organic compounds. Table 2.1 shows several common reduction reactions that might occur in an aqueous metal nitrate solution (Chen, 2012; Mook et al., 2013). The presence of hydrogen gas and oxygen needs to be minimized due to safety issues. On the other hand, a common reaction is the oxidation of hydroxide ions taking place at the anode. However, prevailing chlorides will be oxidized at the anode if these are present in the electrolyte. In practice, the overvoltage for the oxidation of the water molecules is large enough to make it more difficult for these to be oxidized compared to the chlorides, even though the standard oxidation potential of water (E^o= -1.23 V) is more positive than that of chloride (E^o= -1.36 V). Such behaviour is commonly encountered in the electrolysis of brine, which produces chlorine, hydrogen and caustic soda.

Table 2.1: Reduction and oxidation reactions at the electrodes in the electrodeposition process.

Compound	Reduction reaction at the cathode
Metal ion to metal element	M^{n+} (*aq*) + ne^- → M (*s*)
Hydrogen ion to hydrogen gas	$2H^+$ (*aq*) + $2e^-$ → H_2 (*g*)
Nitrate to nitrite	NO_3^- (*aq*) + $2H^+$ (*aq*) + $2e^-$ → NO_2^- (*aq*) + H_2O (*l*)
Nitrite to nitrogen gas	$2NO_2^-$ (*aq*) + $8H^+$ (*aq*) + $6e^-$ → N_2 (*g*) + $4H_2O$ (*l*)
Nitrogen gas to ammonium	N_2 (*aq*) + $8H^+$ (*aq*) + $6e^-$ → $2NH_4^+$ (*l*)
Water to hydrogen	$2H_2O$ (*l*) + $2e^-$→ H_2 (g) + $2OH^-$(*aq*)
Oxygen to water	O_2 (g) + $4H^+$ (*aq*) + $4e^-$ → $2H_2O$ (*l*)
Oxygen to hydrogen peroxide	O_2 (g) + $2H^+$ (*aq*) + $2e^-$ → H_2O_2 (*l*)
	Oxidation reaction at the anode
Hydroxide ion to oxygen and water	$4OH^-$(*aq*) → O_2 (*g*) + $2H_2O$ (g) + $4e^-$
Water to oxygen	$2H_2O$ (*l*) → $4H^+$ (*aq*) + O_2 (g) + $4e^-$
Chloride to chlorine gas	$2Cl^-$ (*aq*) → Cl_2 (*g*) + $2e^-$

Exhaustive mechanisms of heavy metal electrodeposition can be explained according to the discharge of metal ions at an electrode (cathode) surface. According to the atomic level consideration in the electroplating process, metal ions accept electrons from the electrically charged solid-electrolyte interface and are then deposited onto the cathode as metal atoms (Kanani, 2004). The electrons are supplied by an external potential source.

Kanani (2004) briefly explained that the process involves a number of intermediate stages, the most important of which are: (1) the transport of hydrated metal ions or complexes from a bulk solution to the cathode, primarily by convection and solution diffusion; (2) the stripping of the hydration sheath from the metal ion at the cathode-solution interface; (3) the charge transfer with the formation of adsorbed atoms on the surface of the cathode. The discharge of adsorbed ions to form adsorbed atoms takes place within the electrolyte double layer, which forms spontaneously at the cathode-solution interface; (4) the formation of crystal nuclei by the diffusion of the adsorbed atoms at the cathode surface; and (5) the fusion of thermodynamically stable crystal nuclei to form a metallic layer. The crystal growth process commences once the nuclei have reached their critical size.

The economic feasibility of the electrodeposition process is mainly dependent on the rate of mass transfer, the current density and the current efficiency (Koene & Janssen, 2001). These factors are generally associated with the design of the electrochemical reactor and the parameter settings for the process. In optimizing the operating parameters for the electrodeposition of Pb^{2+}, Abou-Shady et al. (2012) studied the effects of pH, applied voltage, concentration, flowrate and temperature using the Taguchi approach. Prior to that, electrodialysis was introduced to increase the concentration of Pb^{2+} from 600 mg/L to 2600 - 3000 mg/L. Up to 91% of the Pb was recovered from the concentrated Pb^{2+} by electrodeposition. They concluded that the most important parameters affecting electrodeposition are in the following sequence of voltage > concentration > pH > flowrate > temperature. Using a similar approach (Taguchi method), Peng et al. (2014) also reported that applied voltage has an important effect on the recovery of nickel compared to the initial concentration and pH. However, the cathodic electrodeposition of wastewater reportedly results in inadequate performance that fails to meet the standard discharge limit (Abou-Shady et al., 2012; Peng et al., 2014). On the other hand, Basha et

al. (2008) claimed that 99.7% of Pb was successfully removed from copper smelting wastewater at a low pH. Thus far, numerous studies have examined the effects of applied voltage, metal salt concentration and pH on the removal or recovery efficiency. Voltage, associated with current density, is likely to be the most important operating condition that needs to be considered to obtain high percentage removal of heavy metal. Other parameters, namely pH and initial concentration, also contribute to the performance of the cell system, although they are slightly less significant than voltage. However, some findings, which have reported inadequate metal removal and recovery performance, require further attention. The proper design of electrochemical cells and the optimization of the operating conditions for the process are crucial for high removal or recovery with reasonable energy consumption.

2.2.1 Design of electrochemical reactor

The electrochemical process takes place in a cell, which is often called an electrochemical reactor. The design of the reactor is the heart of electrochemical technology. The basic principle of an electrochemical reactor consists of a cathode, an anode and an electrolyte. In the application of the electrochemical process for wastewater treatment, the electrolyte is referred to as the wastewater carrying the pollutants to be removed or recovered. The design of the reactor can be classified according to its electrode configuration; 2D or 3D, batch or continuous, static or moving electrode, the electrode compartment separation (divided or undivided) or the electrical connection (monopolar or bipolar) (Bebelis et al., 2013). Each design is noted for its advantages and has certain shortcomings with regard to the overall performance of the electrochemical process. In designing an economical and operative electrochemical reactor, several important characteristics must be considered. Some of the desired specifications are high mass transport rate, high current efficiency, high current density, large active surface area per unit reactor volume, low cell voltage, uniform distribution of electrode potential and

low maintenance cost (Baghban et al., 2014; Scott, 1993). Despite the many parameters for the measurement of the performance of an electrochemical reactor, the current efficiency, CE (Equation 2.2), space-time yield, Y_{ST} (Equation 2.2) and energy consumption, E_c (Equation 2.3) are the most important (Chen, 2004; Goodridge & Scott, 1995).

$$CE = \frac{z_i F \Delta m}{M_i I \Delta t} \times 100 \qquad \text{Equation 2.2}$$

$$Y_{ST} = \frac{iaM_i}{1000 z_i F} CE \qquad \text{Equation 2.3}$$

$$E_c = \frac{VIt}{1000m} \qquad \text{Equation 2.4}$$

Equation 2.2, 2.3 and 2.4 are deduced from several input values whereby z is charge number, F is Faraday's constant (96485 A·s/mol), Δm is the mass (g) deposited in the interval time, Δt (s), M is a molecular mass (g/mol), I is the current passed (A), i is the current density (A/m^2), a is the specific electrode area (m^2/m^3) (electrode area per unit volume of the reactor), V is the cell voltage (V) of the process, t is the electrolysis time (h) and m is the mass of the product (kg). The CE (%) represents the ratio of the current that is consumed in producing a targeted product to the total consumption of current that is determined using Faraday's law. Y_{ST} (kg/m^3s) represents the production rate of the metal per unit of the reactor volume, whereby E_c (kWh/kg) is dominantly contributed by the electrolytic process. However, the energy consumed during the circulation of the electrolyte and the heating treatment may also require attention (Su et al., 2009).

Since electrodeposition occurs at the cathode's surface, a high specific surface area of the cathode can remarkably promote a better space-time yield. However, reports on the space-time yield are largely unavailable, as most authors have preferred to highlight the removal efficiency of heavy metals. Even though this information is essential to some extent, it is challenging to compare the results of one study to another as these results are

largely dependent on the initial concentration, the volume of the reactor and the surface area of the electrode. For instance, batch experiments performed with very low initial concentrations can approach 100% removal in a very short electrochemical treatment time. In such experiments, the chosen initial concentrations are likely not a sensible operating condition to present the maximum capability of the electrode and cell system. It is more useful to evaluate the performance of the electrode/system under a broader range of initial concentrations, for which satisfactory CE, Y_{ST} and E_c can be obtained.

2.2.1.1 Electrode dimensions: 2D and 3D

A two-dimensional (2D) reactor consisted of planar plate electrodes. It was later improved to become a three-dimensional (3D) reactor, which is comprised of particulate or porous electrodes. Generally, the 3D configuration was proposed to enhance the 2D reactor, which had not only a small space-time yield but also a short electrode lifespan, low current efficiency, limited mass transfer, low area-volume ratio (Zhang et al., 2013) and low recovery rate of metal from a dilute solution (Chellammal et al., 2010). The limitation of current efficiency for low metal concentration by the 2D electrode is illustrated by the dashed curve in Figure 2.1. For the 2D electrode (which is addressed as planar in Figure 2.1), the current efficiency approaches zero percentage for a metal concentration below 100 ppm. On the other hand, for the purpose of electroplating or electrowinning on the 2D electrode, the conventional electrochemical process is generally conducted at a metal concentration above 20000 ppm (Keating & Williams, 1976) to achieve higher current efficiency. In addition, Keating and Williams (1976) suggest that the 3D electrode offers a combined effect of hydrodynamic reduction of the diffusion layer and a larger surface area to improve the current efficiency. This concept is described as extended-surface electrolysis (ESE), and the current efficiency trend with respect to the reduction of metal concentration is illustrated in Figure 2.1. By referring to this figure, using a 3D electrode, which is considered as ESE, is promising to remove metal ions from

wastewater to meet the allowable metal ion limit in the effluent. A 3D electrode is designed to facilitate the metal reduction for wastewater that consists of less than 100 ppm concentration. Additionally, they reported that 30% of current efficiency is considered satisfactory from the economic perspective. The wastage of electrical energy in low metal concentration, as be seen by low current efficiency is due to some other competing electrochemical activities such as electro reduction of oxygen and evolution of hydrogen with metal reduction reaction (Ottewill et al., 2005). Thus, the metal ion is transferred to the electrode surface at a lower rate.

Figure 2.2 illustrates several common configurations of reactors for heavy metal removal and recovery. A 2D reactor may be further classified according to the motion of the electrode, whether it is static (Figure 2.2a and b) or moving (Figure 2.2c). Many researchers investigated 3D reactors in various arrangements because they offer a high specific surface area and a high mass transfer rate (Chellammal et al., 2010). With the same geometrical area, a 3D electrode offers a significantly larger active surface area compared to a 2D cell of the same volume. Therefore, the space-time yield of a 3D reactor can be improved by increasing the active surface area per unit of reactor volume. It is a potential alternative for the removal and recovery of heavy metals from very dilute solutions when the reaction occurs at low current densities (Colli & Bisang, 2015). Several studies using 2D electrodes for the removal and recovery of heavy metals are listed in Table 2.2. The 2D electrochemical cell configuration listed in Table 2.2 is specifically focussing on the electrodeposition of metal of interest on the cathode. Whereas the anodes are inert electrode and has not been consumed during the electrochemical process. As shown in Table 2.2, the most common anode that has been employed was titanium mesh coated with RuO_2 and IrO_2, while many utilised stainless steels as the cathode. Only a small number of works studied graphite as the electrode either as the anode or cathode.

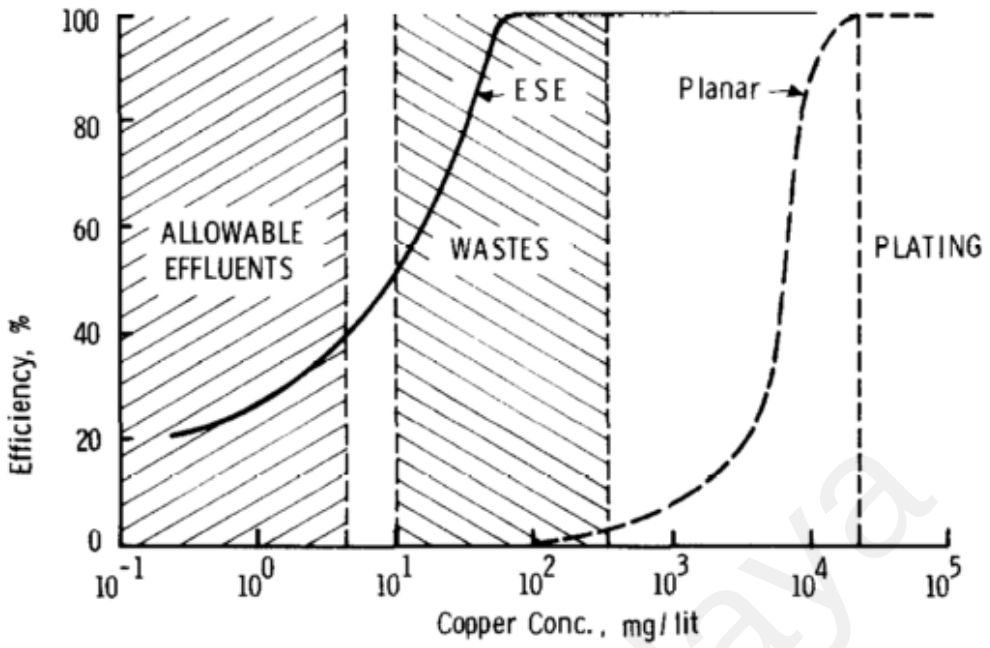

Figure 2.1: Effect of concentration on current efficiency in metal reductions (Keating & Williams, 1976).

A 3D reactor configuration can consist of a packed bed (Figure 2.2d), fluidized bed (Figure 2.2e) or spouted bed electrodes (Figure 2.2f), where particle electrodes are introduced into the cell. Additionally, a porous plate electrode is also classified to function as a 3D reactor. Packed bed and fluidized bed electrodes have been used for hydrometallurgy purposes for many years (Coeuret, 1980; Coeuret & Paulin, 1988). Several recent studies have focused on the use of spouted bed reactors (Britto-Costa & Ruotolo, 2015; Darwish et al., 2015; Grimshaw et al., 2011a; Grimshaw et al., 2011b; Martins et al., 2012; Shirvanian & Calo, 2005), which incorporate many of the advantages of packed and fluidized beds while minimizing the drawbacks of such bed reactors. Several recent studies using 3D electrodes are listed in Table 2.3, and various particle electrode of several types such as metal (copper), graphite, glass bead, polymer bead and resin was introduced in the cell system to provide a larger active surface area. Like Table 2.2, important parameter settings such as pH, temperature, and current density for each study are also listed in Table 2.3.

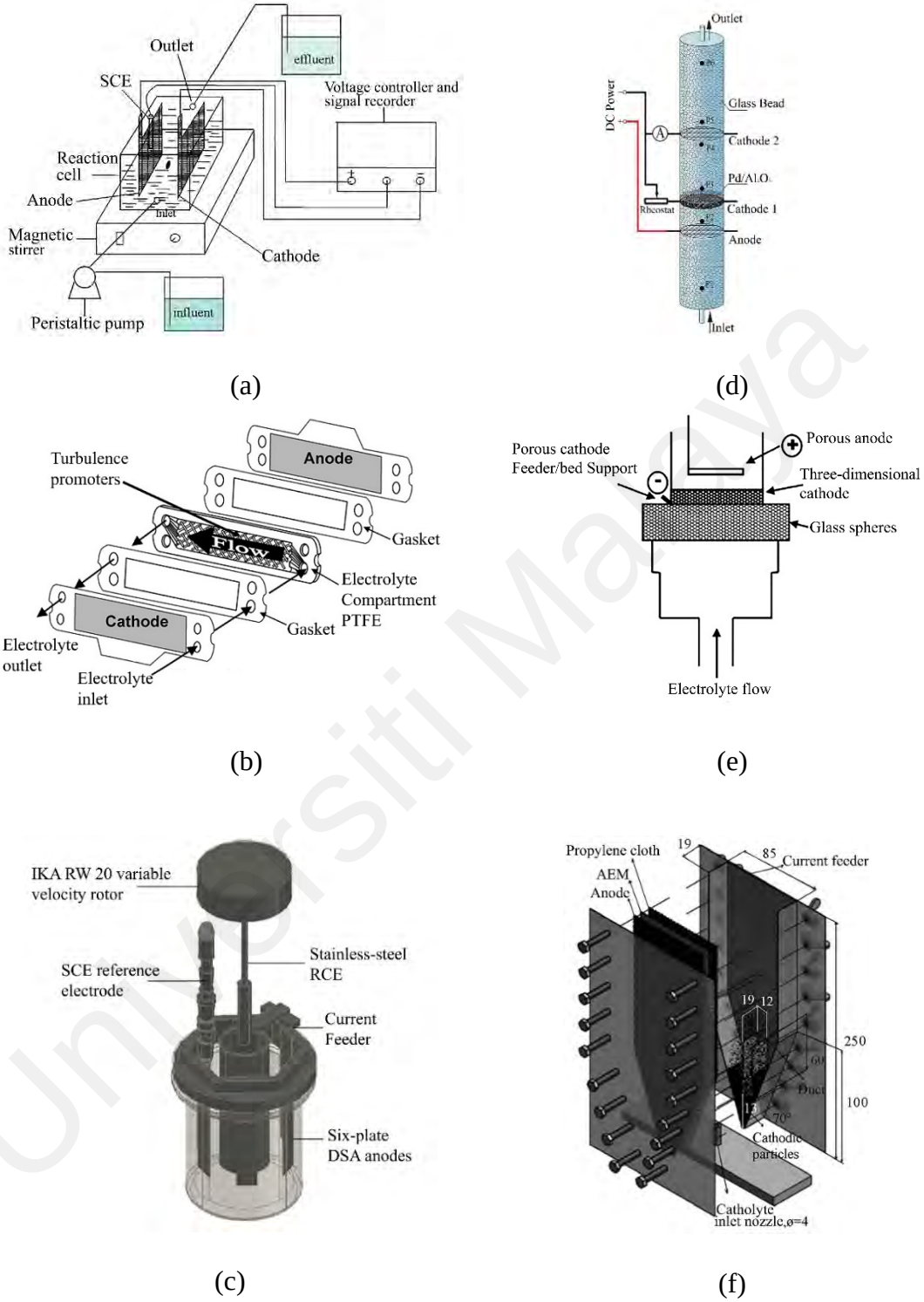

Figure 2.2: Typical 2D: a) parallel plate in tank-cell with recirculation mode (Liu et al., 2013b), (b) parallel plate in filter press (Terrazas-Rodriguez et al., 2011) (c) rotating cylindrical electrode (RCE) (Arredondo et al., 2014) and 3D: (d) packed bed (Qian et al., 2014), (e) fluidized bed (Kaminari et al., 2007), (f) spouted bed (Baghban et al., 2014) reactors.

Table 2.2: Several 2D electrochemical cell configurations and important findings for removal and recovery of heavy metals.

Wastewater	Targeted metal ion: Initial concentration, mg/L	Process	Electrode material		Conditions	Treatment time, min	Removal, %	References
			Anode	Cathode				
Synthetic HgSO4	Hg^{2+}: 10, 25 & 50	Batch Undivided	Ti/IrO2	Titanium plate	10 mA/cm^2	1440	90	Du et al. (2022)
Synthetic Hg^{2+} solution	Hg^{2+}: 1, 10, 200	Batch Undivided	Platinum wire	Nanostructured polymer	300 rpm -1.0 V *vs* Ag/AgCl	60	>95	Candeago et al. (2020)
Municipal wastewater	Hg^{2+}: 0.078					300	97.5	
Synthetic Hg^{2+}	Hg^{2+}:10	Batch Undivided	Platinum wire	Platinum film	0.16 V 20°C	1440	99.4	Tunsu and Wickman (2018)
Synthetic $NiSO_4 \cdot 6H_2O$ solution	Ni: ≈1000	Batch Undivided	Titanium mesh coated with RuO_2 and IrO_2	Graphite	pH 5 4 V	4800	Ni: 88.04	Peng et al. (2014)
		Batch (recirculation mode) Undivided			pH 5 4 V 4 L/h	120	Ni: 65	
Synthetic $Pb(NO_3)_2$ solution	Pb^{2+}: 20-150	Batch Undivided	Stainless steel nets coated with single-wall carbon nanotubes	Stainless steel nets coated with single-wall carbon nanotubes	pH 6.5 -2 V (vs SCE) ≈0.35 mA/cm^2	90	Pb: 97.2-99.6	Liu et al. (2013b)

Wastewater	Targeted metal ion: Initial concentration, mg/L	Process	Electrode material		Conditions	Treatment time, min	Removal, %	References
			Anode	Cathode				
Synthetic $Pb(NO_3)_2$ solution	Pb^{2+}:1500	Batch (recirculation mode) Undivided cell	Titanium mesh coated with RuO_2 and IrO_2	Stainless steel	pH 4 35°C 3.3 V	180	91	Abou-Shady et al. (2012)
Copper-phthalocyanine dye manufacturing plant effluent	Cu^{2+}: 1450	Batch (recirculation mode) Undivided cell	Titanium mesh covered with TiO_2, IrO_2 and RuO_2	Stainless steel	pH <1 100 mA/cm^2	3000	98	Chellammal et al. (2010)
Silver-plating wastewater	Ag^{+}: 1000	Batch Undivided cell	Graphite	Stainless steel	pH 9 45°C 0.5 mA/cm²	-	Ag: 99	Su et al. (2009)
Copper smelting wastewater	As^{2+}: 1979 Cu^{2+}: 165 Cd^{2+}: 76 Zn^{2+}:456	Batch Divided cell	Titanium mesh coated with IrO_2 and TiO_2	Stainless steel	pH 0.64 4.13 V 20 mA/cm²	3600	As: 98.6 Cu: 87.5 Cd: 70 Zn: 69.2	Basha et al. (2008)
		Batch (recirculation mode) Undivided cell			pH 0.64 2.24 V 7.5 mA/cm² 20 L/hr	4800	As: 94.8 Cu: 98.8 Cd: 48.3 Zn: 63.6	

Note: Condition including pH, temperature (°C), voltage (V), current density (mA/cm^2) or voltage (V).

Table 2.3: Several 3D electrochemical cell configurations and important findings for the removal and recovery of heavy metals.

Wastewater	Targeted metal ion: Initial concentration, mg/L	Process	Electrode material			Conditions	Removal, %	References
			Anode	Cathode	Particle			
Synthetic $CuSO_4$ & $NiSO_4$ solution	Cu: 3810 Ni: 3522	Batch	Platinum coated titanium	carbon fibre cloth	-	10 V pH 6.8 20 h	97	(Tran et al., 2017)
Synthetic Cd ions solution	Cd: 180	Spouted bed reactor (batch recirculation mode)	Titanium mesh coated with IrO_2 and RuO_2	Aluminium	Copper wire	pH 4.4 0.95 mA/cm²	>97.8	Baghban et al. (2014)
Synthetic Cr(IV) ion solution	Cr(IV): 5	Packed bed (continuous)	Titanium diamond coated with metal oxides	Titanium diamond coated with metal oxides	Pd/Al_2O_3 and glass beads	3.1 mA/cm² 2.5 mL/min	Cr(III): 71	Qian et al. (2014)
Synthetic $CuSO_4$ solution	Cu: ≈8000	Fluidized bed (batch)	Lead	Copper	Ion-exchange resin	pH 3	NA	Abdel-Aziz et al. (2013)
Synthetic $CuSO_4 \cdot 6H_2O$ solution	Cu^{2+}: 500	Fluidized bed (continuous)	DSA	Copper	Copper	8 A	NA	Tonini et al. (2013)
Synthetic solution	Cd^{2+}: 150 Pb^{2+}: 150	Fluidized bed (recirculation mode)	Expanded 3D mesh DSA	Perforated stainless steel 316	Glass sphere	pH 2	Pb: 99 Cd: 41	Segundo et al. (2012)

Wastewater	Targeted metal ion: Initial concentration, mg/L	Process	Electrode material			Conditions	Removal, %	References
			Anode	Cathode	Particle			
Copper smelting wastewater	As^{2+}: 1979 Cd^{2+}: 76.06 Cu^{2+}: 164.46 Ni^{2+}: 12 Zn^{2+}:455.6 Pb^{2+}: 4 Fe^{2+}: 88.0	Batch (recirculation mode)	Titanium mesh coated with IrO_2 and TiO_2	Graphite particles	Graphite	0.2 mA/cm² 61 mL/min	As: ≈100 Cd: 99.7 Cu: 99.7 Ni:≈100 Zn: 99.7 Pb: 99.7 Fe: 99.8	Basha et al. (2011)
Synthetic Ni_2SO solution	Ni: ≈4000	Spouted bed reactor (recirculation mode)	Expanded platinized niobium mesh	Copper-coated polymer beads	Copper-coated polymer beads	pH 4 15 A	≈95	Grimshaw et al. (2011b)

Note: Condition including pH, temperature (°C), voltage, (V) or current density, mA/cm^2, DSA: Dimensionally stable anode, NA: Not applicable

Meanwhile, Martins et al. (2012) obtained a high space-time yield (86 $kg \cdot m^{-3}hr^{-1}$) of copper removal with low energy consumption (5 kWh/kg) using a spouted bed electrode whose the cathode was comprised of 1.0 mm copper particles. Other than spouted, the particles are commonly designed to be placed in the cell as being packed or fluidized. Table 2.4 compares the advantages and disadvantages of packed and fluidized bed reactors. Additionally, it has been proven that in a small-scale laboratory setup, a 3D system works better than a 2D system in terms of current efficiency and energy consumption (Chellammal et al., 2010) On the contrary, a comparison of the identical geometrical areas of a 2D and 3D stainless steel cathode for the recovery of a precious metal (palladium) indicated no significant difference in their current efficiency except that a faster electrodeposition time was achieved by using the 3D electrode (Terrazas-Rodriguez et al., 2011). The important findings of studies comparing 2D and 3D reactors by Chellammal et al. (2010) and Terrazas-Rodriguez et al. (2011) are listed in Table 2.5. However, the information about the space-time yield, for which the effects of the surface area might be further justified, has not been provided by the authors.

Table 2.4: Studies on fluidized and packed bed reactors for removal and recovery of heavy metals, their advantages, and disadvantages.

Types of 3D reactor	Advantages	Disadvantages	References
Fluidized bed	Particle motions prevent the particle agglomeration	Weak charge transfer in the bed	Segundo et al. (2012)
		Non-uniform potential distribution	Tonini et al. (2013)
Packed bed	Easy charge transfer in the bed	Packed particles form particle agglomeration	Almeida et al. (2008)
		May have flow channelling	Britto-Costa and Ruotolo (2014)

The 3D electrode is more favourable than the 2D in a system where both of the reactant and the product are soluble due to its high specific surface area (Koene & Janssen, 2001). However, in many cases, the product will be deposited on the electrode surface and reduce the effective surface area. Subsequently, the 3D electrode will behave essentially like a 2D electrode, where the entire effective surface will be covered by metal deposits (Reade et al., 2004b). During operating hours, even the moving 3D electrodes tend to be less suitable for metal ion removal (Koene & Janssen, 2001) due to the blockage of the active surface area of the porous electrodes. Nevertheless, the number of studies on 3D electrodes continues to grow. For instance, electrochemical cells with reticulated vitreous carbon (RVC), a micro porous glassy carbon material, is well-known for offering a highly efficient and low-cost electrochemical process (Friedrich et al., 2004) for the removal of copper (Britto-Costa & Ruotolo, 2013), lead (Ramalan et al., 2012), cadmium, (Reade et al., 2004a) zinc (Bertazzoli et al., 1997), silver (de Radigues et al., 2010) and nickel (Dell'Era et al., 2014) ions. The electrochemical cell configuration varies in a static or dynamic flow-by (the electrolyte and current flow is perpendicular) or flow-through (the electrolyte and current flow is parallel) mode. In considering product blockage in the porous electrode, the nature of the deposited metal and the frequency of metal removal from the reactor should be clearly addressed in designing a reactor, whether it is a 2D or 3D reactor (Walsh & Reade, 1994). Such important criteria are very crucial for upscaling purposes. However, recent studies have not treated the characteristics of the metal deposits in much detail. Evaluating the lifecycle or lifespan of the electrode, which may reduce its active site after a certain period of operation, also requires critical attention. Therefore, in parallel with the aim of increasing the mass transfer rate for the higher removal of heavy metals, it is beneficial to produce a low adherence of metal deposits on the 2D or 3D cathode so that the metal deposit can be stripped or separated by mechanical means. Elsewhere, it is suggested that 2D electrode is used to recover the metal ions from

concentrated solution for the purpose of metal reclamation, followed by a 3D electrode for reducing further the remaining metal up to allowable limit prior to discharge (Tatapudi & Fenton, 1995).

Table 2.5: Performance comparison of 2D and 3D reactors.

Pollutant	System	Metal recovery, %	Current efficiency %	Energy consumption, kWh/kg	References
Copper	2D	97.5	12.0	11.23	Chellammal et al. (2010)
	3D	99.5	56.8	2.37	
Palladium	2D	98	27	1.76*	Terrazas-Rodriguez et al. (2011)
	3D	99	24	2.86*	

*kWh/m^3

2.2.1.2 Operation mode: batch and continuous

The electrodeposition process can be conducted via batch or continuous mode. The suitability of the operation mode is mainly according to the characteristics of the wastewater and the purpose of the application. The batch recycle mode using a continuous stirred tank reactor (CSTR) has received more attention from many researchers compared to the continuous mode, as listed in Table 2.2 and Table 2.3. In the batch recycle mode, the wastewater is subjected to a continuous flow of more than a single pass through the electrolyser. The batch mode is preferable for a feasibility study of the electrode and cell performance under controlled experimental conditions. The recirculation of the electrolyte is introduced to homogenise the solution and is claimed to be more efficient than using the rotating cylindrical electrode (RCE) to improve mass transfer (Su et al., 2009). In small scale industries, electrochemical processes that operate under batch recirculation are more suitable, so that maximum recovery of valuable metals can be successfully removed or achieved at reasonable energy consumption without compromising the treatment time. Other than the CSTR type of reactor, several continuous electrodeposition processes utilize the flow-through (Almeida et al., 2008;

Bertazzoli et al., 1997; Issabayeva et al., 2006; Widner et al., 1998) or flow-by configuration (de Radigues et al., 2010; Dutra et al., 2000; Terrazas-Rodriguez et al., 2011). The continuous operation mode is suggested to increase the low kinetic rate of the electrodeposition process of static RCE (Arredondo et al., 2014). However, only a limited number of works have been reported using the continuous mode. For instance, Issabayeva et al. (2006) and Almeida et al. (2008) studied the performance of a continuous flow-through electrochemical cell for the electrodeposition of lead using a single pass of synthetic metal solution at a concentration of 50 ppm. Due to the low removal and recovery of metal ions, the single-pass operation has not received much attention. Thus, limited information is available in the literature, which might be useful for dealing with a large volume of water or wastewater. With an appropriate design of a single-pass mode electrochemical cell, a cascade identical reactor may be economical for use in large scale applications.

2.2.2 Electrode material

The cathode in the electrodeposition process is made of a conductive material such as metal (e.g., copper, aluminium, platinum), carbonaceous material (e.g., graphite, carbon nanotube), metal oxide or stainless steel, as listed in Table 2.2 and Table 2.3. The emergence of nanotechnology has led to several modifications being made to the electrode to improve the performance of the electrodeposition process. For instance, Liu and co-workers (Liu et al., 2013a; Liu et al., 2013b; Liu et al., 2011) carried out an extensive study of a stainless-steel electrode coated with a single layer of nanotubes for the removal of nickel, chromium and lead. However, the controlled laboratory conditions needed to be scaled up further to verify their feasibility, particularly when dealing with real wastewater treatment. On the other hand, microporous materials, such as reticulated vitreous carbon (RVC), are recognised as being able to enhance the electrodeposition of metals in a dilute stream (Agarwal et al., 1984) due to the high specific surface area. RVC

has been employed as an RCE and parallel plate electrode for the cathodic electrodeposition of heavy metals in a number of works (Britto-Costa & Ruotolo, 2011; Dell'Era et al., 2014; Ramalan et al., 2012; Reade et al., 2004a; Reade et al., 2004b). RCE provides a high mass transfer rate and a uniform current distribution (Almazan-Ruiz et al., 2012). Whenever specific ion selectivity becomes a concern, the choice of the electrode material must focus on the high activation energy for the undesired reactions. If the side reaction (e.g., hydrogen evolution) is to be reduced, the cathode should have a high over-potential hydrogen evolution. On the other hand, the anode is chosen from insoluble material such as stainless steel, graphite, platinum, or metal oxide (e.g., dimensionally-stable anode, DSA). With emerging efforts to explore superior materials for the fabrication of electrodes, the focus should be on finding cheap and abundantly available sources of electrode materials.

Only a few studies have looked into the electrochemical removal of mercury from wastewater. As a result, the number of electrodes that have been investigated is limited. Recently, the electrode, particularly cathode material that has been studied for the electrochemical removal of Hg were titanium plate (Du et al., 2022), nanostructured polymer (Candeago et al., 2020) and platinum film (Tunsu & Wickman, 2018). All these electrodes are considered to have a 2D electrochemical cell configuration. Employing 2D metal material such as titanium and platinum provide the advantage of having a stable electrode without additional electrode modification or preparation. However, the selectivity of the metal deposit is not becoming the main goal and it is expected that the electrodeposition of metal ion (as the pollutant) will provide an acceptable result. Unlike the work by Candeago et al. (2020), they designed a nanostructured poly(3hexylthiophene-2,5-diyl)-carbon nanotube composite electrode, coated on titanium as the cathode for reversible Hg deposition. They reported that the functional electrode provides 12-fold higher release kinetics compared to nonfunctionalized electrodes.

Hence, the effort to explore superior electrodes for Hg removal is necessary to improve the electrochemical process in terms of having a high reaction rate, low energy consumption and high selectivity.

2.2.3 Types of wastewaters

It has been well noted that most of the studies on electrodeposition have dealt with the removal efficiency of a particular cell configuration towards a single metal ion under controlled laboratory conditions. Of interest is synthetic metal salt that is prepared to represent industrial wastewater, for which recommendations are often made for the treatment of real wastewater. Only a limited number of studies have been carried out using real industrial wastewater, such as the effluent of copper-phthalocyanine dye manufacturing plants (Chellammal et al., 2010), silver-plating wastewater (Su et al., 2009) and copper-smelting wastewater (Basha et al., 2008; Basha et al., 2011). Some other types of wastewaters that have received less attention by the electrodeposition process are photographic production, printed circuit board production and the batteries manufacturing industry.

Industrial wastewater often contains several cations and anions with different concentrations. As a result, the performance of the developed electrode or the proposed cell configuration towards a metal ion in a complex multi-component aqueous medium is highly compromised due to competition between the ions that are present. For instance, a rinsing bath in Ni-Cu electroplating comprises not only Ni and Cu ions but also contains high total dissolved solids (TDS) from carried over precipitates in the plating bath. The effluents might need to be filtered to remove suspended solids prior to the electrodeposition process in order for the process to be more effective. Plating baths are also prepared from a specific ratio of ingredients such as additives for brightening and methanesulfonic acid for the electrolyte.

Furthermore, the selectivity of the metal ions in a complex matrix wastewater stream is a crucial aspect to be considered for the successful application of electrodeposition in industrial effluents. For example, gold plating generates a large amount of aqueous cyanide wastewater containing several metal ions. The main component is gold (100 mg/L) and copper (600 mg/L), with minor components of silver, nickel and zinc (Spitzer & Bertazzoli, 2004). A suitable working potential range and the material for the electrode in the electrodeposition process become crucial in order to improve the selectivity of precious metal recovery compared to other metal ions. Elsewhere, Doulakas et al. (2000) also claimed that high purity of metal by selective electrodeposition could be achieved by manipulating the overpotential value during the process. To date, the interaction of other ion constituents with heavy metals and their selectivity have yet to be investigated in significant depth, except for a few works by Doulakas et al. (2000) and Spitzer and Bertazzoli (2004).

Although it is tempting to evaluate the electrochemical removal of metals from a real wastewater, it is a challenge to understand the characteristics of a real wastewater prior to the study of the performance of a new developed electrode. The wastewater could consist of several species and may varies in its contents from one batch to another. Hence, many works that focus on the preparing, developing, or innovating new electrodes for electrochemical removal of metals have designed the experimental work under a controlled laboratory condition. Therefore, the synthesis of wastewater contains single metal has been employed, for instance, the work by Du et al. (2022); Li et al. (2015); Shen et al. (2021).

2.2.4 Electrode reaction and mass transport

The electrochemical reaction process that occurred at the electrode is ruled by charge transfer (also known as electron transfer) and mass transfer steps. Brownson and Banks

(2014) described a general electrochemical reaction pathway using Figure 2.3. It illustrates that the electrode current is dependent of mass transport, and is followed by other processes, namely chemical reactions, adsorption/desorption, and the heterogeneous rate constant for the electron transfer reaction. Elsewhere, Seeber et al. (2016) highlighted a similar pathway but adding in structural reorganization as another accompanying step. Comparing between the mass transport and charge transfer, the later step has received substantial consideration in electrochemical reaction studies.

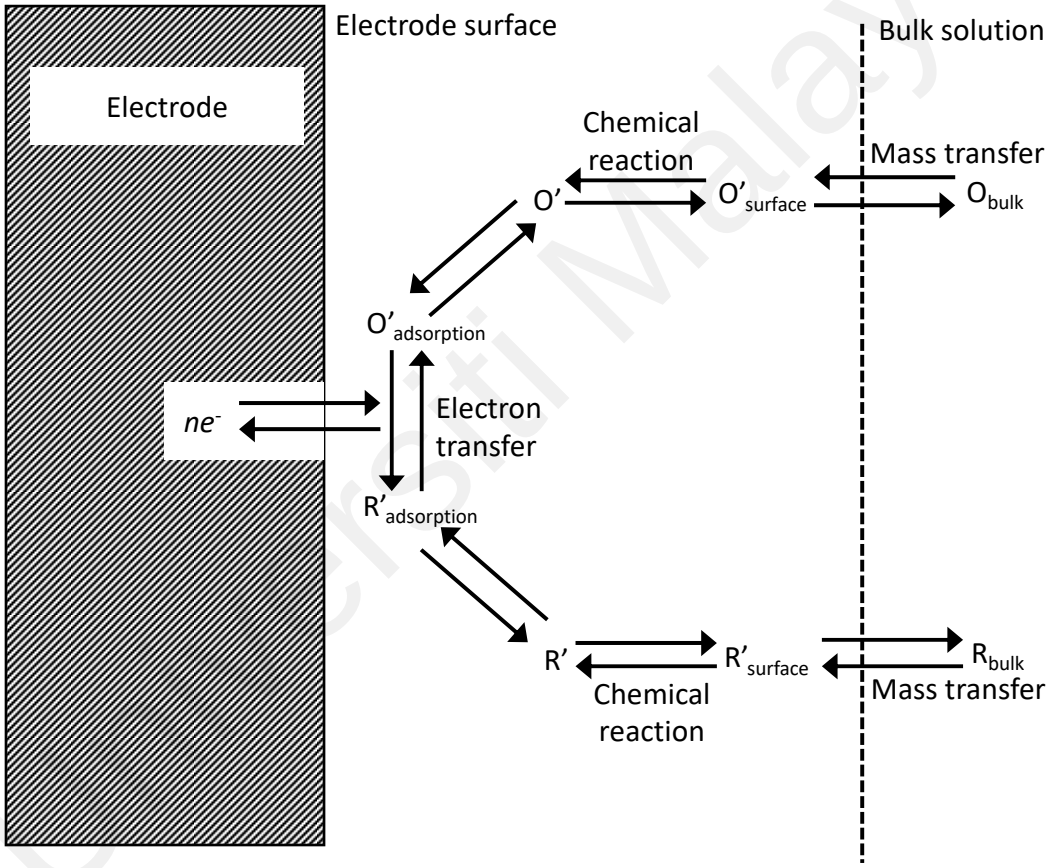

Figure 2.3: General electrochemical reaction pathway. Redraw from Brownson and Banks (2014).

Charge transfer is governed by Erdey-Grúz Volmer, which is also known as the Butler-Volmer equation (Equation 2.5). This mathematical expression describes the electrical current at the electrode as a function of electrode potential.

$$j(t) = j_o(t)\left\{\exp\left[\frac{\alpha F(E - E^o)}{RT}\right] - \exp\left[\frac{-(1-\alpha)F(E - E^o)}{RT}\right]\right\} \quad \text{Equation 2.5}$$

Where j(t) is the electrode current density (Am^{-2}), j_o is the exchange current density (Am^{-2}), E is the electrode potential (V), E^o is the equilibrium potential (V), T is the absolute temperature (K), z is the number of electrons involved in the reaction, α is the charge transfer coefficient, R is the universal gas constant, and F is the Faraday constant. Several studies reported using this expression to describe the electrochemical process for heavy metal removal and recovery. For instance, Low et al. (2014) deduced a mathematical expression from the Butler-Volmer equation. They demonstrated a log-scale plot of j_o versus chloride ion concentration to determine the stoichiometry number of chloride ions involved in the electrodeposition of copper under the influence of different chloride ion concentrations. Using this approach, they evidenced a transition from one step (two electrons) to a two-step (one electron) electron transfer reaction involved in the electrodeposition of copper from Cu^{2+}, as the concentration of chloride ions was increased. Moreover, the Butler-Volmer equation is frequently employed in electrochemical modelling and simulation studies. For example, Cheng et al. (2005) developed a one-dimensional model using the Butler-Volmer equation to describe the kinetic electrodeposition of Pb and PbO_2, as well as the oxygen reaction for removal of Pb^{2+} from industrial wastewater by monopolar and bipolar flow-through reactors. Similarly, Rivero et al. (2015) and Sarkar and Aquino (2011) also incorporated the Butler-Volmer kinetic equation with several other mass transfer equations in their theoretical modelling analysis and simulation of an electrochemical process. In addition, Wang et al. (2012) claimed that the value of the standard heterogeneous rate constant, k^o and charger transfer, α was well predicted by Butler-Volmer, compared to the Marcus-Hush model for the reduction of europium ion.

Mass transfer or the movement of the active species in the bulk solution to the surface of the electrode is governed by three possible processes. These are diffusion, migration and convection. The mechanism of mass transport is given by the Nernst-Plank equation (Equation 2.6), written for a one-dimensional mass transfer along the x-axis.

$$J(x) = -D\frac{\partial C(x)}{\partial x} - \frac{zF}{RT}DC\frac{\partial \emptyset(x)}{\partial x} + Cv(x) \qquad \text{Equation 2.6}$$

Where J(x) is the molar flux density (mol s^{-1} cm^{-2}) at a distance x from the surface of the electrode, D is the diffusion coefficient (cm^2 s^{-1}), $\partial C(x)/\partial x$ is the concentration gradient, $\partial \emptyset(x)/\partial x$ is the potential gradient, z is the charge, C is the concentration (mol cm^{-3}) and v(x) is the velocity (cm/s) with which a volume element in solution moves along the axis. From the right-hand side, the three terms represent the contribution of convection, migration, and diffusion, respectively, to the flux of the active species, J(x). Diffusion is always considered due to the undeniable presence of the concentration gradient of the active species between the region near to the electrode and the solution bulk. In principle, the active species is transported under the influence of chemical potential. The migration process is described by the movement of the charged active species under the influence of an electric field (inner potential gradient). The charge transfer certainly alters the charge balance of the chemical species close to the electrode. However, several mass transfers studies, as well as those who employed the voltammetry technique in the electrode characterization, simplified their electrochemical analysis by neglecting the effect of migration, as excess supporting electrolyte is introduced into the solution to compensate for the unbalance of the electric charges.

Meanwhile, the solution resistance will be lowered by the presence of the supporting electrolyte and hence increase conductivity. Another means of mass transport process is convection, which refers to the movement of active species through the bulk fluid motion. This can take place in either natural or forced convection. Natural convection can be

generated by density gradient while solution stirring, electrode movement and continuous recirculation are called forced convection. However, in the most widely used diffusion-controlled potential techniques, such as linear sweep voltammetry, cyclic voltammetry and chronoamperometry, mass transport governed by convection is carefully prevented. For this reason, voltammetry or chronoamperometry studies are carried out in a quiescent solution with a supporting electrolyte. Therefore, among the mass transport mechanisms, diffusion becomes the main contribution of the mass transfer process, particularly in an electrode characterization study by voltammetry technique.

2.3 Electrosorption

It is crucial to differentiate between the electrodeposition and electrosorption process, although both steps may take place simultaneously in the attempt to remove and recover metal ions from the wastewater stream. Several researchers pronounced their system only to involve electrodeposition, and this is essentially true when it only involves a planar electrode (2-dimensional). On the other hand, electrosorption is expected when the porous electrode (3-dimensional) is employed, whereby the proposed electrochemical system is designed to eliminate the reduction of metal ions to form a metal element.

Electrosorption is a combination of electrochemical and adsorption/desorption processes. This process is usually used to illustrate the mechanism that takes place in capacitive deionization (CDI) technology. CDI technology is also referred to as the electrochemical demineralization or electrosorption of salt ions. During the electrosorption process, ionic contaminants in the aqueous solution move towards the oppositely charged electrode under the imposed electrical field. The ions are temporarily stored via the formation of an electrical double-layer inside the porous electrodes. Hence, high-quality purified water is delivered as a product. Once the electric field is removed or reversed, the ionic contaminants move back to the bulk solution, and the electrode is

regenerated by desorption (Hu et al., 2015). The working principle is similar to that of an electrochemical capacitor. It is well recognized that the growth of CDI technology is rapid and is mainly focused on the production of portable water from seawater or brackish water. The performance of CDI systems is most often accomplished based on experiments using sodium chloride, typically with a concentration of between 5-50 mM (Suss et al., 2015). However, recently this method has been explored for the removal of heavy metals such as copper (Hu et al., 2015; Huang et al., 2014) and lead (Li et al., 2015). The conventional electrodes for electrosorption are carbonaceous material such as activated carbon, carbon nanotubes, carbon nanofibers and carbon aerogels (Li et al., 2015). They are renowned for their good electrical conductivity and high specific surface area properties.

A review of the development of electrodes employed in CDI technology for desalination was discussed in detail by Porada et al. (2013) and Liu et al. (2015). On the other hand, Suss et al. (2015) emphasised that whenever a metal reduction takes place to form a metal deposit on the electrode, such a process should not be classified as electrosorption but appropriately metal electrodeposition involving electron transfer. Further, the presence of metal deposits on the surface of the electrode in an electrosorption process will likely reduce the surface area of the electrode due to pore blockage. For this reason, an appropriate applied voltage is required to suppress metal electrodeposition (Huang & He, 2013; Huang et al., 2014). Additionally, Huang and He (2013) claimed that their applied operating condition successfully eliminated the metal electrodeposition by the evidence of capacitor-like characteristics obtained from the cyclic voltammetry analysis. Moreover, only a low atomic percentage of copper deposits (0.17%) was observed on the electrode under the x-ray photoelectron spectroscopy (XPS) analysis after the electrosorption has been taken placed. Similarly, Huang et al. (2016) reported

that a dotted crystal metal deposit was observed on the surface of the electrode after the electrode has undergone an electrosorption process.

Although extensive research has been reported on desalination, whereby sodium chloride has commonly become a constituent of interest, there a limited number of works that adequately analyses the performance of CDI systems for heavy metal removal. It is strongly suggested that the key criteria, which are comparable to the current established practice in the desalination of brackish water, be applied when analysing the performance of CDI systems for the removal of heavy metals. Such key metrics include the adsorption capacity, average adsorption rate, charge efficiency and current efficiency (Suss et al., 2015). While exploring CDI technology for the removal of heavy metals, some major challenges for the development of an economical electrochemical system need to be considered. The system may have unwanted reactions at the electrode, which will lead to high energy consumption, inadequate electrical conductivity or limitation of electrode materials, such as high manufacturing costs, poor wettability or poor mechanical stability (Liu et al., 2015). Only limited studies have been carried out to adequately address the limitations of the electrosorption process and the electrode design for the purpose of heavy metal removal. For example, Li et al. (2015) introduced a large specific surface area of natural cationic clay mineral in preparing a conducting polymer composite electrode to improve the removal of Pb(II) via physisorption. However, the clay did not contribute considerably to the overall electrosorption performance, in which the chemisorption and electrostatic interaction between Pb(II) and the electrode prevailed.

Classical adsorption isotherms, namely the Langmuir and Freundlich adsorption isotherms, have been frequently employed to fit the data of electrosorption equilibrium (Li et al., 2015). However, these theories do not fully explain the real phenomenon of electrosorption, as they do not take into account the presence of the applied potential. The

charged ions in electrosorption have very different underpinning physical characteristics compared to the uncharged ions in the adsorption process. Electrosorption is predominantly based on the storage of ions in the electric double-layer (EDL) by an electrostatic attraction under the external electrical charge supplied. This electrostatic charge can be controlled by adding to or subtracting from the electrical charge in the electrode. Obviously, a classical adsorption isotherm is unable to make any useful prediction about the electrosorption or charge behaviour as a function of the cell voltage and ion composition. Yang et al. (2001) explained that the total electrosorption capacity of an electrode is dominantly affected by two factors. The first factor is the EDL capacity due to the electrostatic attraction force between the ions and the electrode. The EDL capacity is predominantly affected by the ion concentration in the solution and the applied voltage on the electrodes. The second factor contributing to the total electrosorption capacity is the pseudocapacity initiated by Faradic reactions. The pseudocapacity depends on the chemical characteristics of the solute and the functional groups at the electrode surface (Liu et al., 2011).

2.4 Development of porous carbon-based electrodes

Most of the studies in electrochemical technologies for the removal of heavy metals have been concentrating on investigating the effects of process parameters and developing new electrode materials. Several core characteristics and explanations have been considered in the process to develop efficient and economical electrodes. In general, the selection of electrode material is based on the functionality and the economic value of the material. For example, carbon fibre was coated with MnO_2 for copper electrosorption, whereby MnO_2 is reported to be an effective adsorbent for many metal ions as it has a good and high specific capacitance, good cycle stability, has a low cost and is abundantly available (Hu et al., 2015). In addition, a composite electrode prepared from conductive polymers (polyaniline) and natural clay mineral (attapulgite) was evaluated for the

electrosorption of Pb(II) (Li et al., 2015). As an individual component, polyaniline has been proven to play an important role in the removal of heavy metals by chelation, while attapulgite is a natural cationic clay mineral with a large specific surface area. Porous activated carbon has also gotten attention to be employed as the raw material of electrodes for electrochemical removal of heavy metals from water and wastewater (Liu & Wang, 2020; Macias-Garcia et al., 2017; Rajumon et al., 2020). The porosity characteristics of activated carbon provide a high surface area per unit volume (or mass) of the electrode and high rates of electron transfer reactions (Punckt et al., 2013). The fabrication of electrodes for the removal and recovery of heavy metals varies, and several well-established methods will be discussed in the following sections.

2.4.1 Polymeric binders

A conventional activated carbon electrode often uses polymeric binders, such as polyvinylidene fluoride (PVDF) (Duan et al., 2015; Wang et al., 2013) or polytetrafluoroethylene (PTFE) (Ajeel et al., 2015b; Lee et al., 2011), to hold the carbon particles together. Even though this method is being widely applied for the preparation of the electrode for desalination (Choi & Choi, 2010; Wang et al., 2013), recent works have also adapted such a technique for the removal of heavy metals (Huang & He, 2013; Huang et al., 2014). However, the polymeric binders can obstruct fractions of the activated carbon surface and increase the electrical transfer resistance (Liu et al., 2011). Although this method is widely employed because of its simplicity, the mixture is usually blended with carbon black, which acts as a conductive additive (Oda & Nakagawa, 2003; Wang et al., 2013). Mesoporous conductive carbon black is added to activated carbon electrodes to improve the electrical conductivity and enhance the electrode capacitance (Nadakatti et al., 2011).

Dong et al. (2012b) also claimed that when the ratio of PTFE to activated carbon was less than a certain amount, the paste cannot be firmly bound. In their electrode preparation study, the activated carbon/PTFE ratio was varied between 3 and 11. This ratio is equivalent to 8% to 25% of PTFE in each electrode. They reported that if less than 8% of PTFE was used, the composite could not be tightly rolled on the matrix (stainless steel) due to the lack of binder. Ultimately, they found that 14% PTFE was the best amount because it gave the highest power densities for the fuel cell. Elsewhere, Hou et al. (2012) claimed that 10% polyvinylidene fluoride (PVDF) was the optimum because it gave the highest Brunauer-Emmett-Teller (BET) surface area of nano porous carbon sheet electrode for desalination. Increasing the amount of binder has reduced the specific surface area of the electrode. The mechanical strength of the electrode with 10% PVDF was also claimed to be adequate for the desalination process. However, the mixture of powder activated carbon, PVDF and N,N-dimethylacetamide (DMAc) as the solvent required a long stirring duration (6 hours) to ensure homogeneity despite of a little mass of electrode was produced (ca. 1.5 g).

Furthermore, Nadakatti et al. (2011) claimed that by introducing an optimum electrode composition consisting of activated carbon, a polymeric binder and carbon black, the preparation of the electrode could be carried out under an aqueous phase without the introduction of any organic solvent. Such a preparation simplifies the complexity of the electrode manufacturing process. On the other hand, Hou et al. (2012) immersed the polymeric binder-bonded carbon sheet electrode in a KOH solution to improve the electrosorption properties of the electrode. Table 2.6 lists several studies on the preparation of electrodes using polymeric binders.

Ionic liquids have been exploited in various electrochemical applications such as electrolytes for fuel cells and batteries, a medium for electroplating baths and a solvent

for semiconductor electrodeposition (Armand et al., 2009). An ionic liquid-modified electrode has been patented for the construction of secondary lithium batteries (Yong et al., 2008). Additionally, it has been used extensively to improve electrodes for sensors (Bagheri et al., 2015; Bijad et al., 2013; Elyasi et al., 2013; Ismaiel et al., 2014a, 2014b; Jamali et al., 2014; Khani et al., 2010; Maleki et al., 2006; Najafi et al., 2014). Figure 2.4 illustrates the publications and citation trends related to 'ionic liquid* and electrode' as the search topics from 2010 until 2021, as reported in the database of the Web of Science™ Core Collection by Clarivate. From 2010 until 2014, a gradual increase in the number of published articles and an exponential rise in the number of citations have proven the tremendous works that have been carried out in exploring ionic liquids for the development of electrochemical technology via electrode modifications. However, the number of publications slightly decreased in 2015 (about 4%). The number of publications increased in the following year (2016) and reached a plateau in 2018 and 2019. A decreased trend was observed in 2020 and 2021. Therefore, it is an urge to put more effort into exploring the benefit of ionic liquid for electrode improvement in the near future. Several studies have reported using ionic liquids as binders for carbon paste electrodes in the development of sensors (Bagheri et al., 2015; Khani et al., 2010; Maleki et al., 2006) and supercapacitors (Wei et al., 2013). They are attractive for electrode modification due to their hydrophobicity, high viscosity, ionic conductivity, very low volatility and biocompatibility properties (Opallo & Lesniewski, 2011). However, a limited number of works have been carried out to explore ionic liquid-based electrodes to remove and recover heavy metal.

Table 2.6: Several studies on electrode preparation using polymeric binders.

Electrode precursor	Binder (Content)	Percentage of binder (wt%)	Conductive agent	Solvent	Current collector	References
Activated carbon	PVDF	10	-	N-methyl-2-pyrrolidone (NMP)	Titanium plate	(Shen et al., 2021)
Activated carbon	PVDF	10	Carbon black	NMP	Graphite foil	Tran et al. (2020)
Activated carbon	PTFE	20	-	Ethanol	Graphite sheet	Duan et al. (2015)
Activated carbon (Filtrasorb 400)	PVDF	9-18	-	Di-methylacetamide (DMAc)	Titanium plate	Huang et al. (2014)
Ordered mesoporous carbon	PVDF	10	Carbon black	-	Titanium plate	Huang and He (2013)
Activated carbon	PVDF	10	Carbon black	-	Graphite sheet	Wang et al. (2013)
Activated carbon (Filtrasorb 400)	PVDF	10-40	-	DMAc	-	Hou et al. (2012)
Nano diamond	PTFE	≈8	Carbon black	1,3-propanediol	Graphite sheet	Lee et al. (2011)
Activated carbon	Polyethylene	20	Carbon black	Ultra pure water	Graphite sheet	Nadakatti et al. (2011)
Activated carbon (P-60)	PVDF	9-18	-	DMAc	Graphite sheet	Choi and Choi (2010)

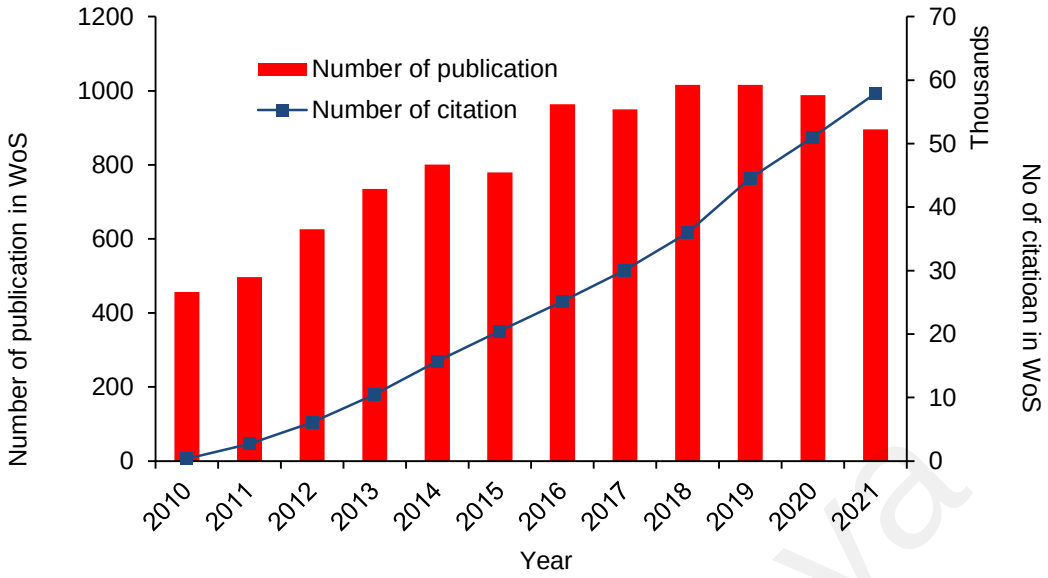

Figure 2.4: Publication and citation trend related to "ionic liquid*" and 'electrode' as the search topics from 2010 until 2021. Citation Report graphic is derived from Web of Science, Copyright THOMSON REUTERS ® 2022. All rights reserved.

A feasibility study on the use of ionic liquid-modified electrodes for the removal and recovery of heavy metals is probably a promising work to be explored in the near future. Functionalized ionic liquid appears to be a broad and promising field to be studied. Besides, ionic liquid has been reported as a selective extractant and ion carrier of heavy metal ions from aqueous solutions (Pospiech & Kujawski, 2015). Task-specific ionic liquid (TSIL), which has been developed as a functionalised ionic liquid to extract specific pollutant, for instance, $Cu^{2+,}$ are considered to be promising to be impregnated with an electrode of high surface area. Further, an ionic liquid-impregnated electrode is expected to have a higher selectivity for electrodeposition of Cu^{2+} compared to other components of wastewater (e.g., chelating agent, other metal ions). This would be beneficial for copper recovery for recycling purpose.

Meanwhile, a proper study in evaluating the possibility of maintaining the effective electrochemical surface area of such electrode after the recovery or detach of metal deposit from the electrode surface is crucial to predict the electrode life spent and its reusability. This may be conducted via electrode regeneration and/or process optimization

studies. The main drawback of ionic liquid is claimed to be its high cost as it is generally synthesized on a small scale in the laboratory. However, by intensifying the present ionic liquid production steps on a large scale, the production cost, which is contributed mainly by the cost of the raw material and the process steps, is reported to be effectively reduced (Chen et al., 2014).

2.4.2 Electrophoretic deposition

In order to eliminate the limitations of polymeric binders in the fabrication of electrodes, several studies were carried out on the preparation of the carbon electrodes using electrophoretic deposition methods. For this kind of deposition, the particles of interest are dispersed or suspended in a liquid medium and deposited onto a conductive substrate under the application of an electric field. Organic liquid is preferable to water. For example, Liu et al. (2011) and Liu et al. (2013b) prepared an electrode by depositing colloidal suspended particles of carbon nanotubes in dimethylformamide liquid on a stainless steel net under the influence of electric fields. The electrode was fabricated without the addition of a polymeric binder. Further, the prepared electrode was employed for the removal of lead ions (Liu et al., 2013b) and the reduction of Cr(VI) to Cr(III) (Liu et al., 2011). Liu et al. (2013b) claimed that both electrodeposition and electrosorption took place during the removal of the lead ions. However, electrodeposition was predominant when the applied voltage was higher than 1.5 V (vs. the reference electrode). In addition, Hekmat et al. (2015) utilized an ionic liquid as the dispersing agent for the electrophoretic deposition of carbon nanotubes on a porous aluminium oxide template. They claimed that 1-methyl-3-octadecyleimidazolium bromide was an excellent dispersing agent for the dispersion of carbon nanotubes in an aqueous solution, which showed a homogenous dispersion after the suspension was kept for 10 months.

2.4.3 Chemical electrodeposition

On the other hand, Hu et al. (2015) developed MnO_2/carbon fibre composite electrodes for the electrosorption of copper ions. An aqueous precursor solution of $MnSO_4$ and H_2SO_4 was utilized as the electrolyte. MnO_2 was deposited onto the carbon fibre at a constant current (galvanostatic), where the carbon fibre, graphite and $Hg/HgCl_2$ were used as the working electrode, counter electrode and reference electrode, respectively. It was reported that the specific capacitance (387 F/g) of the prepared electrode was comparable with the literature, which presented an ideal pseudo capacitive behaviour.

2.5 Electrochemical properties of porous carbon electrode

The electrochemical properties of an electrode were commonly studied by cyclic voltammetry (CV), potentio electrochemical impedance spectroscopy (PEIS), chronoamperometry (CA) and chronocoulomb (CC).

2.5.1 Cyclic voltammetry (CV)

Cyclic voltammetry (CV) is a well-established electrochemical technique that measures and provides a unique profile of the current that develops in an electrochemical cell. Potential (*E*) is applied to an electrode in both forward and backward direction while the resulting current (*i*) is monitored over a period of time. The applied potential forces a change in the concentration of an electroactive species at the electrode surface by electrochemically reducing or oxidizing it. For instance, the oxidation/reduction of ferrocyanide/ferricyanide ($Fe(CN)_6^{4-}$/ $Fe(CN)_6^{3-}$), utilising several mM of potassium ferrocyanide and $K_4Fe(CN)_6$ as the electroactive species in a supporting electrolyte (e.g., KCl, KNO_3, NaCl) is commonly employed in electrochemical activity and reversibility studies of the reaction at the electrode using CV. Theoretically, the $Fe(CN)_6^{4-}$/ $Fe(CN)_6^{3-}$ couple exhibits a reversible electrode reaction which can be described by $Fe(CN)_6^{3-} + e^- \leftrightarrow Fe(CN)_6^{-4}$, in which the Fe(III) is reduced to Fe(II) without any complications of

preceding or post chemical reactions. An electrochemically reversible electrode reaction will produce a symmetrical anodic and cathodic current with a ratio close to unity, as shown by Figure 2.5(a). In this technique, the voltage is predetermined at a value in excess of that predicted by the Nernst equation, as shown by Equation 2.7. Additionally, for a reaction that is electrochemically reversible, the peak potential separation, ΔE_p (V), is having a relationship according to Equation 2.8:

$$E = E^0 - \frac{RT}{nF} ln \frac{[Fe(CN)_6^{4-}]}{[Fe(CN)_6^{3-}]} \quad \text{Equation 2.7}$$

$$\Delta E_p = \frac{2.303\ RT}{nF} = \frac{0.059}{n} \quad \text{Equation 2.8}$$

Where R is the universal gas constant, T is the temperature (298 K), n is the number of electrons transferred, F is Faraday's constant (96485 C/mol), and E^0 is the standard reduction potential.

The voltammogram provides information about the Faradaic reaction, which qualitatively and quantitatively measures the electrical current corresponding to electron transfer between the electrode and the active species, resulting in oxidation or reduction of the species. CV scan at various scan rate is also important to verify the reversibility of electrode reaction. Peak current is expected to linearly increase as a function of the square root of the scan rate for a reversible electron transfer. Such trend also suggests a diffusion-controlled process (Peterlevitz et al., 2016). Increasing values of ΔE_p as the scan rate increases indicates the presence of electrochemical irreversibility or quasi-reversible, as shown in Figure 2.5. Additionally, this value is useful to calculate the heterogeneous electron transfer rate constant, k_s, by using the Butler-Volmer equation.

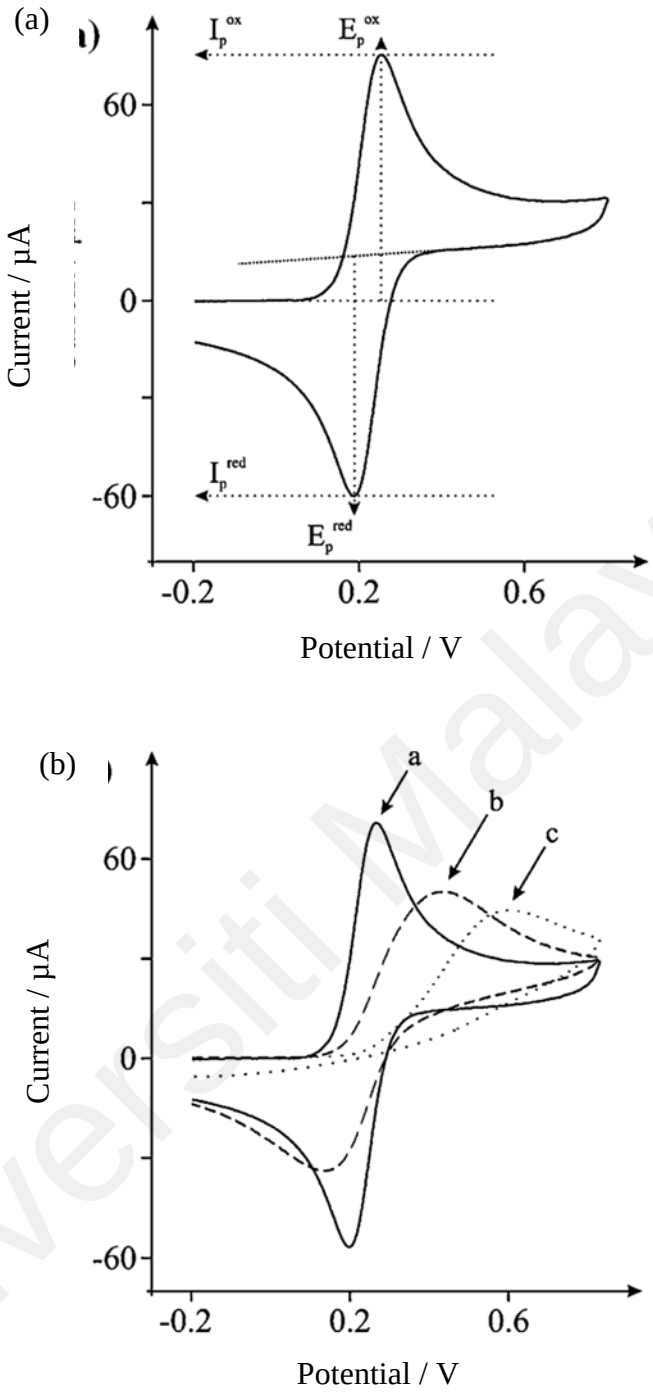

Figure 2.5: (a) Typical CV voltammogram depicting the peak position and peak height. (b) CV for a. reversible b. quasi-reversible and c. irreversible electron transfer (Brownson & Banks, 2014).

An electrochemically quasi-reversible process can be explained by the equivalent effect of both electron transfer and mass transfer rates in an electrochemical process. Nicholson method provides a relationship to estimate the standard heterogeneous electron transfer rate constant, k^o for a quasi-reversible process as shown by Equation 2.9, where Ψ is the kinetic parameter obtained from Nicholson (1965) and tabulated in Table 2.7. For simplification in determining the value of ψ, Lavagnini et al. (2004) suggest an empirical equation (Equation 2.10) to establish a relationship between ψ and ΔE_p. The constants (*a*, *b* and *c*) in Equation 2.10 can be deduced from the nonlinear regression fitting. The plot of ψ versus $v^{½}$ allows the kinetic parameter k^o to be determined from the slope.

$$\psi = k^o \left(\frac{\pi D n v F}{\mathrm{RT}}\right)^{-\frac{1}{2}} \qquad \text{Equation 2.9}$$

$$\psi = \frac{a + b(\Delta E_p)}{1 + c(\Delta E_p)} \qquad \text{Equation 2.10}$$

Table 2.7: Variation of ΔEp with ψ at 25°C. Reproduced from (Nicholson, 1965).

ψ	**ΔE_p x n (mV)**
20	61
7	63
6	64
5	65
4	66
3	68
2	72
1	84
0.75	92
0.50	105
0.35	121
0.25	141
0.10	212

It is crucial to verify that the redox that happened is principally due to active species under studies. For this reason, CV is always run firstly, using only supporting electrolyte

without active species and later with the active species, either using the species of interest or the standard redox probe such as ferricyanide/ferrocyanide [$Fe(CN)_6^{4-}/Fe(CN)_6^{3-}$] or ferrocene/ferricenium [$Fe(C_5H_5)_2/Fe(C_5H_5)_2^{+}$]. For example, the absence of distinctly formed peaks in Figure 2.6(a) and Figure 2.7(a) suggests that no electron transfer had been taken place on the surface of the electrode. On the other hand, numerous works related to electrode development for desalination employed CV analysis with NaCl as the active species, for which the Faradaic reaction is usually has been proven to be non-existent. Their works nonetheless provide valuable information as a porous electrode are employed. For instance, the work by Dehkhoda et al. (2014) who studied the effectiveness of activated bio-char for electrical double layer (EDL) application. They claimed that the cyclic voltammogram obtained at slower sweep rates (<10 mVs^{-1}) using 0.1 $mol \cdot L^{-1}$ NaCl in 0.1 $mol \cdot L^{-1}$ NaOH electrolyte have a shape that is closer to the ideal EDL capacitive response (i.e., more rectangular-like shape without any peak). Similar finding was reported by Tran et al. (2020) for which the CV test was carried out for activated carbon as the working electrode at sweep rate of 1 mV/s and applied potential from −0.7 to +0.5 V.

With the presence of active species (i.e., ferricyanide), the CV is expected to produce at least a peak, as shown by Figure 2.6(b), Figure 2.7(b) and Figure 2.7(c). It was reported that the working potential window of carbon nanospheres electrode in 0.1 M potassium nitrate is about 1 V. However, it is clearly seen in Figure 2.7(a) that a potential window of 0.75 is more acceptable as the potential window is determined corresponding to the range of onset potential of hydrogen (at -0.25 V) and oxygen evolution (at 0.5 V). On the other hand, there is no convincing information about the working potential window of the activated carbon electrodes in Figure 2.6(a) as the CV analysis was carried out at a limited potential range. Additionally, a comprehensive study on the selective recovery of copper and silver from a cyanide leaching solution has been reliably described by CV studies by

Reyes Cruz et al. (2002). They observed that the copper reduction took place at more negative potential than silver. Hence, in the presence of high Cu(I) concentrations, a well-defined potential range for Ag(I) deposition was identified.

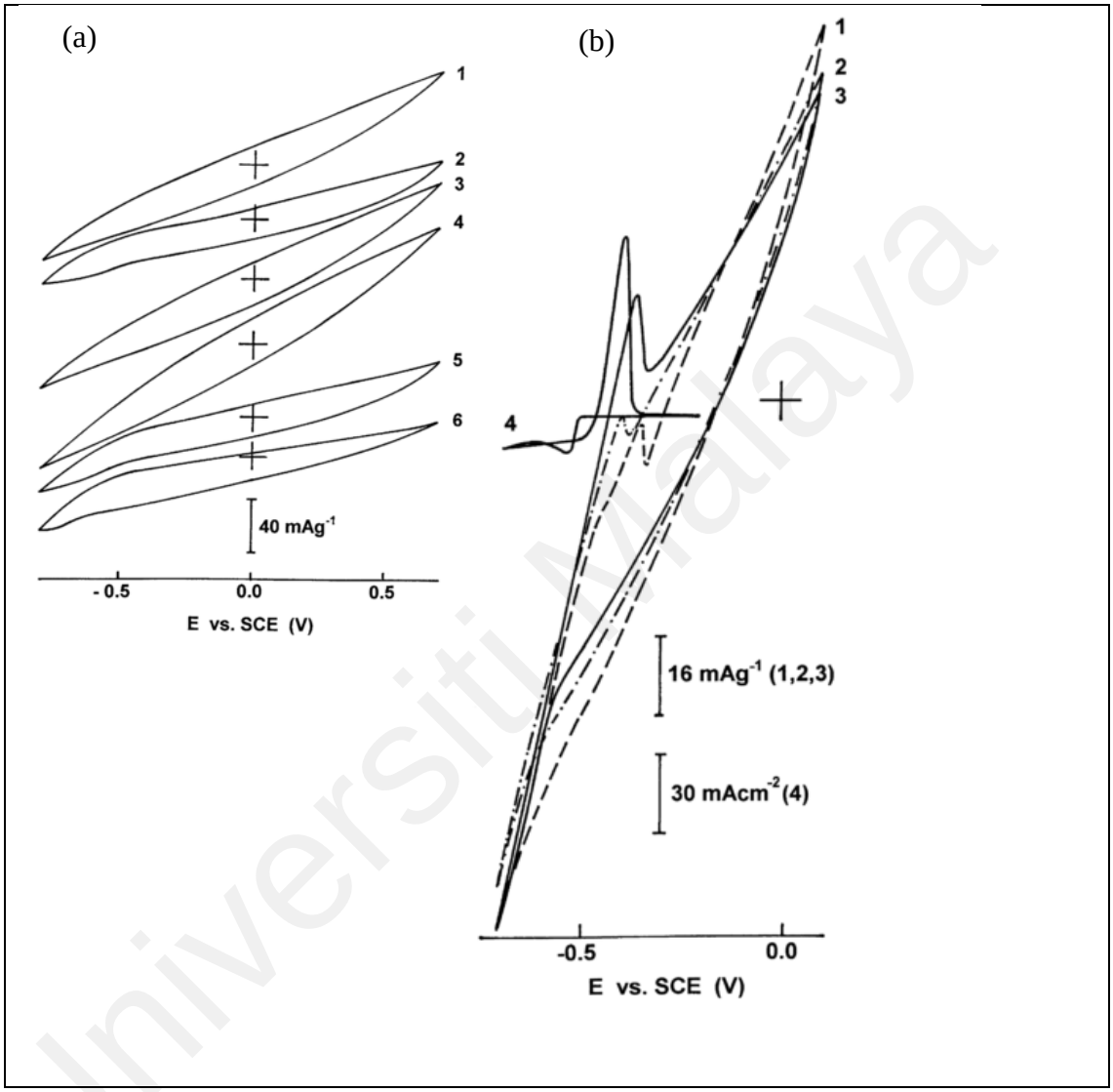

Figure 2.6: Cyclic voltammograms of (a) six different activated carbon electrode (b) activated carbon with pre-adsorbed lead ions (curve 1-3) and glassy carbon electrode (curve 4), recorded in a solution of lead ions in 0.1 M ($NaNO_3$ + HNO_3) at a scan rate of 3 mV/s (Swiatkowski et al., 2004).

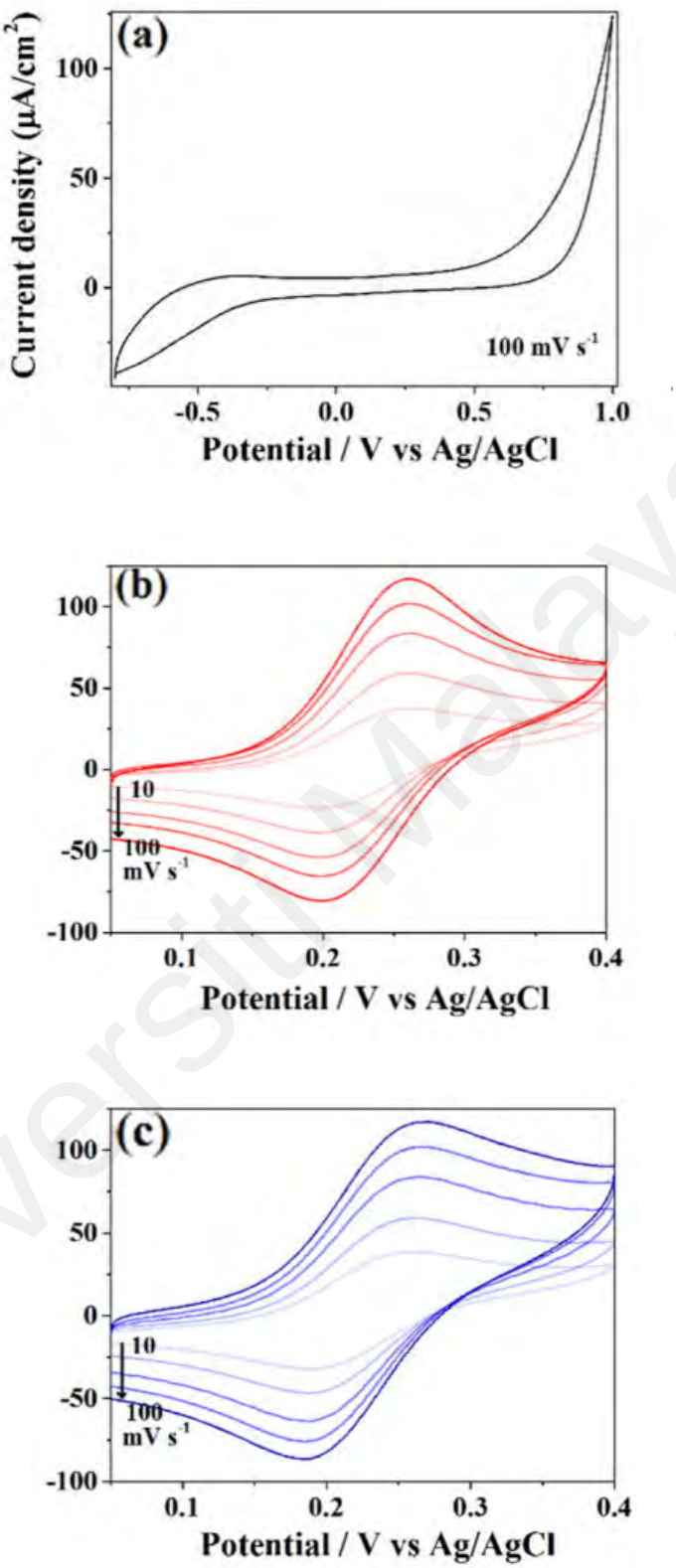

Figure 2.7: Cyclic voltammograms of carbon nanospheres electrode in (a) 0.1 M potassium nitrate at scan rate of 100 mV/s, (b) 0.5 mM ferrocene-methanol in 0.1 M potassium nitrate, and (c) 0.5 mM ferrocyanide in 0.1 M potassium nitrate at different scan rate (10, 25, 50, 75 and 100 mV/s) (Peterlevitz et al., 2016).

The presence of double-layer capacitance could also be discussed from a set of CV studies conducted by Choi and Choi (2010) and Farma et al. (2013). Such studies disclosed the ability of electrode application for the electrosorption of metal ions. However, there is little common understanding of the electrode reaction, particularly of porous electrodes employed for the removal and recovery of heavy metals from water and wastewater. It is crucial to identify the chemical process that taking place in the electrochemical cell, whether it is an electrosorption or an electrodeposition process. Such concern was studied and highlighted by Huang et al. (2014). They claimed that redox of copper ions on activated carbon was observed when the applied potential was widened to a higher range (-1.4 to 1.4 V) while, at the lower range of applied potential (e.g., -0.8 to 0.8 V), the electrochemical mechanism was governed by pure electrostatic interaction in terms of electrical double layer formation as shown by Figure 2.8. If one aims to remove the metal ion by electrosorption rather than electrodeposition, the applied voltage must be controlled at an appropriate value or range to prevent the electrodeposition of metal ions on the electrode surface and vice versa.

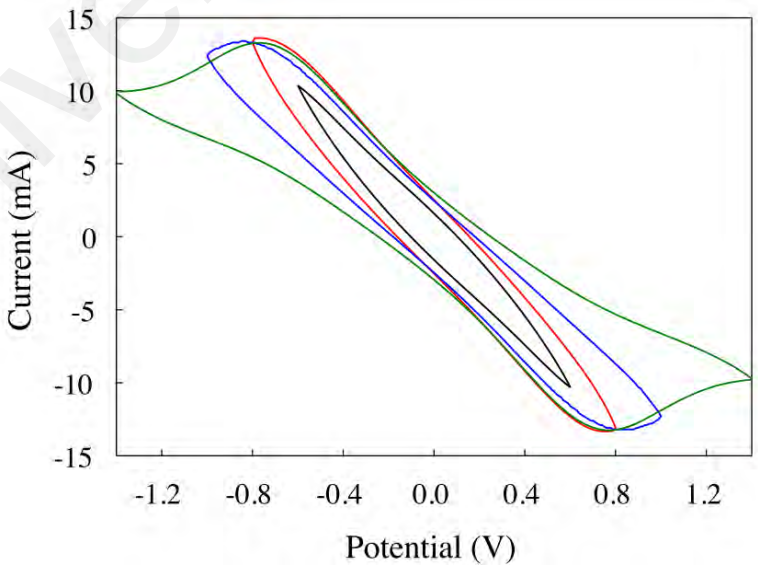

Figure 2.8: CV voltammograms for activated carbon electrode in 50 mg/L copper solution at various sweep potential at a scan rate of 5 mV/s (Huang et al., 2014).

2.5.2 Potentio electrochemical impedance spectroscopy (PEIS)

PEIS is a technique to measure an electrochemical impedance in an electrochemical cell by applying an AC potential in a perturbative manner and then measuring the current through the cell. Generally, it is a tool for unravelling a complex non-linear process by exploiting Faraday's Law to characterize a chemical process in terms of electrical measurements. A small excitation signal (~10 mV) is applied, and the measurement is carried out at different AC frequencies. Using a small excitation signal, the cell response is expected to be linear or pseudo-linear. In a linear system (or pseudo-linear), the current response to sinusoidal potential will also be sinusoidal at the same frequency but shifted in phase, as shown by Figure 2.9. The excitation signal, *E*, and the response signal *I* at time *t* are expressed as a function of time by Equation 2.11 and Equation 2.12, respectively. Additionally, by generalization according to Ohm's law, an expression to calculate impedance, *Z* is shown by Equation 2.13.

$$E = \Delta E \sin(2\pi f t) \qquad \text{Equation 2.11}$$

$$I = \Delta I \sin(2\pi f t + \emptyset) \qquad \text{Equation 2.12}$$

$$Z = \frac{E}{I} \qquad \text{Equation 2.13}$$

Where ΔE is the sinusoidal potential at maximum amplitude, ΔI is the response current at ΔE, f is the frequency, $\emptyset$ is the phase angle between excitation potential and produced current, and *t* is the time. Further, Equation 2.13 can be expressed as a complex function composed of a real and an imaginary part. Plotting the real part on the x-axis and the imaginary part on the y-axis produces a Nyquist plot. The Nyquist plot is named after Harry Nyquist, an electronic engineer who had made lots of contribution to the communication theory.

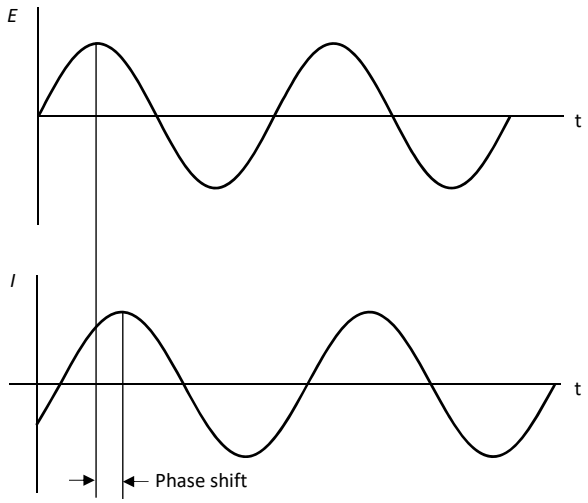

Figure 2.9: Sinusoidal current response in a linear system.

PEIS data is commonly interpreted by an equivalent circuit model. The most common equivalent circuit models for electrode studies is according to Randle's cell for which represents mixed kinetics and charge transfer control. The Nyquist plot and the equivalent circuit model for such a model are presented by Figure 2.10 and its inset, where R_s is the series solution resistance, R_p is the polarization impedance, W is Bounded Warburg impedance, and the C is double-layer capacitance. Meanwhile, it is more convenient to use the constant phase element (CPE) instead of a double layer capacitance as the capacitance in PEIS experiments often do not behave ideally (Liu et al., 2007). The depression of the semicircle indicates the CPE. The interpretation of Figure 2.10 expresses specific electrochemical meanings for which the diameter of the semicircle represents the polarization resistance, R_p or charge transfer resistance, R_{ct}. R_p is equivalent to R_{ct} for a very simple reaction like ferro/ferric cyanide redox. The intercept of the semicircle on the left side of the real axis expresses the solution resistance, R_s. On the other hand, diffusion creates an impedance called a Warburg impedance. On Nyquist plot, when semi-infinite diffusion is the rate-determining steps with a series of solution resistance as the only other cell impedance, the Warburg impedance appears as a diagonal line with a slope of 45°C. This element is named after German physicist Emil Warburg.

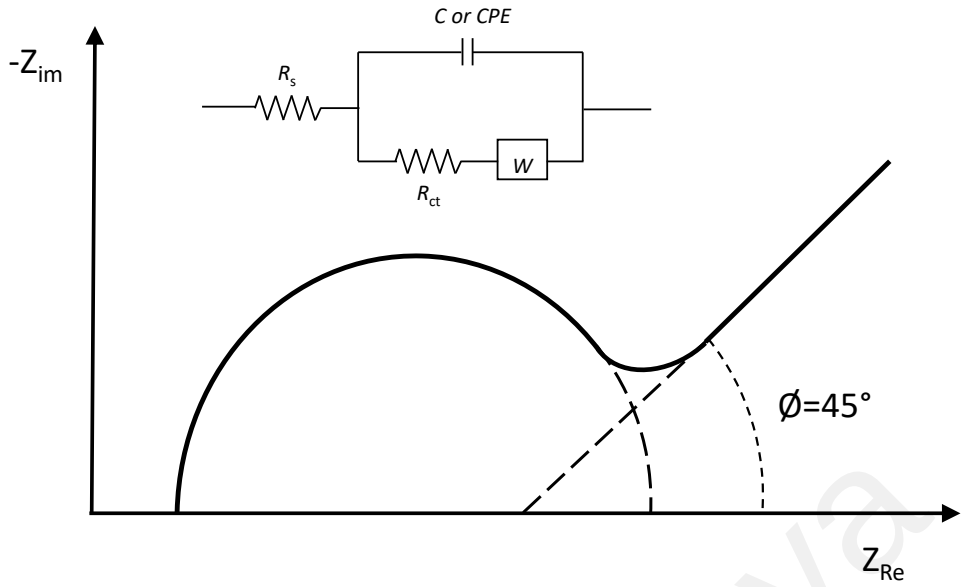

Figure 2.10: A Nyquist impedance diagram for mixed kinetic and charge transfer control. Inset is the corresponding equivalent circuit model.

2.5.3 Chronoamperometry (CA) and chronocoulometry (CC)

CA is a time-dependent technique where a square-wave potential is applied to the working electrode. The output response is current, and it is measured as a function of time, varies according to the diffusion of an analyte from the bulk solution toward the electrode surface. CA can therefore be used to measure current–time dependence for the diffusion-controlled process occurring at an electrode. An empirical equation representing the relationship between the current as a function of time is given by the Cottrell equation (Equation 2.14).

$$I = \frac{\mathrm{nFACD}^{\frac{1}{2}}}{\pi^{\frac{1}{2}} \mathrm{t}^{\frac{1}{2}}} \qquad \text{Equation 2.14}$$

Where *I* is the current (A), n is the number of electrons transferred, F is Faraday's constant (96485 C/mol), A is the electrode area (cm^2), C is the concentration of the analyte (mol/cm^3), and D is the diffusion coefficient (cm^2/s). The derivation of the Cottrell equation is available in many open literatures, namely, Franklin et al. (2016), Franklin et al. (2008) and (Strong, 2004). An ideal plot for CA output response as a function is illustrated in Figure 2.11.

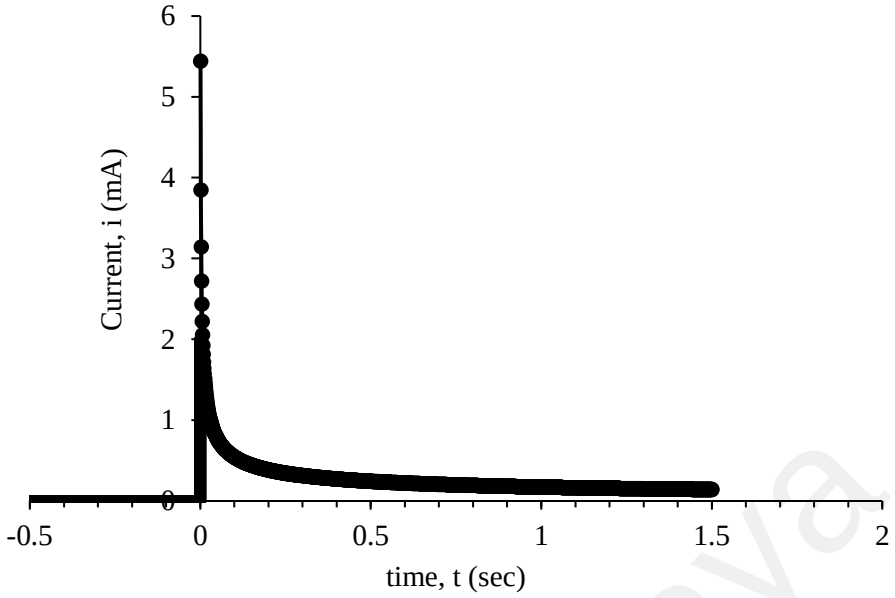

Figure 2.11: Ideal CA current response as a function of time. Assumption: analyte concentration of 1 mM, electrode area 1 cm^2, diffusion coefficient of 10^{-6} cm^2/s and n=1

By referring to Figure 2.11, initially, no potential is applied to the cell for which no current is produced during this period. At t=0, the potential is applied to allow the electron transfer and the instantaneous reduction of all the active species at the surface of the electrode. Additional active species from the bulk solution will arrive at the electrode's surface via diffusion, and it will be immediately reduced. After a period, the applied potential is stepped back to a voltage that allows the product at the electrode surface to oxidize. By considering an ideal CC result (according to Equation 2.14), the most important data points that contribute to the exponential trend of the output response (current) is at time less than 0.5 seconds recorded at a very short interval time, for instance, 0.001 seconds, as shown in Figure 2.11. In several works, chronoamperometry was employed to estimate the electrochemical active surface area of novel electrodes for which the diffusion coefficient, D, is taking from other reported findings with a similar cell system. Such approach was carried out by Ajeel et al. (2015a). Additionally, the diffusion of ferric- and ferrocyanide ions in aqueous media was experimentally studied

by Konopka and McDuffie (1970), and diffusion coefficient values were tabulated according to several different concentration of active species.

Chronocoulometry (CC) is an insightful approach that works on the same concept as CA, but instead of measuring current and time, it quantifies the relationship between the charge and time. CC differs from CA in the following aspect, and for some reasons, it is always preferred as compared to CA in certain studies, particularly those related to porous electrode:

- the signal is opposite trend to CC
- the integration reduces the noise
- provide a smooth hyperbolic response curve
- contribution from double-layer charging and absorbed species are easily noted

CA and CC have been applied in many studies independently or alongside other electrochemical techniques such as CV. Furthermore, CC is also useful to verify any deviation of the electrochemical system from the Cottrell equation. Such deviation can be described by Equation 2.15. The Faradic current is presented by the first term, while Q_{dl} and $nFA\Gamma_o$ represent the double-layer charging and the interfacial interaction, respectively.

$$Q = \frac{2nFAD^{1/2}t^{1/2}C}{\pi^{1/2}} + Q_{dl} + nFA\Gamma_O \qquad \text{Equation 2.15}$$

The description of the parameters in the above equation is similar ro Equation 2.16 with Γ_O is defined as surface concentration of adsorbed species (mol·cm^{-2}). Moreover, Zhou et al. (2021) claimed that the interfacial interaction is referring to the Faraday charge due to the adsorption of active species on the electrode and noted the last term in Equation 2.17 as Q_{ads}. Such claim was adopted from Anson (1964) for which the Q_{dl} was obtained by

CC test with supporting electrolyte alone. While Q_{ads} was estimated from the observed intercept of Q versus $t^{1/2}$ plot for a cell setup with the presence of the active species in a similar supporting electrolyte.

2.6 Palm shell activated carbon (PSAC)

Activated carbon or also called activated charcoal, is a form of disordered amorphous carbon with small pores and large surface area. It is well known for its porous characteristics. According to the IUPAC classification, the pore structure of porous material can be classified into (1) micropores with a pore diameter of less than 2 nm, (2) mesopores with a pore diameter between 2 to 50 nm and (3) macropores with a pore diameter greater than 50 nm. Due to its porous characteristic, the surface area of activated carbon can be reach up to 2395 m^2/g, as reported by Tran et al. (2020). This is equivalent to 1/3 a football field. The surface chemistry of activated carbon was also reported as one of the main factors contributing to its superior performance as adsorbent and catalytic materials. Various surface functional groups are available on a typical activated carbon due to the presence of heteroatoms (e.g., H, O, N, Cl, S) that bound to the edges of the graphene layer. Typical oxygen and nitrogen surface groups are illustrated in Figure 2.12. The surface oxygen functional groups can be classified into acidic, neutral and basic. The acidic groups are favourable towards metals ions by ion exchange and complex formation (Daud & Houshamnd, 2010). The primary source of surface acidity of activated carbon is mainly carboxylic acids or anhydrides, lactones or lactols, and phenolic.

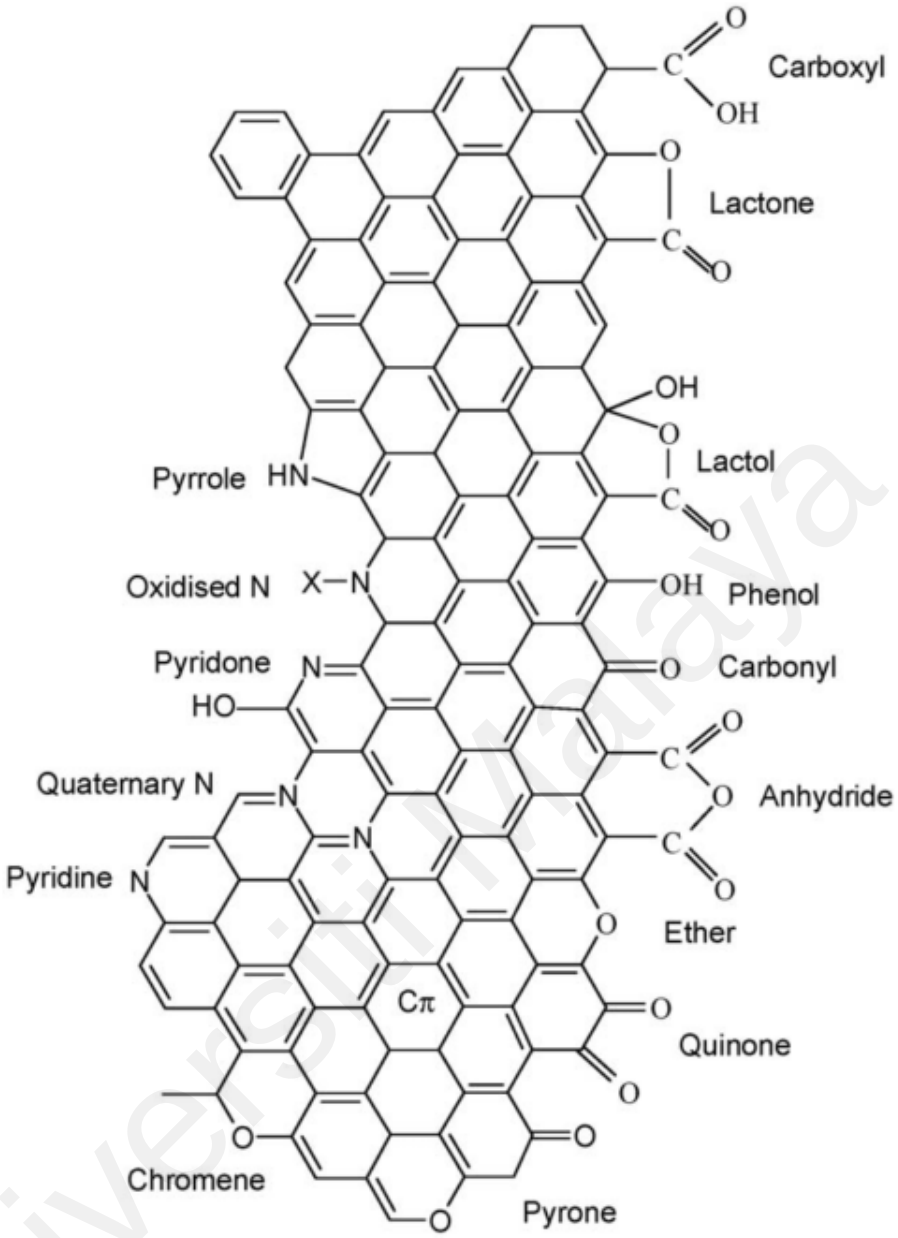

Figure 2.12: Nitrogen and oxygen surface functional groups on carbon material (Figueiredo & Pereira, 2010).

Activated carbons are prepared by thermal decomposition and activation of carbonaceous material, including an extensive selection of natural and synthetic precursors. A commercial activated carbon is mainly produced by coal, wood, sawdust, bamboo. They are also produced from an abundantly available raw material, particularly by-product generated by agro-industrial industry such as almond shell, coconut shell and

palm shell. In Malaysia, the effort to explore the feasibility of palm shell (or also called palm kernel shell) as activated carbon was first reported in open literature in 1996 (Hussein et al., 1996). The idea was initiated due to the gradual expansion of palm oil production, which leads to the generation of a huge amount of palm shell as a by-product. Oil palm shell is the solid waste produced during the milling process of palm oil.

PSAC was employed in various water and wastewater treatment applications, particularly for the adsorption of heavy metal and dyes (Ismaiel et al., 2014a; Mook et al., 2016; Nomanbhay & Palanisamy, 2005; Tan et al., 2008). The use of PSAC for electrode fabrication could demonstrate a valuable repurposing of local agricultural solid waste as it is available in huge quantities in tropical countries such as Malaysia, Indonesia and Thailand. For example, several studies have proved the effectiveness of PSAC as an electrode for the removal of nitrate (Ghafari et al., 2009), copper and lead from wastewater stream (Issabayeva et al., 2006). However, the electrochemical properties of PSAC as a prominent porous carbon-based electrode have not been investigated in detail. PSAC is known to offer a high surface area, is cheap, and is abundantly available from local palm oil mill industries. While there have been some reports on the electrical double layer properties of PSAC and its application as a supercapacitor (Misnon et al., 2015), the potential of PSAC to provide the faradaic reaction for metal ions reduction has not yet been well acknowledged in sufficient depth.

2.7 Task-specific ionic liquids (TSIL)

Task-specific ionic liquids (TSILs) are the terminology used to refer to functionalized ionic liquids (ILs) designed and synthesized with high specificity toward a target species. It is widely used as a component in the sensor. Modifying ILs with metal-chelating functional groups (e.g., urea, thiourea, thioether, phosphoryl, ethylene glycol, maltolate or thioglycolate) is expected to increase its selectivity towards target metal cations.

Figure 2.13 shows a comparison between ordinary ionic liquids and TSILs. To date, a very limited number of works were carried out to utilise TSIL in preparing electrode for heavy metal removal. Studies focuses on employing TSIL for metal speciation and detection. For instance, trihexyltetradecyl- phosphonium-, methyltrioctylphosphonium- and methyltrioctylammonium 3-hydroxy-2-naphthoate were used or multi-elemental micro-extraction of Cu, Ag, Cd and Pb from various synthetic aqueous solutions (Pirkwieser et al., 2018). Meanwhile, 1-(3-aminopropyl)-3methylimidazolium hexafluorophosphate was coupled to multi-walled carbon nanotubes for the speciation analysis of Hg (Esmaeili et al., 2020). Elsewhere, Stanisz et al. (2013) introduced trioctylmethylammonium thiosalicylate (TOMATS) coated polymeric tube for solid phase microextraction for determination of Hg in soil samples.

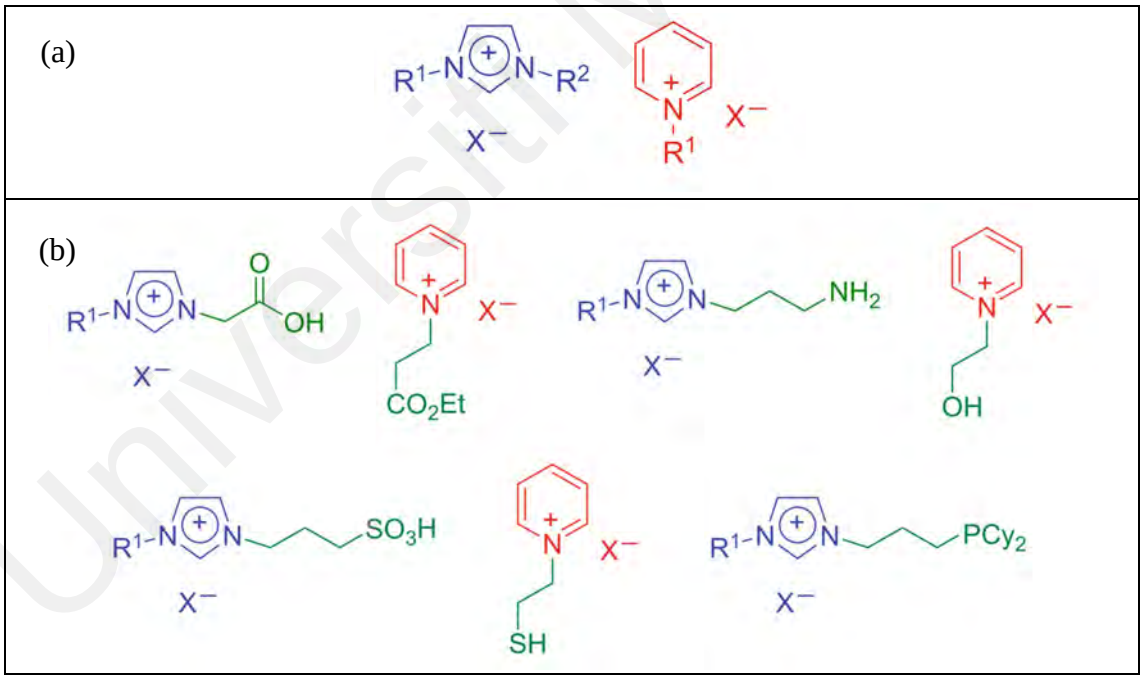

Figure 2.13: Examples of (a) ordinary ionic liquids (ILs) (imidazolium and pyridinium-based ILs) and (b) functional groups (green) chained at the cations allowing TSILs (Neto et al., 2019)

TSIL for the selective liquid/liquid extraction of heavy metals from aqueous systems was first published by Robin and co-workers in 2001 (Visser et al., 2001). They developed

functionalized imidazolium cation with thioether-, urea or thioether-derivative side chains act as metal liganding parts. This ionic liquid was the first to contain specific functionalities to enable well-defined chemical properties. As the ionic liquid is identified to have hydrophobic characteristics, PF^{6-} anions was introduced to provide the desired water immiscibility. However, these novel ionic liquids have some significant disadvantages. Kalb and Kotschan (2006) claimed that this pioneering TSIL suffered from several drawbacks; namely, (1) the PF^{6-} anion is very unstable, producing poisonous and corrosive HF or fluorides with regard to hydrolysis, (2) it is difficult to quantify the toxicity of the imidazolium cation for which it is costly to perform a toxicological analysis (3) the disposal of fluorous compounds is expensive and problematic, (4) synthesis on a larger scale is complicated and (5) the starting material are expensive.

Later, Kalb and Kotschan (2006) reported that Proionic Production of Ionic Substances GmbH & Co KG had developed a new ionic liquid called TOMATS to overcome the above drawbacks. TOMATS does not contain any fluorine and is totally hydrolysis-stable. Therefore, HF or fluoride is not released. TOMATS is non-corrosive and considerably easier to dispose than the previously invented TSIL. The low toxicity of cation is identified from similar compounds namely trioctylammonium chloride (a catalyst for phase transfer) and thiosalicylic acids or its salts which categorized as irritants. Additionally, TOMATS is claimed to have heavy metal distribution coefficients values ranging from 50 thousand to over 2 million. A considerably high distribution coefficient can be explained by the chelating effect of ortho-positioned carboxylate group relative to the functionality of thiol. Such configuration is well-known to form metal thiolate complexes. The synthesis is also claimed to be simple and promising to be carried out at a large scale (Kalb & Kotschan, 2006). TOMATS has a high viscosity at 20°C. Therefore, the phase separation at 20°C often takes quite a long time if applied as a solvent for heavy metal extraction. This downside can be resolved by applying a water-

immiscible organic solvent such as ethyl acetate or increasing the operating temperature. However, the diluted TOMATS may deteriorate the extraction process and introducing higher temperature may incur additional cost to the process. The chemical and physical characterization of TOMATS is listed in Table 2.8.

Table 2.8: Physical and chemical properties of TOMATS (Kalb & Kotschan, 2006).

Appearance	Olive green, viscous liquid
Relative Molecular Mass	521.89 g/mol
Empirical Formula	$C_{32}H_{59}NO_2S$
Solubility	- Soluble in alcohols, ethyl acetate, tetrahydrofuran (THF), acetonitrile, acetone, dichloromethane, dimethyl sulfoxide (DMSO) - Insoluble in water, hexane
Nernst Distribution Coefficients*	Cd^{2+} > 50000, Cu^{2+} > 50000 Pb^{2+} and Hg^{2+} > 100000
Melting Point	< 30 °C
Leaching into the aqueous phase	< 100 ppm

* Aqueous phase with 5 to 50 ppm metal, 1:1 extraction, detection using Atomic Absorption Spectroscopy (AAS) and Inductively Coupled Plasma Atomic Emission Spectroscopy (ICP-AES).

Several works have been carried out to explore the feasibility and the performance of TOMATS for various application. Fontas and co-worker have extensively studied the application of TOMATS as the carriers in polymers inclusions membranes (PIMS) (Elias et al., 2019; Elias et al., 2020; Elias et al., 2018; Turull et al., 2017). They proposed a novel and simple method for the preconcentration and determination of mercury from natural waters through its extraction into a polymer inclusion membrane (PIM) containing TOMATS. Recently, Elias et al. (2020) developed novel sorbents, namely, silicon dioxide at a nanoparticle range and cellulose powder at a microparticle range. Both were modified

with TOMATS to determine bioavailable trace concentrations of mercury in water. It was reported that Hg(II) uptake efficiency was 97% for both types of the developed electrode, while only 25% of Hg(II) was taken up using non-impregnated materials. They also reported that Hg collected in the TOMATS impregnated PIM was stable for at least six months without the use of any preservative (Elias et al., 2018). Elsewhere, several works also focus on applying TOMATS to facilitate metal extraction for detection purpose (Ismaiel, 2013; Ismaiel et al., 2014a, 2014b; Mohamadi & Mostafavi, 2011; Saljooqi et al., 2015; Stanisz et al., 2013). Therefore, it can be concluded that TOMATS has received a lot of consideration in sensor development and fabrication, but there is little work has been carried out to evaluate the performance of TOMATS for wastewater treatment, particularly for removal of Hg.

2.8 Summary

In this chapter, it is well acknowledged that electrochemical removal of Hg from wastewater has received limited attention in comparison with other heavy-metal contaminants. Well-versed findings in the literature have proven that the electrochemical process is capable of removing and recovering heavy metal ions from waste and wastewater. Electrochemical technologies are not only aimed at meeting the discharge limit requirements set by the local authorities but also at providing the possibility of water recycling as well as metal recovery in their most valuable forms. Thus, electrochemical approach is seen to be an appealing method for removal of Hg.

The development of electrodes for the removal and recovery of Hg is still scanty in the literature compared to the swift revolution in the construction of electrodes for the desalination of saltwater. Many studies have shown that the electrosorption process by activated carbon is effective in removing undesirable sodium and chlorides from brackish water. This technology should be taken as a point of reference for the removal and

recovery of Hg, either via electrosorption or/an electrodeposition. Additionally, studies have proven the improved characteristics of a 3D electrode in comparison to a 2D electrode. Hence, the development of electrode derived from porous material becoming a pioneering notion for 3D-electrochemical removal of Hg. For this purpose, the local PSAC carbon would be the best candidate to be utilised as the major component of a porous electrode.

Meanwhile, ionic liquid is extensively utilized in the preparation of highly sensitive electrochemical sensors for organic and inorganic detection. However, the application of an ionic liquid in electrode modification to achieve a higher metal ion selectivity and reusability in the treatment of heavy metal-laden wastewater has not yet attracted considerable attention. It is expected that the role of ionic liquids, particularly TSIL will progressively grow with the development of the unique properties of electrodes with high metal ion selectivity (particularly Hg) and less energy consumption.

CHAPTER 3: METHODOLOGY

3.1 Overview

The experimental works consist of three main parts, and it is summarized according to the objectives, namely, (1) the electrode preparation, (2) the electrochemical characterization of the prepared electrode, and (3) the electrochemical removal of Hg as shown in Figure 3.1.

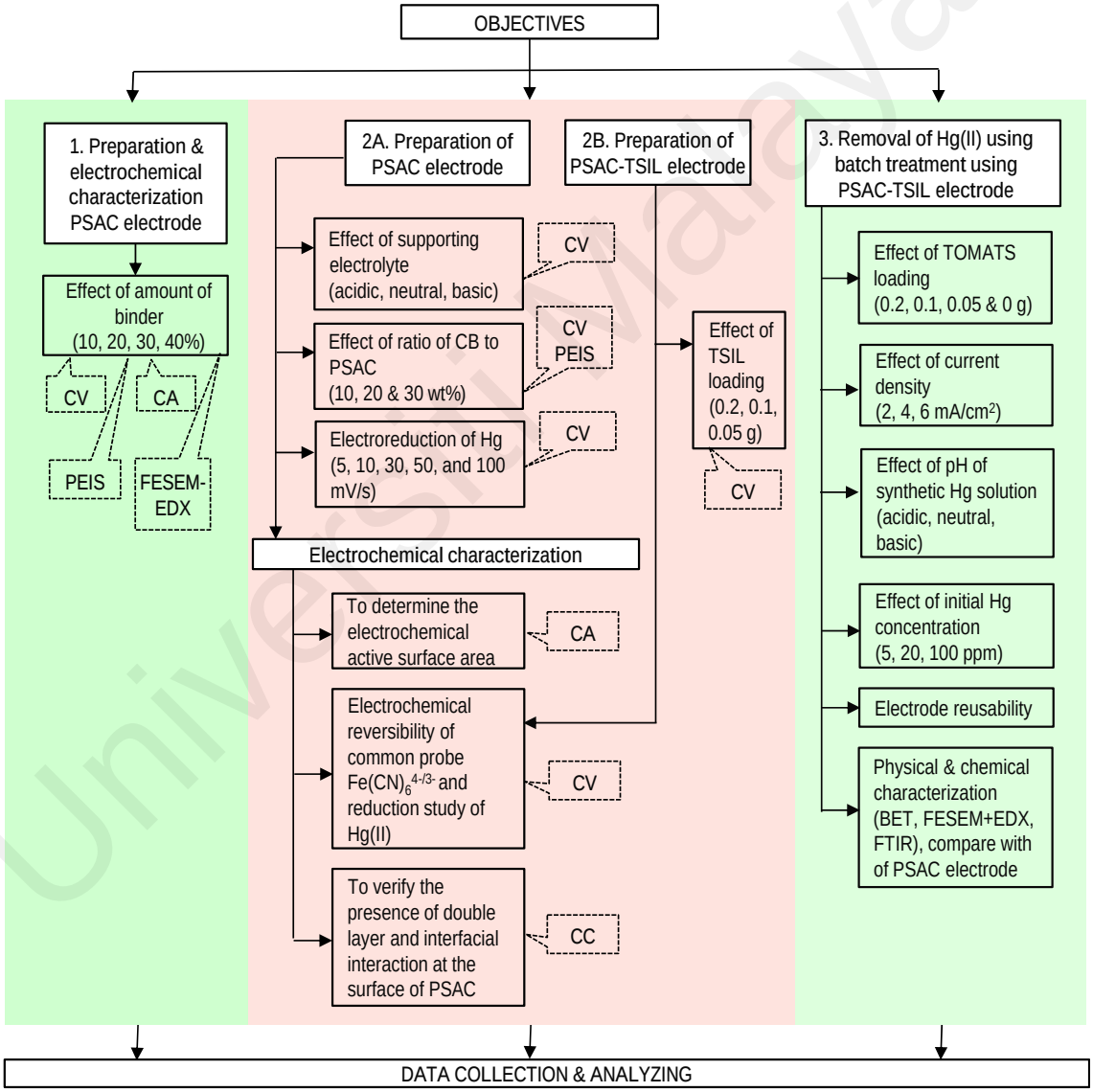

Figure 3.1: Summary of the experimental works for the electrode preparation, electrochemical characterization, and electrochemical removal of Hg.

3.2 Material and chemical

3.2.1 Material

Granular palm shell activated carbon (PSAC) was provided by a local supplier, Bravo Green Sdn. Bhd., Sarawak. The granular PSAC was ground to fine particles and sieved to obtain the desired particle size (<100 µm). Powdered PSAC was dried in an oven at 110°C for 24 hours. It was then stored in an airtight container prior to electrode preparation. Fine powder carbon black (CB) (Super P) and commercial activated charcoal (Supelco) were purchased from Alfa Aesar and Sigma-Aldrich, respectively.

3.2.2 Chemical

Mercury(II) chloride (99.5%, R&M Marketing) was used to prepare the Hg solution. Polytetrafluoroethylene (PTFE), in the form of suspension, 60 wt.% dispersion in water (Sigma-Aldrich) and perfluorinated resin solution containing Nafion^{TM} 1100W (Nafion 1100EW) (5 wt%, Aldrich) were used as the binder. Meanwhile, 1,3-propanediol (98%, Sigma-Aldrich) and 2-propanol were spent as a solvent in the electrode preparation. The pH of the solution was adjusted by adding an appropriate amount of 0.5 M or 1 M HCl, and 0.5 M or 1 M of NaOH prepared from solid NaOH (Emsure®, Merck) and 37% HCl (Emsure®, Merck), respectively. Trioctylmethylammonium thiosalicylate (TOMATS) (Sigma-Aldrich) has a purity of ≥95%. The empirical formula of TOMATS and its molecular weight is $C_{32}H_{59}NO_2S$ and 521.89 g/mol, respectively. The molecular structure of TOMATS is presented in Figure 3.2.

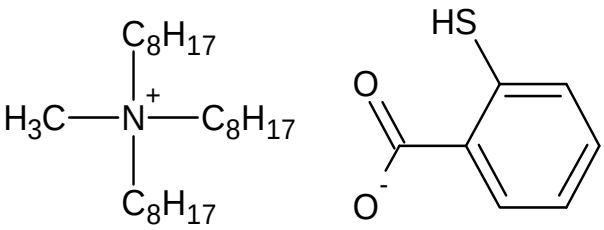

Figure 3.2: Molecular structure of TOMATS

3.3 Electrode preparation

There are two types of prepared electrodes. The first type of electrode was prepared from virgin PSAC, and the second type was the modified PSAC. The modified PSAC was prepared by immobilising the task-specific ionic liquid (TSIL) on the surface of virgin PSAC. This type of electrode is addressed as PSAC-TOMATS electrode. The details of the preparation steps for PSAC-TOMATS electrode are described in Section 3.3.2.

3.3.1 Palm shell activated carbon (PSAC) electrode

The electrode was prepared by mixing a fixed amount of powdered PSAC, CB and PTFE with a predetermined mass ratio. The amount of CB and PTFE in the electrode was varied to determine the effect of these parameters on the electrochemical properties of the prepared electrode. PSAC was replaced by commercial activated charcoal (Supelco) for comparison studies employing the CA & CC analysis. This activated charcoal is addressed as Supelco.

3.3.1.1 Effect of the amount of carbon black (CB)

A mixture of PSAC, CB and PTFE suspension was prepared at a ratio of 4:1:1, for which the electrode was identified as PSAC electrode with 20% of CB and labelled as PSAC20CB. For the electrochemical characterization studies, the actual amount of PSAC, CB and PTFE used for the preparation of PSAC20CB was 0.4, 0.1 and 0.1 g, respectively. The mixture was thoroughly hand-mixed to produce an electrode paste by adding approximately 1 g of 1,3-propanediol as the solvent. The mass ratio of 1,3-propanediol to the total amount of PSAC and CB was 2:1. The paste was then kneaded and pressed in a stainless-steel mould prior to drying at 80ºC for 2 h, at 125ºC for 1 h and at 250ºC for 1 h. The dried electrode was then packed into a 5 mm-diameter empty electrode tip, as shown in Figure 3.3(a), and it was readied for electrochemical

characterization studies. Additionally, for electrochemical removal of mercury from the aqueous solution, the electrode was prepared in a bigger size, a diameter of 24.5 mm, as shown by Figure 3.3(b). The optimum amount of CB was determined by varying the mass ratio of 10, 20 and 30% of CB to the mass of PSAC while maintaining the same amount of PTFE. The equivalent mass ratios of PSAC:CB:PTFE were 45:5:10, 40:10:10 and 35:15:10 for the PSAC10CB, PSAC20CB and PSAC30CB electrodes, respectively. An equal total mass of electrode (ca. 0.5 g for small electrode or 1.5 g for big electrode) was prepared for each type of electrode while the percentage of CB was varied accordingly.

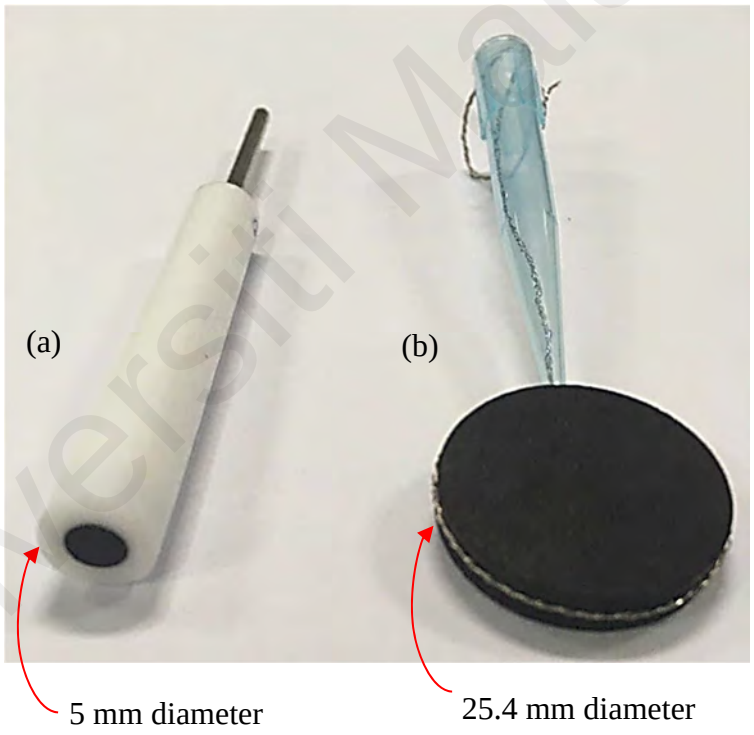

Figure 3.3: Electrode for (a) electrochemical characterization in a three-electrode cell system and (b) electrode for Hg removal in a two-electrode cell system.

3.3.1.2 Effect of the amount of binder

For this study, the amount of binder, namely PTFE, was varied in four different percentage (10, 20, 30 and 40%). The amount of PSAC and CB was fixed at 0.4 g and 0.1 g, respectively. Similar preparation steps as described in Section 3.3.1.1 were carried

out. The electrode with different amounts of binder was investigated for its electrochemical characteristics by using cyclic voltammetry, chronoamperometry, and potential electrochemical impedance spectroscopy (PEIS).

3.3.2 PSAC-TSIL electrode

The prepared modified PSAC electrode was compromised of the optimum amount of CB and PTFE obtained in the previous study of virgin PSAC. The optimum mass ratio of PSAC:CB:PTFE was found to be 4:1:1. Later, the immobilisation of TOMATS on the PSAC electrode was made by applying a mixture of powdered PSAC, Nafion 1100EW as the binder and TOMATS as the active material onto the PSAC electrode. This type of electrode is addressed explicitly as PSAC-TOMATS electrode. Firstly, a predetermined weight of TOMATS (e.g., 0.05, 0.1 and 0.2 g) was diluted in 1 mL of 2-propanol in a 5 mL glass container that was equipped with a cap. TOMATS was rigorously diluted in 2-propanol on a vortex mixer. Next, a 0.1 g Nafion 1100EW was added, and the solution was mixed on a vortex mixer for 3 minutes. Next, 0.1 g powdered PSAC was added, and the solution was mixed again on a vortex mixer. Finally, the TOMATS-coated PSAC suspension (ca. 150 µL) was applied on the PSAC electrode and dried at room temperature. Three layers of TOMATS-coated PSAC suspension was applied on both sides of the PSAC electrode. The suspension was well shaken on a vortex mixer prior to applying them on the PSAC electrode. For the study of the effect of TOMATS loading, three different electrodes were prepared, and the mass of TOMATS was varied at 0.05, 0.1 and 0.2 g. This amount was equivalent to a mass ratio of powdered PSAC to TOMATS of 2:1, 1:1 and 1:2, respectively.

3.4 Cyclic voltammetry

Cyclic voltammetry experiments were conducted in one compartment of 100 mL glass cells at room temperature. The supporting electrolyte was prepared at a concentration of

0.5 M, while the electroactive material for the reversibility study was 5 mM potassium ferrocyanide ($K_4[Fe(CN)_6]\cdot 3H_2O$). Three supporting electrolyte have been tested, namely NaCl for neutral, HCl for acidic and NaOH for alkaline conditions. A three-electrode cell configuration was employed, as shown in Figure 3.4. Platinum wire (counter electrode) and Ag/AgCl (3M KCl) reference electrodes were used for the measurement. The prepared electrode was addressed as the working electrode.

The cyclic voltammetry experiments and analysis were performed by a potentiostat instrument (Autolab PGSTAT101, Metrohm) controlled by the NOVA 1.10 software. In addition, the solution was stirred between experiments to restore initial conditions but was not stirred during the experiment to maintain the flux to the electrode under diffusion-controlled behaviour. For the electro-reduction study of Hg^{2+}, the active electroactive material was 5 mM $HgCl_2$ in 0.5 M NaCl, and the scan rate was varying at 5, 10, 30, 50, 100 mV/s. The second cycle of each cyclic voltammetry was reported unless otherwise noted. Additionally, prior to evaluating the electrochemical characteristics, the electrode surface was polished using the micro pad polishing cloth. Each electrode was held vertically, and 8-motions were performed 20 times on the wet polishing pad, which was pre-wetted by distilled water. The electrodes were then dried using a hot air blower, cooled at room temperature, and made ready for electrochemical characterisation studies.

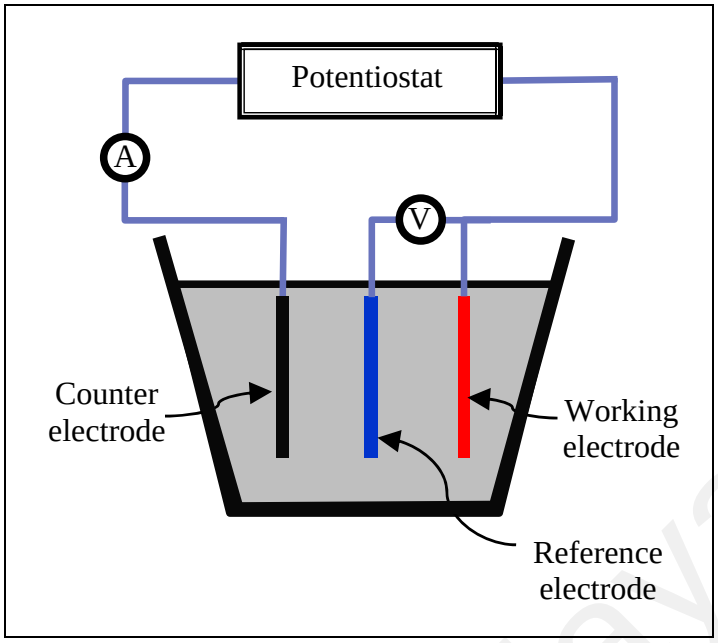

Figure 3.4: Schematic diagram for three-electrode system setup

3.5 Potentio electrochemical impedance spectroscopy (PEIS)

PEIS studies employed a potentiostat (Biologic, SP-300), and the data were analysed using EC-Lab®software. PEIS was performed at a potential bias of 0.26 V (vs Ag/AgCl) over the frequency range of 300 kHz to 1 Hz with an AC perturbation of 10 mV. A higher frequency (5 MHz) was applied for PSAC00CB. The analysis was conducted using an aqueous solution of 5 mM potassium ferrocyanide in 0.5 M NaCl as the electrolyte. PSAC electrodes of 5 mm diameter were used as the working electrode. Platinum wire and Ag/AgCl (3M KCl) were used as the counter- and the reference electrodes, respectively, for the PEIS analysis. The result from PEIS is illustrated by a Nyquist impedance diagram.

3.6 Chronoamperometry (CA) & chronocoulometry (CC)

CC studies employed a potentiostat (Biologic, SP-300), and the data were analysed using EC-Lab®software. The analysis was conducted using an aqueous solution of 5 mM potassium ferrocyanide in 0.5 M NaCl as the electrolyte. The effective surface area was

obtained by the Cottrell equation (Equation 2.14), where I is the current (A), n is the number of electrons transferred, F is Faraday's constant (96485 C/mol), A is the electrode area (cm^2), C is the concentration of active species (mol/cm^3) and D is the diffusion coefficient (cm^2/s). Furthermore, CC was utilised to verify any deviation of the electrochemical system from the Cottrell equation. Such deviation can be described by Equation 2.15. The Faradic current contributes the first term, while Q_{dl} and $nFA\Gamma_o$ represent double-layer charging and interfacial interaction, respectively. For this analysis, PSAC20CB, Supelco and Pt with a 3 mm-diameter were used as the working electrode for a comparison study.

3.7 Surface area and porosity analysis

The surface area and the porosity of the electrode component and prepared electrodes were measured by the nitrogen adsorption-desorption isotherms at 77 K using an automated surface area and porosity analyser (Micromeritics, ASAP 2020). The samples were degassed at 250°C under vacuum for 8 hours. The specific surface areas, S_{BET}, of the samples were estimated according to the Brunauer-Emmett-Teller (BET) equation at a range between 0.05 to 0.3 P/P^o. The pore size distribution was analysed according to slit shape carbon pore by the Density Functional Theory (DFT) for micropores and Burnett, Jeyner, Halenda (BJH) methods for mesopores characteristics.

3.8 Fourier-transform infrared spectroscopy (FTIR) analysis

Fourier Transform-Infrared Spectroscopy (FTIR) is an analytical technique used to identify the functional groups of organic material present in the electrode. This technique measures the absorption of infrared radiation by the sample material at a range of wavelength. The infrared absorption bands identify molecular components and structures. Infrared energy excites molecular bonds to create unique spectra for various molecules. By comparing unknown spectra to individual standard spectra, molecules can be

identified. The FTIR spectrum and the comparison of IR data for PSAC-TOMATS electrode before and after the electrochemical removal of Hg were compared. The analysis was accomplished using FTIR spectrometer, Perkin-Elmer Spectrum 400, USA.

3.9 Electro-reduction of Hg^{2+}

This experiment aimed to evaluate the effectiveness of the prepared electrode for the removal of metal ions, Hg^{2+} in particular. The electrochemical cell consisted of a two-electrode system where the anode was graphite felt with a 99% metal basis (Alfa Aesar) with a dimension of 20 x 40 mm. The schematic diagram for the two-electrode cell system is illustrated in Figure 3.5. The cathode was the PSAC based electrode with a diameter of 2.54 cm (1 inch). Conventional batch mode experiments were performed at room temperature with a 100 mL initial Hg concentration of 100 mg/L and a small amount of 0.1 M NaCl as a supporting electrolyte (ca. 5 mL). The experiments were conducted at a constant applied current density of 6 mA/cm^2 (60 mA per 10.134 cm^2), controlled by a programmable power supply (IPS 3201). The solution was subjected to the stirring mode at 250 rpm for 5 hours of reaction time. The initial Hg^{2+} concentration was varied at 25 and 50 mg/L to investigate the effect of initial metal concentration on the reaction kinetics. The removal of Hg^{2+} was examined by Inductively Couple Plasma-Optical Emission Spectroscopy (ICP-OES) (Perkin Elmer, Optima 7000 DV) or Inductively Coupled Plasma-Mass Spectroscopy (ICP-MS) (Agilent, ICPMS 7500 Single Turbo System) for lower initial Hg concentration (25 ppm) studies. ICP-MS allows a detection of trace level of Hg, at a range of part per billion (µg/L). The calibration curve for Hg concentration vs intensity using ICP-OES and ICP-MS are presented in Appendix A, Figure A.1 and A.2, respectively. The current efficiency, space-time yield and energy consumption were calculated using Equation 3.1, Equation 3.2 and Equation 3.3, respectively.

$$\text{Current efficiency} = \frac{z_i F \Delta m}{M_i I \Delta t} \times 100 \qquad \text{Equation 3.1}$$

$$\text{Space} - \text{time yield} = \frac{iaM_i}{1000 z_i F} CE \qquad \text{Equation 3.2}$$

$$\text{Energy consumption} = \frac{VIt}{m} \qquad \text{Equation 3.3}$$

These equations were deduced from several input parameters, whereby z is the charge number, F is Faraday's constant (96485 A·s/mol), Δm is the mass (g) of reduced metal in the interval time, Δt (s), M is a molecular mass (g/mol), I is the current passed (A), i is the current density (A/m^2), a is the specific electrode area (m^2/m^3) (electrode area per unit volume of the reactor), V is the cell voltage (V) of the process, t is the electrolysis time (h), and m is the mass of the product (kg).

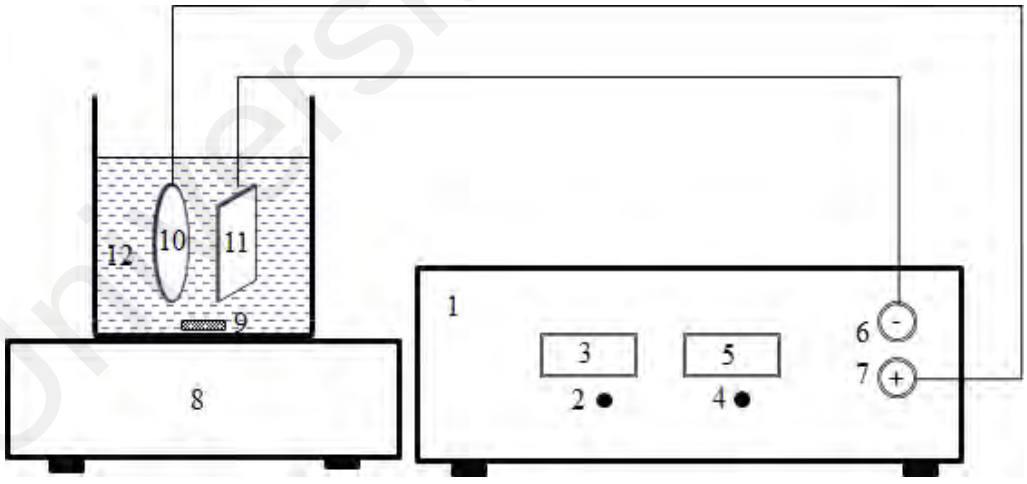

1. DC power supply
2. Current controller
3. Instantaneous/setting current
4. Voltage controller
5. Instantaneous/setting voltage
6. Negative terminal
7. Positive terminal
8. Magnetic stirring plate and controller
9. Magnetic bar stirrer
10. Anode
11. Cathode
12. Synthetic wastewater

Figure 3.5: Schematic diagram for two-electrode system setup

CHAPTER 4: RESULTS AND DISCUSSION

This chapter is divided into three parts and is organized according to the objectives of this study. However, this section on the results and discussion is sometimes interrelated with other parts.

Part I: Preparation and electrochemical characterization of palm shell activated carbon (PSAC): Effect of the amount of binder.

Part II: Electrochemical properties of palm shell activated carbon immobilised with task-specific ionic liquid (PSAC-TSIL).

Part III: Palm shell activated carbon immobilised with a task-specific ionic (PSAC-TSIL) electrode for the removal of mercury from wastewater.

4.1 Part I: Preparation and Electrochemical Characterization of Palm Shell Activated Carbon (PSAC) Electrode: Effect of the Amount of Binder

A binder is an essential component in electrode preparation as it helps in the binding of discrete porous particles to form an electrode that facilitates the electrochemical activities in a system. Fluorine-containing resin materials such as polytetrafluoroethylene (PTFE) are widely used as binders, as they have excellent chemical and thermal resistance and are best known for their binding properties. PTFE is widely used as a binder for the fabrication of cathode for energy storage, particularly fuel cell (Cheng & Wu, 2013; Dong et al., 2012a; Dong et al., 2012b; Lin et al., 2021; Zhang et al., 2014) and capacitor/supercapacitor (Gambou-Bosca & Belanger, 2015; Wu et al., 2021; Zhu et al., 2016). The effect of varying the amount of PTFE in the preparation of the PSAC electrode was studied for their electrochemical properties. The electrochemical properties that will be discussed in the following subtopics are the electrochemical active surface area, cyclic voltammogram, double-layer capacitance and electron transfer resistance. Additionally, the surface morphology and the elemental composition of the prepared electrodes are highlighted.

4.1.1 Electrochemical active surface area

Porous properties of the PSAC led to a higher active electrochemical surface area of an electrode when compared with its geometrical area. However, the introduction of binder in electrode preparation steps may reduce the electrochemical active sites. Therefore, PSAC electrodes with different amounts of PTFE were prepared, analysed, and compared. Figure 4.1 shows the current-time output response obtained from the chronoamperometry (CA) analysis of PSAC electrodes which were prepared using four different amounts of binder (PTFE) (10, 20, 30 and 40%). Additionally, the relationship between the current and the time can be described by the Cottrell equation (Equation 2.14) with the specific known value of the diffusion coefficient, *D*, of ferrocyanide in an

aqueous solution at 25°C, i.e. $D = 7.6 \times 10^{-5}$ cm^2/s (Bard & Faulkner, 2001). A linear plot of i vs $t^{-0.5}$ was obtained as illustrated by the inset in Figure 4.1, and the electrochemical active surface area of the electrode was estimated from the slope corresponding to Equation 2.14. The electrochemical active surface area was compared to the geometrical surface area (0.196 cm^2) and listed in Table 4.1. The 10PTFE was found to have the highest amount of electrochemical active surface area among others with 1.57 cm^2, which was 8 times higher than its geometrical surface area. The electrochemical active surface area decreased by 42% when the amount of PTFE was increased to 20%. Such an outcome suggests that increasing the amount of PTFE decreases the available high surface area of porous PSAC for electrochemical activities. In addition, almost a similar value of the electrochemical active surface area was observed for 20PTFE, 30PTFE, and 40PTFE, which was between 0.92 and 0.96 cm^2. It was about five times greater than its geometrical surface area.

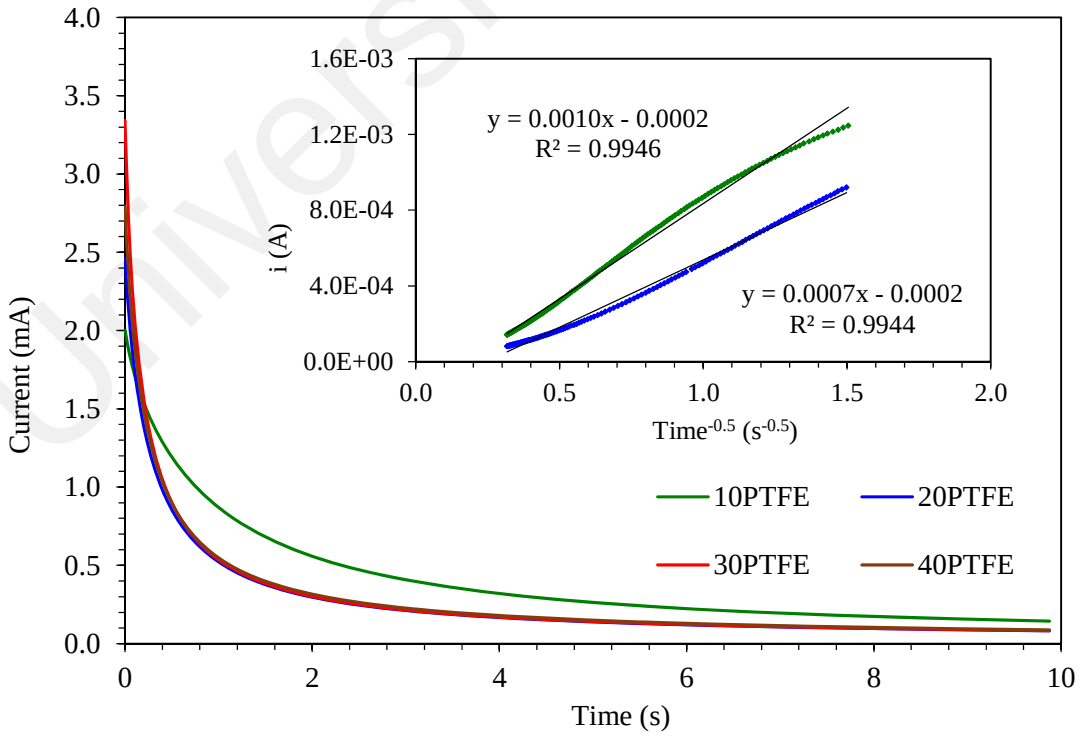

Figure 4.1: A single-step CA plot of the PSAC electrode using electrodes prepared using different amounts of PTFE at a voltage step from 0 to 0.4 V. Inset shows the plot of i vs. $t^{-0.5}$, which has been employed to deduce the electrochemical active surface area of electrodes.

Table 4.1: Electrochemical active surface area of prepared electrodes deduced from CA analysis

Electrode	10PTFE	20PTFE	30PTFE	40PTFE
Electrochemical active surface area, cm^2	1.572	0.917	0.959	0.940
Electrochemical / Geometrical active surface area, cm^2/cm^2	8.0	4.7	4.9	4.8

4.1.2 Surface morphology

Figure 4.2 illustrates the Field Emission Scanning Electron Microscope with Energy Dispersive X-Ray (FESEM-EDX) elemental mapping for the electrodes with a different PTFE composition Figure 4.3 presents the larger scale of elemental mapping of 20PTFE electrode. Accordingly, EDX detects the emission of four major elements on the surface of the PSAC electrode, namely carbon (C), oxygen (O), fluorine (F), and a small percentage of silica (Si), as listed in Table 4.2. These compositions are with reference to the same mapping area as shown in Figure 4.2. The fluorine element represents the distribution of PTFE on the electrode surface. Generally, all the elements are heterogeneously scattered on the surface of the electrode. It is clearly seen in Figure 4.2 that fluorine dots are sparse (blue colour) in the 10PTFE and are the least concentrated compared to the other electrodes. As the amount of PTFE increases to 40%, the intensity of fluorine dots also increases as the blue spots become denser. This is in agreement with the atomic percentage of fluorine, which increases proportionally as the amount of PTFE increases from 10% to 40%, as listed in Table 4.2. On the contrary, the percentage of carbon present on the surface of the electrode is inversely proportional to the atomic percentage of fluorine. For instance, in the 10PTFE electrode, the least amount of PTFE introduced in the electrode results in a larger amount of PSAC available on the same imaging area. This trend is on opposite for 40PTFE. The high intensity of fluorine dots

in 40PTFE suggests an excess amount of PTFE on the surface which hinders the electrochemically active surface area of the PSAC electrode.

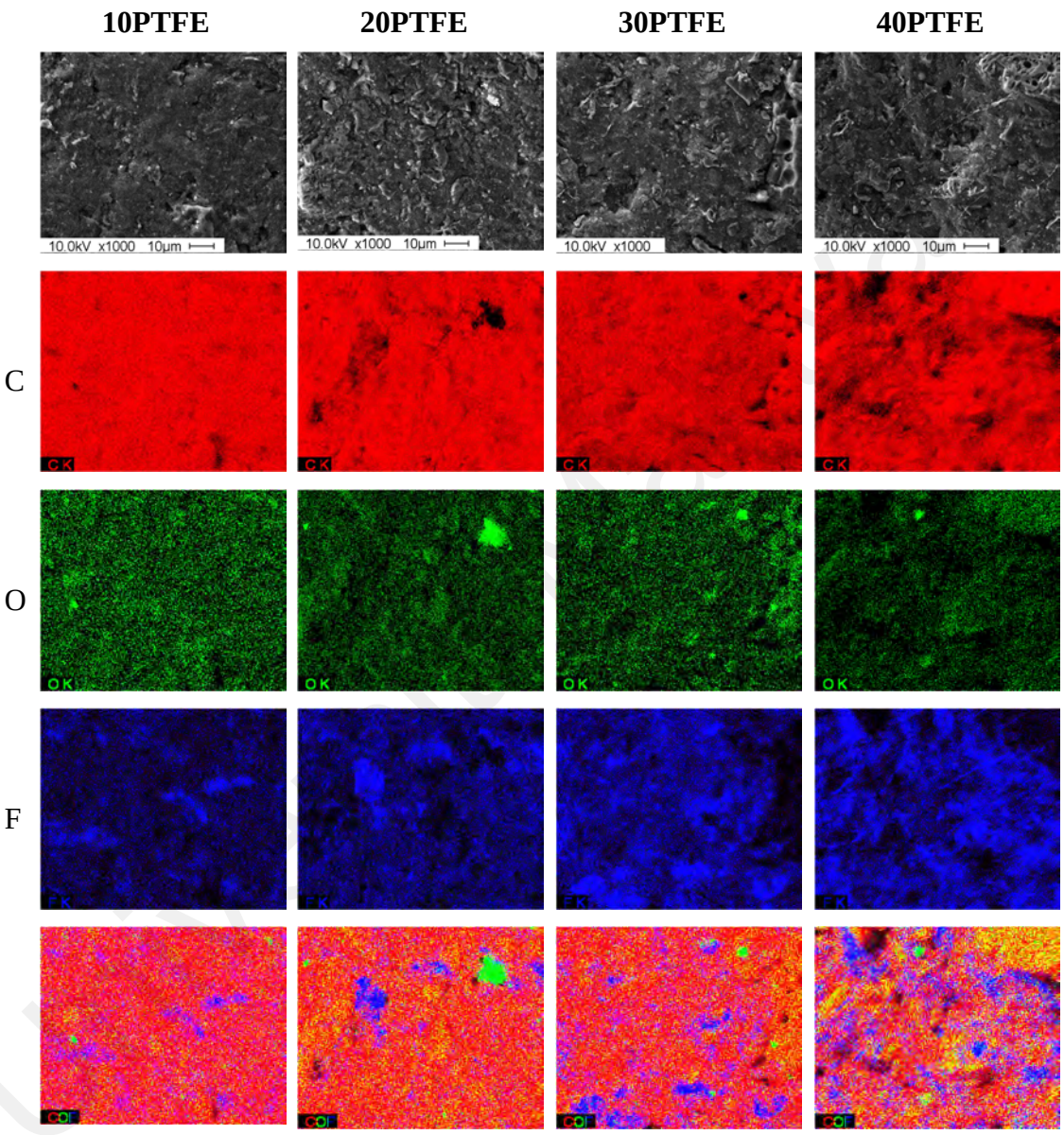

Red, green and blue represents carbon (C), oxygen (O) and fluoride (F), respectively.

Figure 4.2: FESEM-EDX elemental mapping of prepared electrodes using different amount of PTFE.

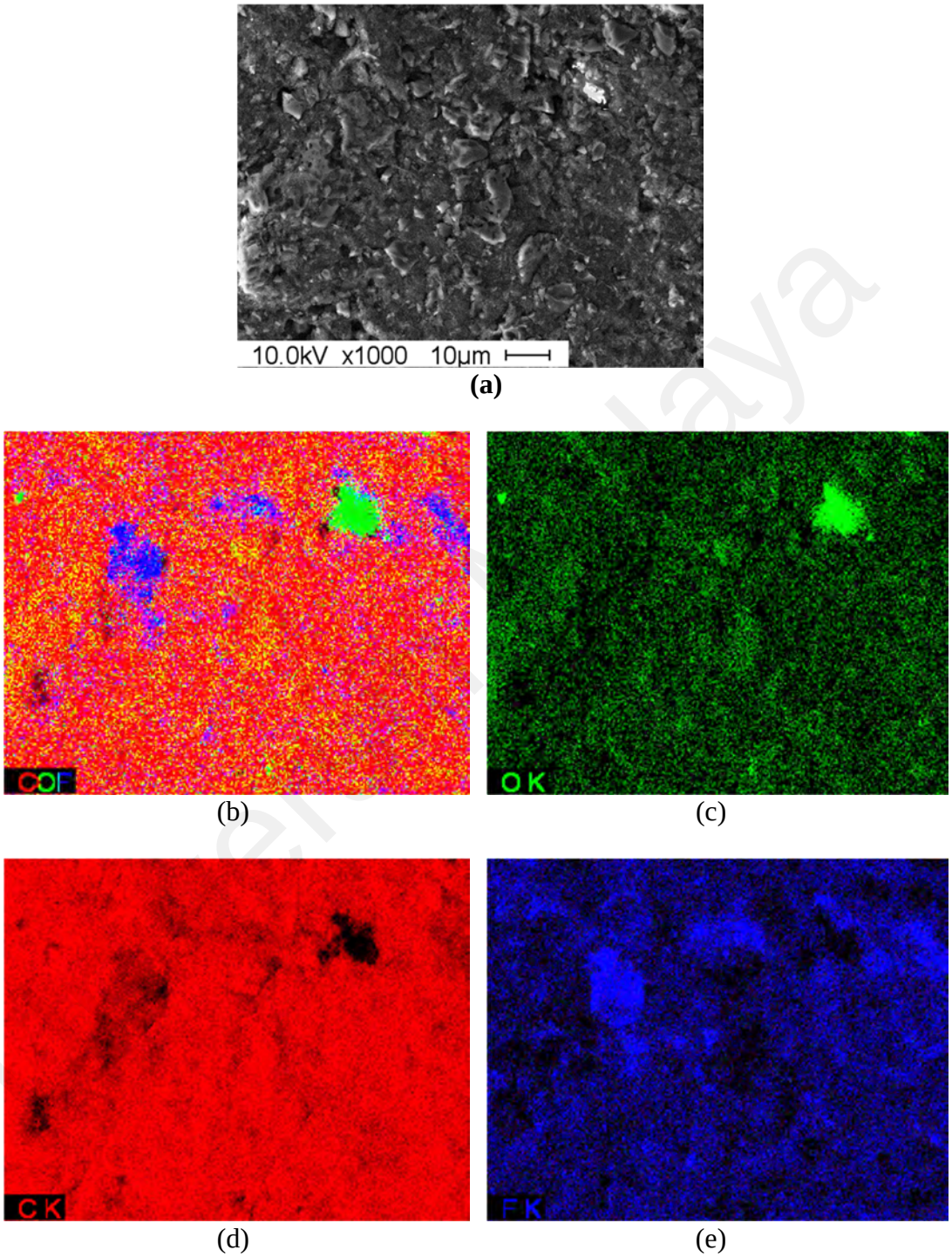

(a)

(b) (c)

(d) (e)

Figure 4.3: FESEM-EDX elemental mapping that captures (a) surface morphology and the distribution of (b) carbon-oxygen-fluorine, (c) oxygen, (d) carbon and (e) fluorine on the surface 20PTFE electrode.

Table 4.2: Elemental composition of electrodes with different compositions of PTFE

	Atomic percentage, %			
Elemental	**10PTFE**	**20PTFE**	**30PTFE**	**40PTFE**
C	91.47	86.24	84.40	79.81
O	3.79	4.58	3.00	2.82
F	4.58	9.04	12.41	17.11
Si	0.15	0.14	0.18	0.26

Additionally, Figure 4.4 illustrates a higher magnification of emission scanning on the surface of the 20PSAC composite electrode. Figure 4.4(a) captures a particle of PSAC, which has a size of approximately 80 µm, as depicted by the dimension in red. This length matches the predetermined particle size of powdered PSAC for electrode preparation (upon grinding and sieving), which is less than 100 µm. The non-uniform pore size is also evident on the surface of the electrode. Generally, the 20PSAC electrode surface is rough, consists of a wide range of particle sizes. It is also clearly seen that this composite electrode consists of a wide range of pore sizes on its surface, from meso (2-50 nm) to macro (>50 nm) pores. FESEM at higher magnification on one of the pores reveals the presence of a smaller pore at the opening of a bigger pore, as shown by Figure 4.4(b). Referring to a nanoscale dimension specified in Figure 4.4(b), it validates the presence of mesopores. However, due to the irregular and uneven surface of the electrode, the presence of micropores (<2 nm) cannot be visually proven.

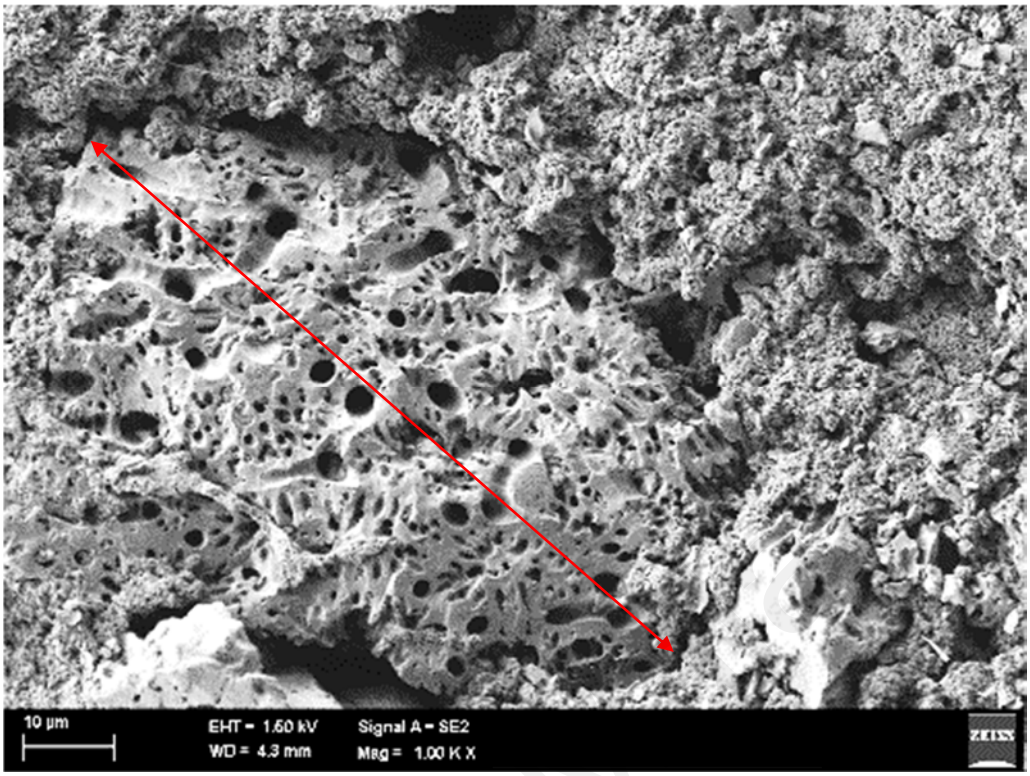

(a)

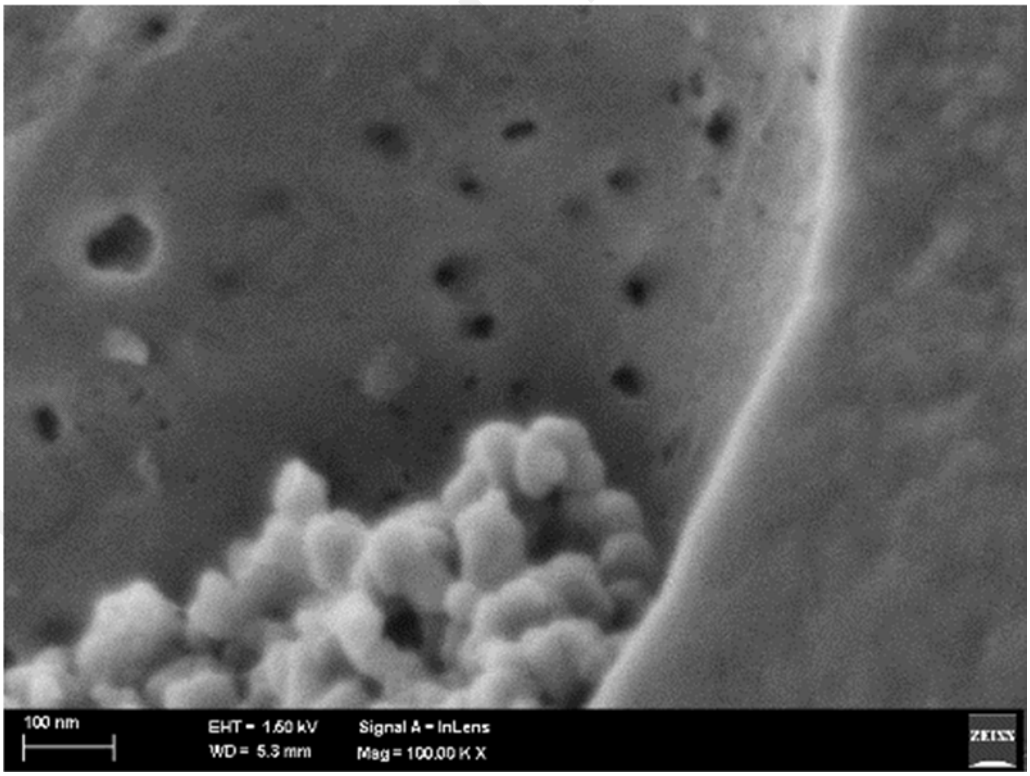

(b)

Figure 4.4: FESEM imaging showing a wide range of pore size available in PSAC-PTFE composite electrode (a) 1000X and (b) 100000X magnification.

4.1.3 Cyclic voltammetry, CV

Figure 4.5 shows the cyclic voltammogram of the prepared electrodes. The error bar is deduced from the standard deviation of the triplicates run. In between each run, the electrode surface was subjected to polishing and drying steps. The average standard deviation for each electrode is listed in Table 4.3. 10PTFE shows the highest value of average standard deviation (± 91 μA). After every polishing step, a new surface area on 10PTFE has been introduced, but it leaves a noticeably large amount of carbon particles on the polishing pad. The PSAC and carbon black easily come out from the electrode during the typical polishing step. This suggests that 10% of PTFE is not sufficient to bind the PSAC and carbon black. Meanwhile, a lower value of the average standard deviation is found for the electrode with a higher percentage of PTFE (20PTFE, 30PTFE & 40PTFE), suggesting a satisfactory amount of binder has been used in preparing the PSAC-PTFE composite electrode.

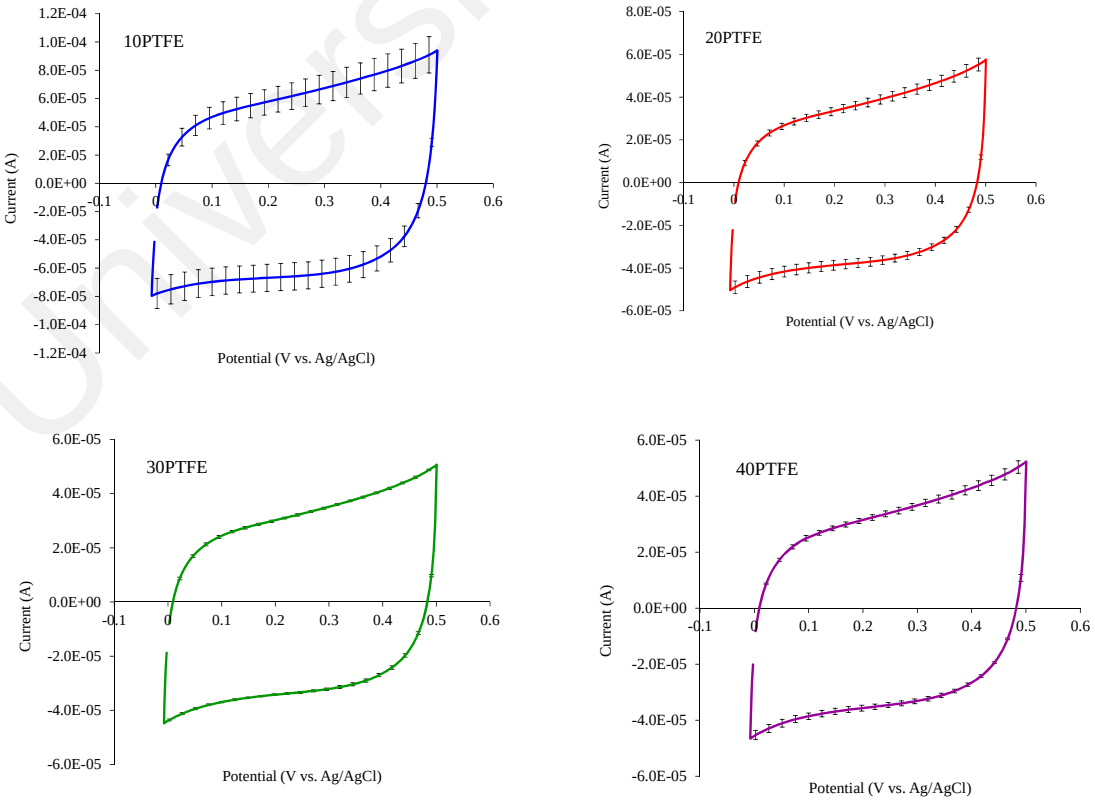

Figure 4.5: Cyclic voltammograms of 10PTFE, 20PTFE, 30PTFE and 40PTFE in 0.5 M NaCl at a scan rate of 5 mV/s.

Table 4.3: Average standard deviation deduced from the triplicates run of CV by different compositions of PTFE.

	10PTFE	20PTFE	30PTFE	40PTFE
Average standard deviation, µA	± 91	± 21	± 0.4	± 10

4.1.4 Double-layer capacitance, C_E

Double-layer capacitance for each electrode is estimated from the average value of current produced by the CV analysis. The effect of varying the amount of PTFE on the geometrical area normalised electrode double-layer capacitance, C_E is calculated using Equation 4.1,

$$C_E = \frac{1}{2(E_2 - E_1)Av} \int_{E_1}^{E_2} i(E)\ dE \qquad \text{Equation 4.1}$$

where E_1 and E_2 are the lower and upper limits of potential, $i(E)$ is the instantaneous current, $\int_{E_1}^{E_2} i(E)dE$ is the total voltammetric charge obtained by integration of forward and backward sweep in CV, (E_1−E_2) is the selected potential width (e.g., 0.2-0.3 V), A is the geometrical surface area of the electrode (0.196 cm^2), and v is the scan rate.

The estimated values of C_E obtained from four electrodes with different PTFE amounts are presented in Figure 4.6. The highest C_E (63.7 mF/cm^2) is attained by 10PTFE, and it has the lowest amount of PTFE, among others. As for 20PTFE, the amount of C_E is found to be decreased by 42%. Further increase of PTFE from 30% to 40% does not show a steep reduction in capacitance where it remains at a value of 33 to 34 mF/cm^2, respectively. Thus, this proves that the reduction of C_E is mainly due to the reduction of the electrode surface area. As the amount of PTFE is increased, it impairs the available surface area of PSAC, including its pores. However, all these C_E values are apparently overestimated as the electrode has a large surface area due to its porous characteristics. To consider the effect of the electrochemical active surface area on the double layer

capacitance, the electrochemical active area normalised electrode double-layer capacitance, C_E* is deduced. The geometrical surface area term in Equation 4.1 is now replaced by the estimated electrochemical active surface area tabulated in Table 4.1. The electrochemical active area normalised electrode double-layer capacitance, C_E* is presented in Figure 4.6. From this figure, the relationship between the capacitance and the electroactive surface area is clearly seen as the C_E* lies between a small range of C_E* (6.7 to 8.0 mF/cm^2) for all the electrodes which have different compositions of PTFE.

The capacitance of electrodes is well reported in various studies of supercapacitor. It is commonly addressed as specific capacitance for which the term geometrical area in Equation 4.2 is replaced by the mass of the active material in the electrode. On the other hands, Pandolfo and Hollenkamp (2006) reported values of capacitance for several typical carbonaceous electrode materials range between 8 to 35 µF/cm^2 depending on the electrolyte used and the properties of carbon material (e.g., surface area). Elsewhere, Ji et al. (2014) reported on a range electrode's capacitance between 4 to 16 µF/cm^2 and it stabilized at 4 to 5 µF/cm^2 for carbon materials with surface area of 1500 m^2/g. In this present work, the true capacitance of 20PTFE was estimated to be 4 µF/cm^2 for which the specific surface area of the electrode was found to be 384 m^2/g with an estimated of 0.5 mg PSAC (which is considered as the active material) available on the surface area of the electrode during the CV test. Hence, the C_E of the prepared electrode in this study is considered comparable to the range of capacitance reported by Ji et al. (2014).

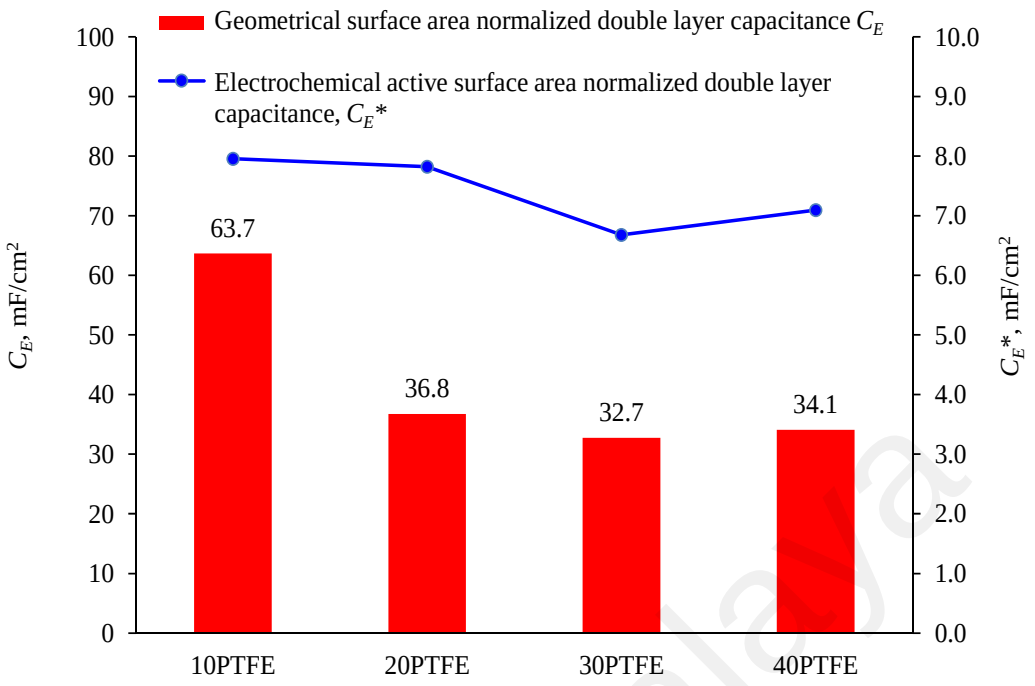

Figure 4.6: Estimated C_E and C_E* by using PSAC electrodes with different amount of PTFE.

Although the 10PTFE electrode gives the highest active surface area and C_E, the requirement for enough strength of binding between the powdered PSAC and carbon black is not achieved. The new surface introduced by 10PTFE after the polishing step, with the apparently high average standard deviation is claimed due to an insufficient amount of binder. On the contrary, Park et al. (2007) reported that the best carbon sheet was prepared using 4 wt% of a binder for the desalination purpose, according to the optimum obtained capacitance calculated from the CV analysis. If the optimum capacitance is to become the main criterion by ruling out the requirement of minimum mechanical strength, then 10% of PTFE seems to be the best amount for the preparation of the PSAC-PTFE composite electrode. However, due to the physical characteristics of the PSAC and the amount of carbon black used, 20PTFE is better than 10PTFE in providing sufficient binding strength between the PSAC (active material) and carbon black (conductive agent).

4.1.5 Electron transfer resistance

The potentio electrochemical impedance spectroscopy (PEIS) for 20PTFE, 30PTFE and 40PTFE are compared. The PEIS data are analysed by fitting them into the Randles equivalent electrical circuit, as illustrated in the inset of Figure 4.7. All the three Nyquist plots similarly display a depressed semicircle over a high-frequency range with the centre lying some distance below the x-axis. A depressed semicircle can be explained by the Constant Phase Element (CPE). CPE is the deviation from true capacitor behaviour, and it can be attributed to the presence of double-layer capacitance (Lvovich, 2012) and electrode surface roughness (De Levie, 1965). This is in agreement with the rough and non-uniform surface area of the PSAC-PTFE electrode, as illustrated by Figure 4.4.

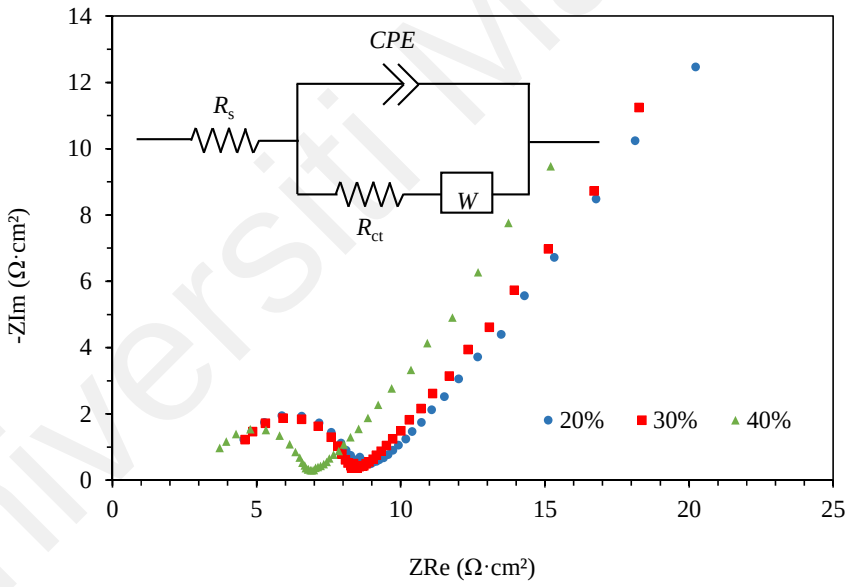

Figure 4.7: Nyquist plot of PEIS for 20PTFE, 30PTFE and 40PTFE. Inset is the equivalent Randles circuit

Meanwhile, the diameter of the depressed loops represents the electron or charge transfer resistance, $R_{ct,}$ due to the Faradaic process. R_{ct} is increasing in the following trend, 40PTFE (3.7 $\Omega \cdot cm^2$) < 30PTFE (4.6 $\Omega \cdot cm^2$) < 20PTFE (5.2 $\Omega \cdot cm^2$). The highest electron transfer by 40PTFE can be described by the high conductivity of the prepared electrode due to the durable binding of PSAC and carbon black using a higher amount of PTFE. However, this value of R_{ct} is considered comparable between the other two electrodes. In

addition, a long straight line with an angle of 45° to the real axis for all the three electrodes represents semi-finite diffusion impedance, also called the Warburg impedance.

4.1.6 Summary

This work demonstrates the effect of PTFE composition as a binder in the preparation of the PSAC-PTFE composite electrode. The 10PTFE electrode provides the highest electrochemical active surface area and C_E. However, it was observed that 10% PTFE was not sufficient to firmly bind the PSAC and carbon black for the purpose of preparing a durable free-standing electrode sheet for water or waste-water treatment. On the contrary, 20PTFE has sufficient binding strength between PSAC and carbon black. It produces an acceptable reproducibility in the voltammogram to deduce the double layer capacitance properties of a PSAC-based electrode. It is proven that increasing the amount of PTFE from 10% to 20% in the electrode preparation does impair the electrochemical properties in terms of the electrochemical active surface area and C_E. Further increase of PTFE up to 40% does not significantly help in improving the electrochemical properties of the PSAC-PTFE hybrid electrode. Meanwhile, the electrochemical active surface area for 20PTFE was estimated 5 times larger than its geometrical surface area. The electrode consists mainly of carbon and a wide range of pore sizes, from meso to macro pores, as proven by the EDX and FESEM analysis. The C_E and R_{ct}, for 20PTFE, 30PTFE, and 40PTFE, were observed to have almost comparable between each other.

In conclusion, the PSAC electrode has been prepared with an appropriate amount of binder. The electrochemical properties of the PSAC electrode have been studied and it have been proven to serve as a 3D electrode for possible use as a porous electrode for electrochemical removal of Hg from an aqueous solution.

4.2 Part II: Electrochemical Properties and Electrode Reversibility Studies of Palm Shell Activated Carbon (PSAC)

The feasibility of PSAC as an electrode for wastewater treatment was studied for the first time using a common redox couple probe, ferro/ferricyanide ($Fe(CN)_6^{4-}/Fe(CN)_6^{3-}$). Prior to the electrode reaction studies, the most suitable supporting electrolyte and the optimum percentage of carbon black (CB) were determined.

4.2.1 Effect of supporting electrolytes

A suitable supporting electrolyte is necessary in cyclic voltammetry test. A good supporting electrolyte (also called inert electrolyte) ensure that the ionic strength of the solution is high. Hence the electric field is homogeneous, near-zero and is not disturbed by the oxidation or reduction of the analyte concerned. The effect of supporting electrolyte was studied by means of cyclic voltammetry in three different types of aqueous electrolytes, namely 0.5 M HCl (acidic), 0.5 M NaCl (neutral), and 0.5 M NaOH (basic). The scan rate was registered at 5 mV/s, and a wide potential range (−1.5 to 1.0 V) was applied to investigate the current-potential behaviour of the PSAC electrode. A substantial reduction peak was observed for all the electrolytes studied, as shown in Figure 4.8. Reduction peaks were observed at −0.36 V, −0.47 V, and 0.59 V for HCl, NaCl, and NaOH, respectively. The reduction of surface oxide is expected at approximately −0.5 V (Besenhard & Fritz, 1983; Georgiou et al., 2010), and the quinone and hydroquinone groups are predicted to be responsible for the redox characteristics of the activated carbon electrode (Pakuła et al., 1995). In addition, a smaller range of potential was applied to closely observe the current-potential behaviour from 0 to 0.5 V. A slow scan rate (5 mV/s) was registered, and it was scanned forward (positively) from 0 to 0.5 V. No anodic and cathodic peaks were observed for the three electrolytes within that small potential range. However, for the acidic environment, a significant decrease of current was observed as the applied potential was scanned backwards from 0.5 to 0 V.

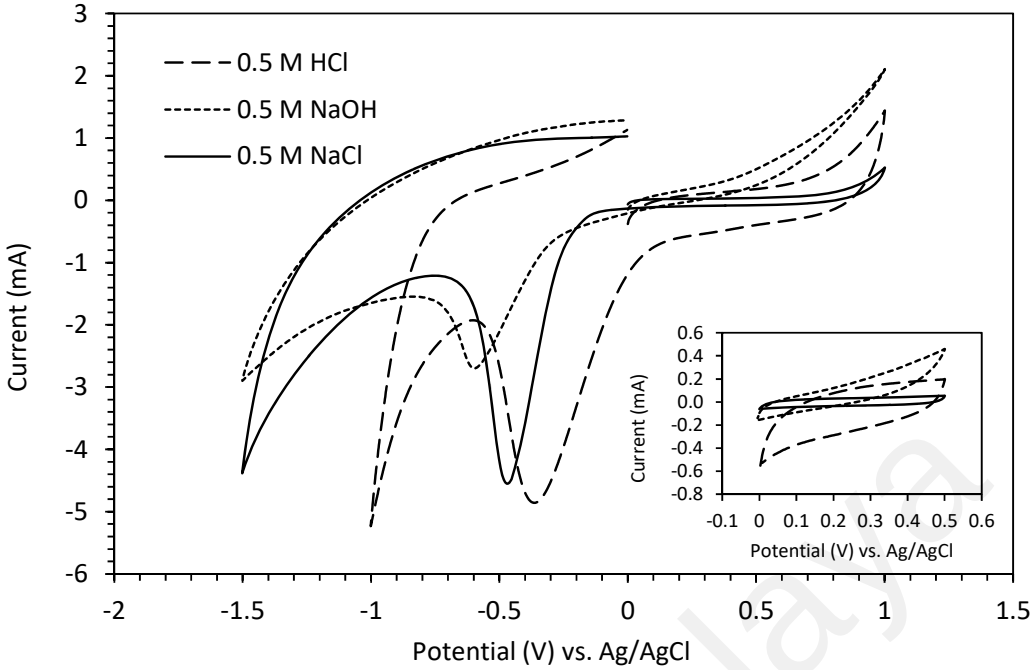

Figure 4.8: Cyclic voltammetry for three different electrolytes (0.5 M HCl, 0.5 M NaOH, and 0.5 M NaCl) without any pH adjustment at a scan rate of 5 mV/s using a PSAC electrode of 5 mm diameter. Inset shows the cyclic voltammetry at 0 to 0.5 V of applied potential.

Due to the porous characteristic and surface chemistry of the PSAC electrode, the selection of supporting electrolyte is crucial for the reversibility study. Hence, according to the voltammogram (Figure 4.8), NaCl was found to be a more suitable supporting electrolyte for the reversibility study of the PSAC electrode than HCl and NaOH. NaCl provides sufficient ionic strength to increase the conductivity of the solution with the smallest background current and the highest hydrogen evolution overpotential, among others. At a distance close to the electrode, both migration and diffusion are responsible for the mass transport. For electrode reaction studies, the migration effect was minimised by the addition of excess supporting electrolyte. A supporting electrolyte to active species ratio of more than 100 was suggested to minimise the effect of migration (Dickinson et al., 2009). Therefore, the molarity of 0.5 NaCl was claimed as sufficient and employed as the supporting electrolyte in the subsequent electrochemical cell setup for electrode reaction studies. Additionally, it is convenient to estimate the geometrical area normalised

electrode double-layer capacitance, C_E using Equation 4.1. The estimated C_E of the PSAC electrode is 33.3 mF/cm^2. When NaOH (87.2 mF/cm^2) and HCl (333.2 mF/cm^2) were used as the supporting electrolyte, C_E showed a higher value. However, these values apparently are overestimated as the electrode has a large surface area due to its porous characteristics.

4.2.2 Effect of amount of carbon black (CB)

CB acts as a conductive agent in an electrode because of its good conducting properties. An appropriate amount of CB in the total electrode mass is crucial to provide sufficient conductivity to the electrode for transferring the electron. The electrochemical characteristics of the PSAC electrode using three different amounts of CB were analysed using cyclic voltammetry and PEIS. Figure 4.9 shows the cyclic voltammogram of redox $Fe(CN)_6^{4-}/Fe(CN)_6^{3-}$ using the PSAC electrode with different amounts of CB (10, 20, and 30 wt%). An electrode without CB (PSAC00CB) was also prepared as a control. The potential was scanned positively from 0 to 0.5 V, and this range was observed sufficiently positive to oxidise $Fe(CN)_6^{4-}$. Along this step, the anodic current, i_{pa}, was produced due to the oxidation of active species. Furthermore, when the potential was reversely scanned from 0.5 to 0 V, the $Fe(CN)_6^{3-}$ was reduced to $Fe(CN)_6^{4-}$, where the cathodic current, i_{pc}, was clearly observed.

In addition, Table 4.4 lists the values of anodic peak current (i_{pa}), cathodic peak current (i_{pc}), the i_{pa} to i_{pc} ratio, as well as the separation peak between the anodic peak potential (E_{pa}) and the cathodic peak potential (E_{pc}). The control electrode (PSAC without CB) produced the most negligible peak current response with the highest background current, among others. Moreover, PSAC without CB showed a wider peak separation between potential E_{pa} and E_{pc}, which can be further interpreted with the slow electron transfer. By contrast, PSAC20CB gives the highest anodic and cathodic current among

others, with the ratio between them close to unity. It may be assumed that increasing the CB amount will increase the peak current response; however, the outcome was the opposite. When the amount of CB was increased to 30%, the peak current response was the least. In this case, as the specific surface area of CB was relatively increased by volume, the amount of PTFE was not sufficient to completely bind the PSAC particles and CB. By contrast, PSAC10CB showed a higher peak current response than 30CB but lesser than 20CB. This finding is further verified by the PEIS analysis, as shown by the Nyquist plot in Figure 4.10.

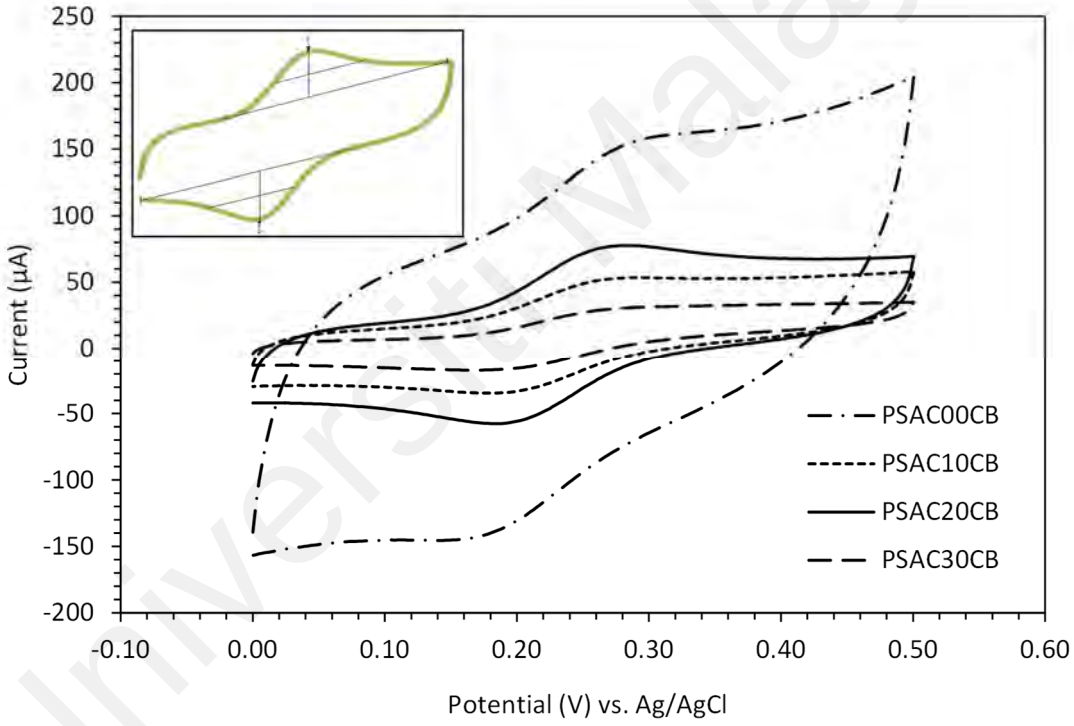

Figure 4.9: Comparison of cyclic voltammogram of $Fe(CN)_6^{4-}/Fe(CN)_6^{3-}$ redox in 0.5 M NaCl using the PSAC electrode (0.196 cm^2 geometrical surface area) with different amounts of CB. Inset shows the identification of oxidation (top) and reduction (bottom) peaks of the PSAC20CB electrode.

Table 4.4: Values of the anodic and cathodic peak current of PSAC with various amounts of CB

Electrode	i_{pa}, µA	i_{pc}, µA	Ratio i_{pa}/i_{pc}	E_{pa}, mV	E_{pc}, mV	ΔE_p, mV
PSAC00CB	28.7	23.4	1.23	281	186	95
PSAC10CB	18.3	22.9	0.80	266	190	76
PSAC20CB	36.5	38.4	0.95	271	193	78
PSAC30CB	11.3	14.5	0.78	271	191	80

Figure 4.10 shows the Nyquist plot for the PSAC electrode with different percentages of CB (0, 10, 20 and 30 wt%) in 0.5 M NaCl, which was used as the supporting electrolyte. The PEIS data were analysed by fitting it to the Randles equivalent electrical circuit model as illustrated in the inset of Figure 4.10. The EIS spectrum of an electrode is divided into the following: (i) the solution/electrolyte resistance, R_s, between the working and reference electrode at >1 kHz, (ii) the capacitive, C, effects at intermediate frequencies at <1 kHz, (iii) the charge transfer resistance, R_{ct}, and (iv) Warburg impedance, W, resulting from the frequency dependence of diffusion in the electrode-electrolyte interface at low frequencies, <5 Hz. The electron transfer resistance of PSAC20CB was the lowest (2.4 $\Omega \cdot cm^2$), while PSAC10CB showed an electron transfer resistance of 12.7 $\Omega \cdot cm^2$. As expected, PSAC without CB had the highest electron transfer resistance (24.6 $\Omega \cdot cm^2$). Hence, PSAC20CB has been proven to provide the fastest electron transfer, among others. Overall, the findings from cyclic voltammetry and PEIS prove that the amount of CB helps to increase the electron transfer of PSAC, and 20% CB is considered the optimum amount for a quasi-reversible electrochemical process.

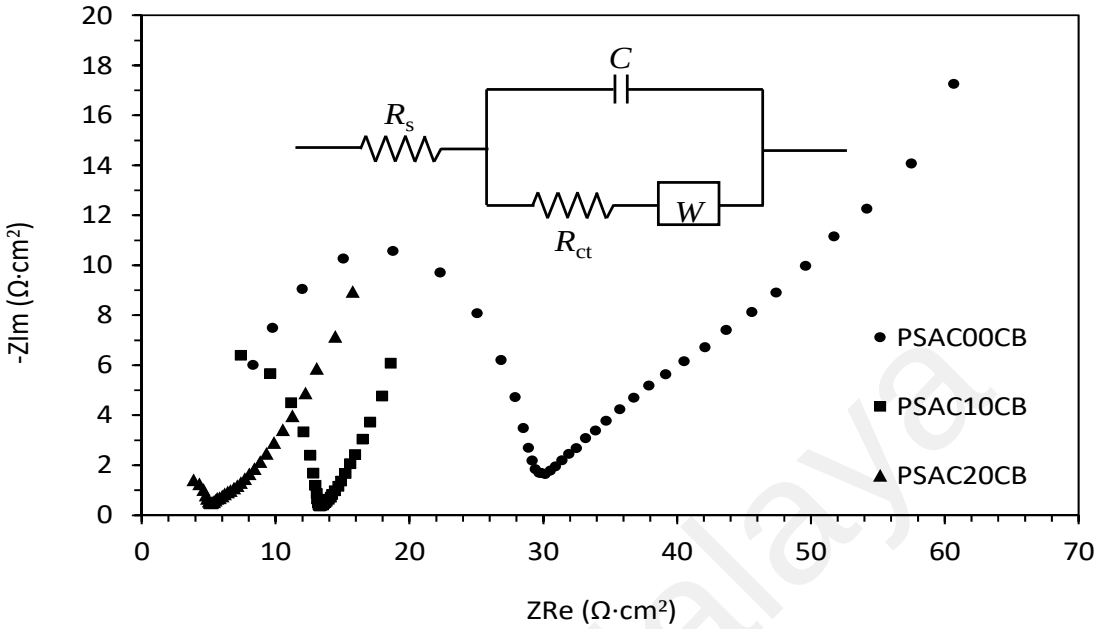

Figure 4.10: PEIS for different amounts of CB in the PSAC electrode.

4.2.3 Deviation from the Cottrell assumption

The inset in Figure 4.11 reveals that the PSAC electrode does not correspond to that predicted by the Cottrell equation for which plot of $it^{1/2}$ vs t should yield a horizontal straight line similar to the Pt electrode. It is well understood that the $Fe(CN)_6^{4-}$/ $Fe(CN)_6^{3-}$ redox using a platinum electrode takes place as per the Cottrell assumption due to a fast electron kinetic reaction. Such results for PSAC are according to the previous findings in CV analysis (showing quasi-reversible reaction). The slow electron transfer might have probably caused this behaviour. The chronocoulometric mode was employed to distinguish further the contribution of charge, Q_t, from double-layer charging and the electrode reaction due to adsorbed active species on the electrode. The two quantified terms were represented by the intercept of the plot of charge, Q_t as a function of time, $t^{1/2}$, as shown in the inset of Figure 4.11. The quantitative parameter was interpreted using Equation 2.15. The intercept represents the double layer charging of the background

current and any presence of interfacial interaction such as adsorption. The amount of charge due to this phenomenon was found to be 244 µA·s and 222 µA·s for PSAC and Supelco, respectively.

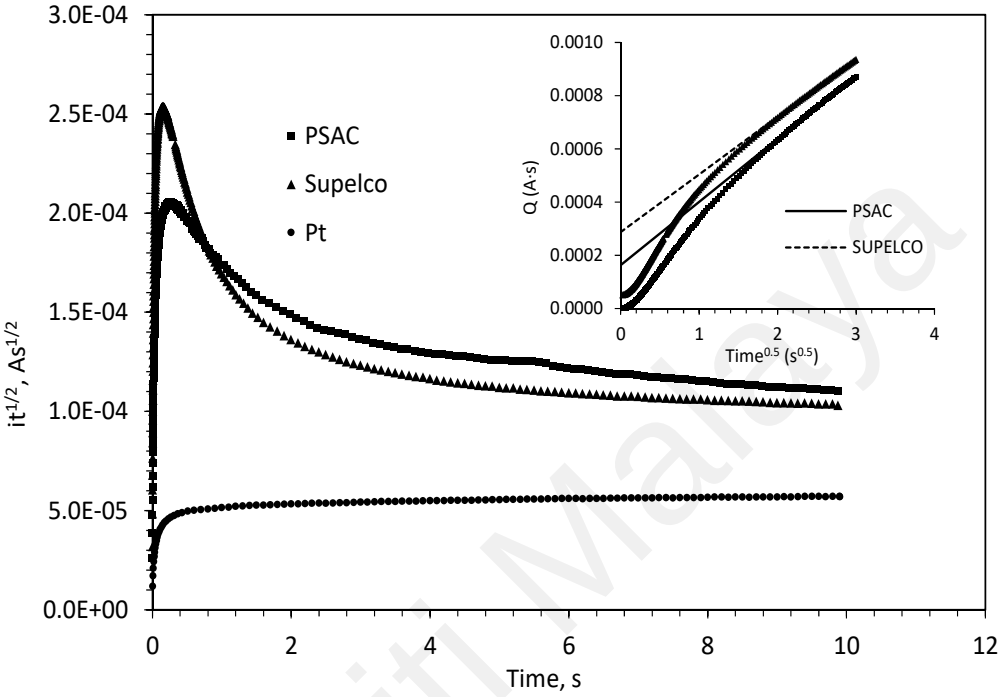

Figure 4.11: A plot of $it^{1/2}$ vs t for a Cottrellian system, showing a deviation of the PSAC and Supelco from the Pt electrode. Inset shows the CC plot of PSAC and Supelco at a voltage step-up from 0 to 0.4 V.

The deviation of electrode reaction of PSAC from Cottrell's assumption is obviously due to the porous characteristics of PSAC itself. Therefore, it is necessary to determine the physical characteristic of powdered PSAC and PSAC electrodes. For this reason, the surface area and porosity analysis were carried out for powdered PSAC, PSAC electrode, and CB. Figure 4.12 shows the nitrogen adsorption-desorption isotherms for powdered PSAC, CB, and PSAC20CB electrodes. At the low relative pressure region (<0.05), steep adsorption of nitrogen corresponding to Type I isotherm was observed, thus indicating the presence of micropores. A slim and long hysteresis loop was observed between 0.3 to 0.6 of relative pressure for powdered PSAC and PSAC20CB, corresponding to Type IV

isotherm according to the IUPAC classification. The hysteresis loops with adsorption and desorption isotherms parallel to each other and nearly horizontal indicate the presence of mesopores with Type H4. These characteristics correspond to the presence of slit-like shaped pores in PSAC. Hence, the adsorption-desorption isotherm for powdered PSAC and PSAC electrodes corresponded to a combination of Type I and IV isotherms, indicating the presence of both micropores and mesopores in the samples. Conversely, the CB isotherm indicates a Type IV isotherm with the Type H3 hysteresis loop, in which there was no evidence of any plateau at high P/P°.

The surface area analysis confirms that powdered PSAC has a specific BET surface area of 1,014 m^2/g and it is considered as acceptable surface area to be used in preparing a porous electrode. During the electrode preparation, by adding a low surface area of CB (62 m^2/g) and PTFE to a high specific surface area of powdered PSAC, the specific surface area of the prepared electrode becomes only 384 m^2/g. This value is higher as compared to the activated carbon electrodes (300 m^2/g) prepared by Duan et al. (2015). Duan et al. (2015) also used PTFE as the binder but have not employed any conductive agent in the electrode preparation. The more the amount of CB added while preparing the electrode, the lower the specific area of the PSAC electrode. Furthermore, according to the *t*-plot analysis, powdered PSAC and PSAC electrodes had micropores predominantly, with 828 m^2/g and 230 m^2/g of the micropores area, respectively. For PSAC20CB, the micropores area contributed about 60% of the total pore area. The insets in Figure 4.12 confirm that powdered PSAC and PSAC20CB exhibit micropores predominantly, with the highest pore size distribution being at 8.4 Å and 9.2 Å pore width, respectively. On the other hand, CB consisted of a considerably larger pore width and mesopores mainly at the peak of 24 Å. For the PSAC20CB electrode, the pore size distribution was slightly shifted to a bigger pore width than the powdered PSAC. This is probably because most of the micropores area of PSAC would have been blocked by the CB and PTFE, as these

acted as the conductive agent and the binder, respectively. Both micropores and mesopores characteristics were observed in the PSAC20CB electrode. This wide range of pore width is considered sufficient to provide an effective electrochemical active surface for the electrode reaction for the removal of metal ions from wastewater. In conclusion, from the surface area analysis, the deviation of Cottrell's assumption is proven due to the porous characteristics of PSAC. The prepared electrodes is also foreseen to provide the 3D electrochemical cell system.

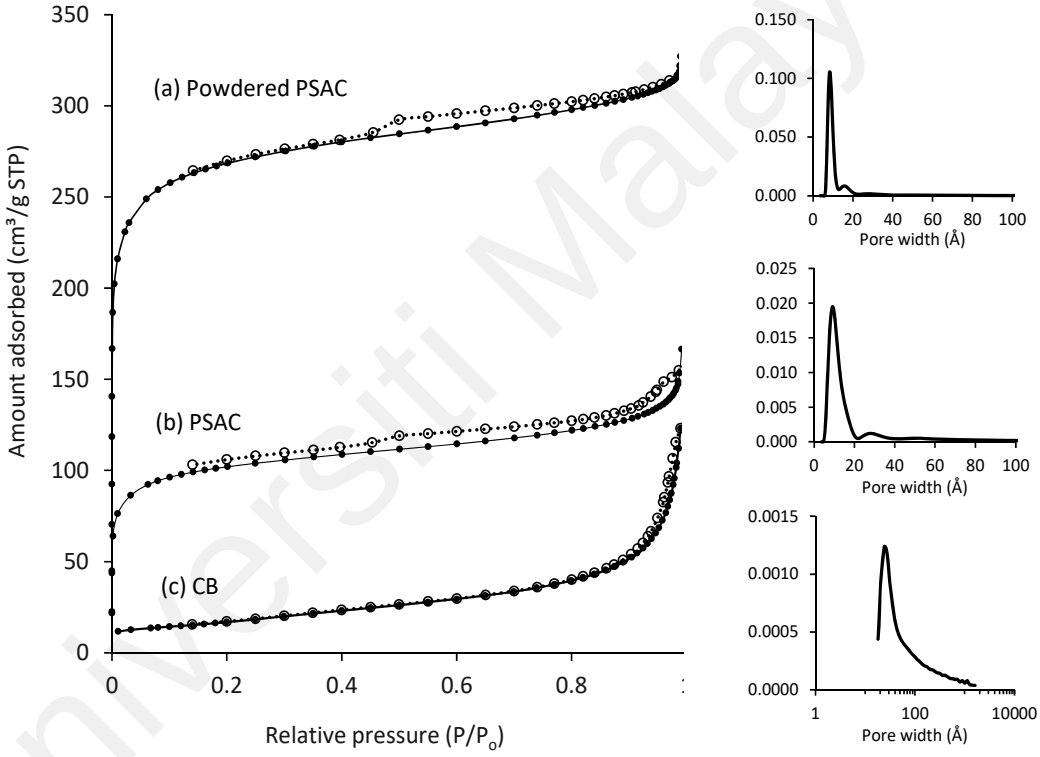

Figure 4.12: Nitrogen adsorption (filled symbols) and desorption (open symbols) isotherms for (a) powdered PSAC (b) PSAC electrode and (c) CB. Insets show the pore size distribution for powdered PSAC, PSAC electrode, and CB.

4.2.4 Electrochemical reversibility study

A comparison of cyclic voltammogram of PSAC20CB and platinum electrodes in 5 mM $Fe(CN)_6^{4-}$ in 0.5 M NaCl at a scan rate of 5 mV/s is shown in Figure 4.13. The measured current was normalised to the geometric area of the electrode surface. It can be seen in Figure 4.13(a) that the background currents in forward and backward scans for

PSAC20CB are well separated. This is in fair agreement with the large capacitance feature of carbon-based material reported by several researchers (Huang et al., 2014; Li et al., 2002). The capacitive current for PSAC20CB was substantially high compared to platinum. As illustrated in Figure 4.13(b), platinum is well known to be governed by the reversible electron transfer reaction ($\Delta E_p \approx 59/n$ mV). It is generally useful to consider the peak current ratio (i_{pa}/i_{pc}) instead of an individual peak current value. This ratio approaches unity for a reversible process as it has been observed for the platinum electrode.

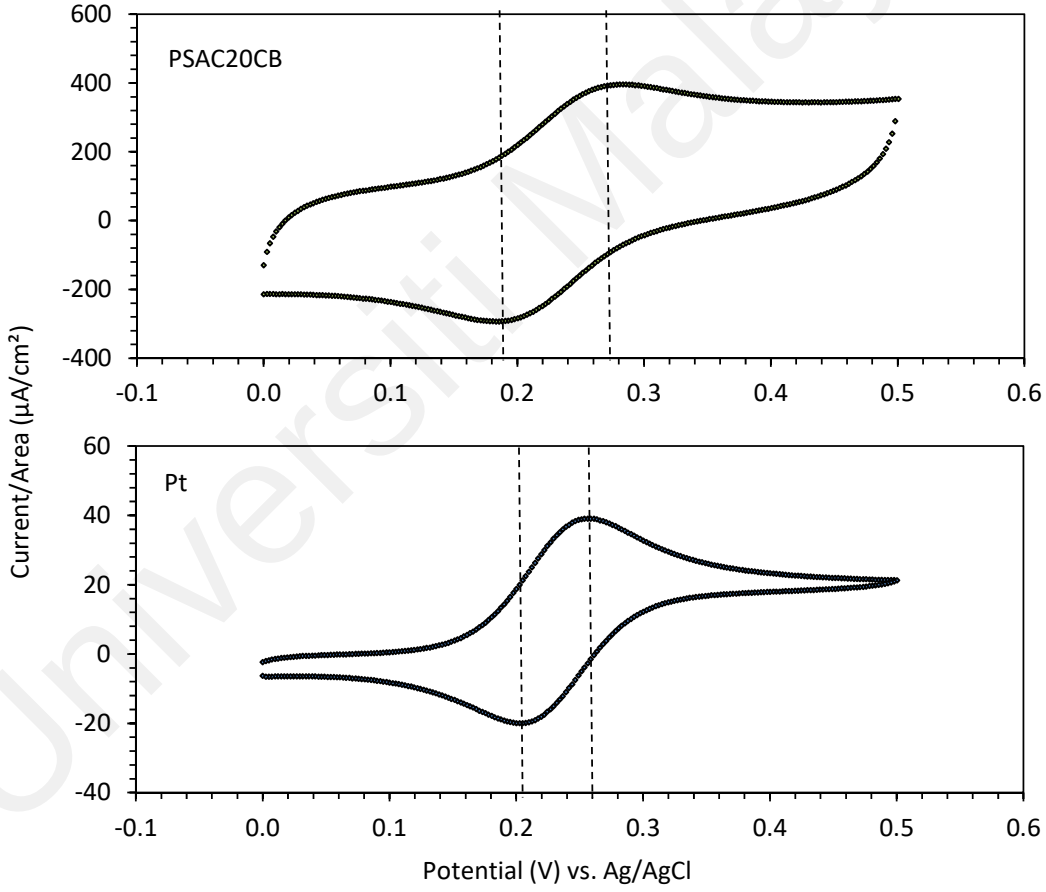

Figure 4.13: Cyclic voltammetry of PSAC20CB and platinum (Pt) electrodes in 5 mM $Fe(CN)_6^{4-}$ in 0.5 M NaCl at a scan rate of 5 mV/s.

Although the i_{pa}/i_{pc} ratio of PSAC is close to unity, PSAC is characterised to have quasi-reversible as the peak-to-peak potential, $\Delta E_p > 59/n$ mV. The CV result for PSAC has a similar pattern to a typical CV voltammogram for a quasi-reversible electron

transfer, as illustrated by Figure 2.5, in Chapter 2. Further analysis of the observed current at various scan rates proved the quasi-reversible behaviour of PSAC, as shown in Figure 4.14. Increasing the scan rate from 1 mV/s to 30 mV/s resulted in a rise in ΔE_p values from 78 to 125 mV by considering that the number of electron transfers, *n*, is equal to 1. The anodic and cathodic peak currents (i_{pa} and i_{pc}) function is proportionally linear to the scan rate as shown by the inset (i_p versus $v^{½}$) in Figure 4.16, with a slope of 0.41. The linear relationship verifies that the reversibility study of PSAC20CB was a diffusion-controlled process. In addition, the quasi-reversible process observed in this study reveals that the electron transfer kinetics are not fast enough to maintain the surface concentrations of the reactant and the product at the values required by the Nernst equation. When the scan rate was increased further (e.g., 50 mV/s), the capacitive current increased much faster than the faradaic current. Suppression of the faradaic current by the capacitive current resulted in difficulties in identifying the highest peak current. A further increase in the scan rate (e.g., 100 mV/s) led to an overlap of the faradaic current with the capacitive current.

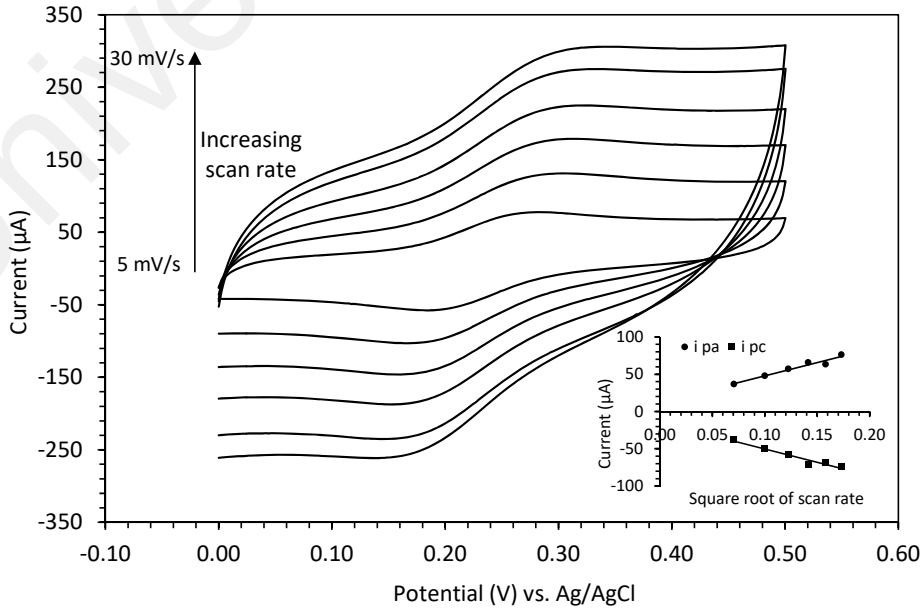

Figure 4.14: Cyclic voltammetry response of 5 mM potassium ferrocyanide on PSAC in 0.5 M NaCl at various scan rates (5, 10, 15, 20, 25, and 30 mV/s). Inset shows the anodic and cathodic peak current versus the square root of the scan rate.

The quasi-reversible process by PSAC can be explained by equivalent effect, both the electron transfer rate and the mass transfer rate. The Nicholson method was used to estimate the standard heterogeneous electron transfer rate constant, k^o, using Equation 2.9, where Ψ is the kinetic parameter obtained from Nicholson (1965). In the absence of the actual measurement, it is assumed that the transfer coefficient is equal to 0.5. For simplification in determining the value of ψ, a relationship between ψ and ΔE_p was computed by an empirical equation, Equation 2.10 (Lavagnini et al., 2004) to represent a working curve at the range of ΔE_p = 72 to 212 mV. The constants were deduced from the nonlinear regression fitting, where a = −0.5405, b = 0.0014, and c = −0.017. The plot of ψ versus $v^{½}$ allows the kinetic parameter, k^o to be deduced from the slope, which resulted in k^o equalling to 3.5×10^{-3} cm·s^{-1}. For the same redox couple, this value is much higher than the other carbon-based electrodes. For comparison, a value of 3.6×10^{-4} cm·s^{-1} was reported by Lavagnini et al. (2004), 1.4×10^{-4} cm·s^{-1} by Modestov et al. (1997) and 6.88×10^{-4} cm·s^{-1} by Ajeel et al. (2016). A larger k^o value implicates a shorter time to achieve equilibrium than a smaller value of k^o (Bard & Faulkner, 2001).

4.2.5 Electroreduction of Hg

The presence of Hg reduction was validated by the cyclic voltammetry analysis using different scan rates (5, 10, 30, 50, and 100 mV/s) as shown in Figure 4.15. Well-defined anodic and cathodic peaks were clearly observed even at a high scan rate (e.g., 100 mV/s). On the contrary, these peaks were suppressed by the double layer capacitance when $Fe(CN)_6^{4-}/Fe(CN)_6^{3-}$ probe was used at a high scan rate. From a low scan rate of 5 mV/s to 100 mV/s, the ΔE_p increased from 49 mV to 100 mV. Cyclic voltammetry analysis shows that PSAC20CB was feasible to reduce Hg under the quasi-reversible electron transfer reaction. Additionally, the reduction potential of Hg was shifted to a more negative value compared to $Fe(CN)_6^{3-}$. There are several possible reaction pathways of Hg reductions in the cell, as listed in Table 4.5 (Harris, 2010). As the standard reduction

potential of $Fe(CN)_6^{3-}$ is E° = 0.356 V, the most possible reactions are reduction of $Hg(OH)^{3-}$ and/or $Hg(OH)_2$, wherein these have a smaller value of standard reduction potential than $Fe(CN)_6^{3-}$. On the contrary, Fleischmann and Kelsall (1984) claimed that calomel precipitation (Hg_2Cl_2) was observed at the bottom of the electrochemical cell due to the following reaction (Equation 4.3) of the elemental mercury at the cathode with aqueous $HgCl_2$.

$$Hg(l) + Hg^{2+} + 2Cl^{-} \rightarrow Hg_2Cl_2(s) \qquad \text{Equation 4.3}$$

In this study, a nickel rotating disc was employed as the electrode. However, such findings were not observed in this work.

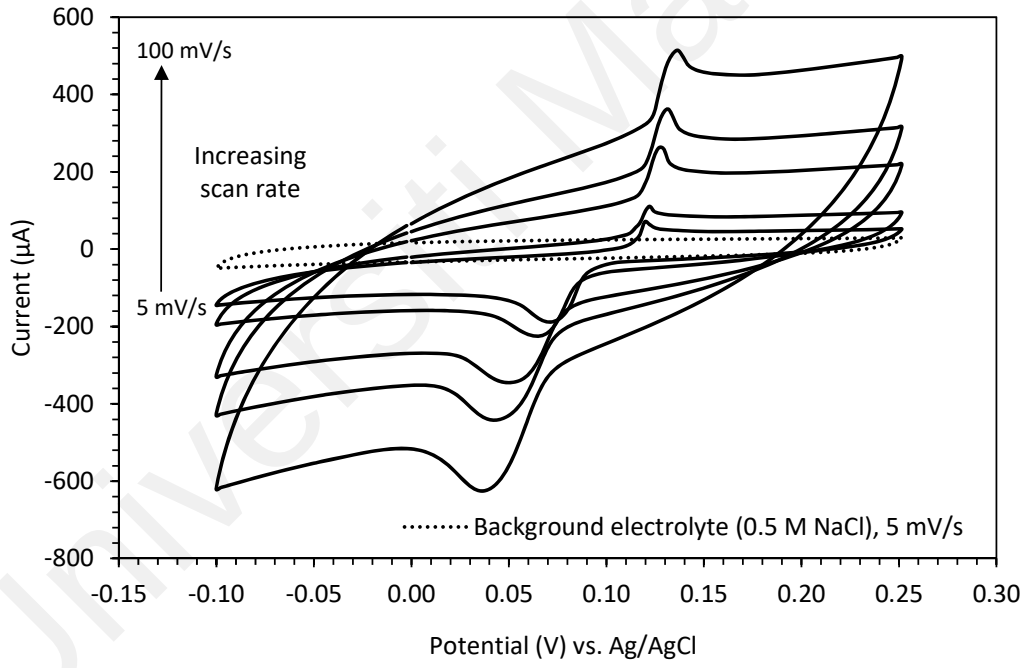

Figure 4.15: Cyclic voltammetry of 0.5 M NaCl as supporting electrolyte and 5 mM Hg^{2+} in 0.5 M NaCl at different scan rates (5, 10, 30, 50, and 100 mV/s) using a 5-mm diameter PSAC20CB.

Table 4.5: Standard reduction potential, E° (V) for possible Hg^{2+} reduction reactions (Harris, 2010)

Reactions	Standard reduction potential, *E°* (V)
$2Hg^{2+} + 2e^{-} \leftrightarrow Hg_2^{2+}$	0.908
$Hg^{2+} + 2e^{-} \leftrightarrow Hg(l)$	0.852
$Hg_2^{2+} + 2e^{-} \leftrightarrow 2Hg(l)$	0.796
$Hg(OH)_3^{-} + 2e^{-} \leftrightarrow Hg(l) + 3OH^{-}$	0.231
$Hg(OH)_2 + 2e^{-} \leftrightarrow Hg(l) + 2OH^{-}$	0.206

4.2.6 PSAC immobilised with task-specific ionic liquid (PSAC-TSIL)

The electrochemical characteristics of PSAC-TSIL and virgin PSAC were compared by cyclic voltammetry runs, for which the $Fe(CN)_6^{4-}$ was the active species. A similar range of potential (-0.2 to 0.5 V) was applied for both types of electrodes. Figure 4.16(a) shows that the virgin PSAC exhibits criteria of quasi-reversible electrochemical reaction. The ratio of the anodic peak current to cathodic peak current was found approximately 1, with the separation of anodic and cathodic peak current is about 80 mV. Additionally, a hydrogen evolution overpotential was clearly observed at 0 V as the potential was scanned backwards from 0 V towards -0.2 V. At this region, hydrogen gas is being formed from hydrogen ions. Furthermore, the pattern of the voltammogram for each cycle remains the same upon proceeding the run for another four consecutive cycles, as shown in Figure 4.16(b). A slight increase in the magnitude of anodic peak and cathodic peak with the number of cycles could be explained due to the increase of double-layer capacitance on the porous 3-dimensional PSAC electrode.

As for PSAC-TSIL, the anodic and cathodic peaks were clearly observed in the first cycle of cyclic voltammetry Figure 4.16(c). The separation peak between the anodic peak potential and the cathodic peak potential was about 140 mV. It can be interpreted that the process using this kind of electrode has a sluggish electron transfer and could be closely

explained as an irreversible electrochemical reaction. Additionally, a larger capacitance was observed in the PSAC-TSIL electrode as compared to the virgin PSAC. Moreover, upon applying a subsequent cycle of potential scanning, the magnitude of anodic and cathodic peaks become smaller and almost vanished at the fourth cycle. Such behaviour emphasises the presence of irreversible electrochemical reaction. On the other hand, an electrode reaction coupled with a chemical is strongly suggested to occur in this process. It is strongly predicted that a metal ligand is formed due to the presence of the thiolate group in TOMATS.

4.2.7 Summary

The PSAC electrode was analysed for its electrochemical properties, specifically for its electrochemical reversibility, using the most suitable supporting electrolyte that is NaCl. The present work shows that the PSAC electrode has a quasi-reversible electrode reaction for common redox probe $(Fe(CN)_6^{4-}/Fe(CN)_6^{3-}$. Adding a 20 wt% of CB in PSAC electrode has improved its conductivity with a value of 2.4 V cm^2 electron transfer resistances. For this ratio, the suitable ratio of PSAC:CB:PTFE was 4:1:1. Due to the porous characteristic of PSAC, this type of electrode provides more electrochemical active area than its geometrical surface area. The Faradaic current was observed, associated with electrode reaction double-layer and some interfacial interaction of electrode-electrolyte. Additionally, PSAC20CB provides 384 m^2/g of specific BET surface area, which consists of 60% of micropore area. Using $Fe(CN)_6^{4-}$/ $Fe(CN)_6^{3-}$ as the redox couple, it was determined that kinetic parameter k^o for PSAC electrode is higher than the several other reported carbon-based electrodes.

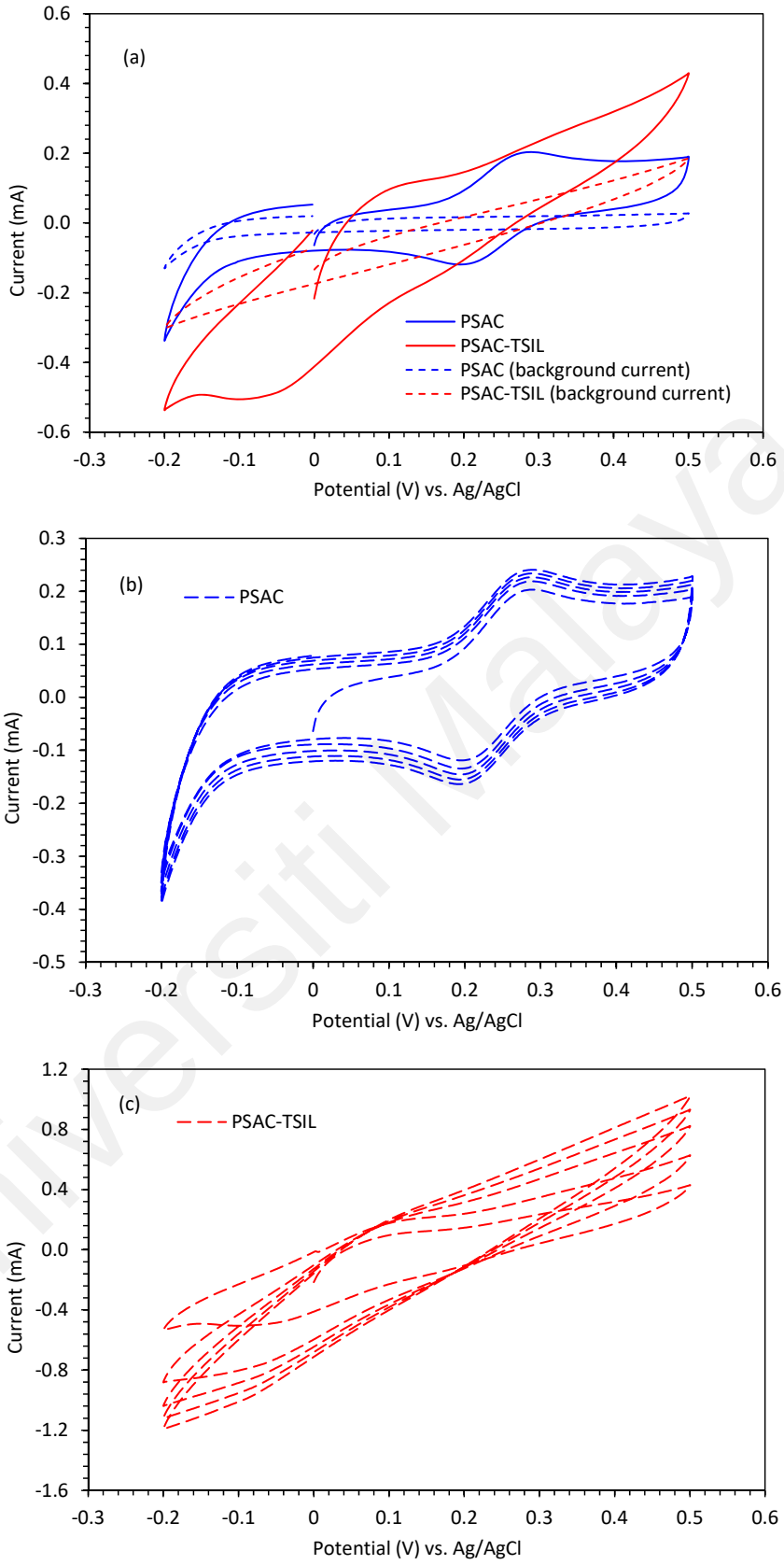

Figure 4.16: Cyclic voltammogram of 10 mM $Fe(CN)_6^{4-}/Fe(CN)_6^{3-}$ redox in 0.5 M NaCl using (a) the PSAC and PSAC-TSIL electrode (b) the PSAC electrode for five consecutive cycles and (c) the PSAC-TSIL electrode for five consecutive cycles at 5 mV/s scan rate.

4.3 Part III: Electrochemical Removal of Hg using PSAC-TOMATS Electrode

In this part, a PSAC-TOMATS electrode was prepared, and its performance was tested for the removal of Hg via an electrochemical process. The TOMATS loading was varied during the preparation of the electrode, and its performance was studied in terms of the percentage removal of Hg and its instantaneous current efficiency. The elemental analysis, surface morphology and presence of functional groups on the prepared electrode before and after the electrochemical process were also highlighted in this part for both the PSAC with and without TOMATS. Other than that, the effect of the solution pH, current density, initial concentration of Hg and electrode reusability for the removal of Hg using the PSAC-TOMATS electrode were also evaluated.

4.3.1 Effect of TSIL loading

Figure 4.17 shows the trend of the percentage removal of Hg from the aqueous solution for three different TOMATS loadings and a PSAC electrode without TOMATS. It can be seen from the figure that the percentage removal increased sharply with treatment time, particularly at the initial stage of the electrochemical treatment (the first 30 minutes). Later, the percentage removal of Hg plateaued over a longer treatment time. The removal rate of Hg was the fastest when a TOMATS loading of 0.2 g was used. However, the removal rate decreased slightly when a TOMATS loading of 0.1 g was used. The maximum percentage removal of mercury by the electrode with 0.2 g and 0.1 g of TOMATS was 99.2% (5 hours of treatment time) and 98.1% (4 hours of treatment time), respectively. The presence of the thiol-group (R−SH functional group), which is the anion of TOMATS (as illustrated by Figure 4.18) on the PSAC prominently improved the removal rate of Hg. Such a finding was in agreement with the properties of Hg, which has a very strong affinity to form thiolate ligands, where Hg replaces the hydrogen attached to sulphur. Sulphur is a relatively soft (polarised) atom that causes the thiol group

to have a high tendency to bind with soft elements such as Hg. Numerous studies have tested the use of thiol-functionalized material for mercury removal and remediation (Billinge et al., 2005). Even so, there are a variety of binding modes of complexes of thiosalicylate ligands that can be expected. The most common and simplest thiosalicylate ligand is formed by the chelating and bridging mode (Henderson & Nicholson, 2004), as illustrated in Figure 4.19. Each thiosalicylate ligand is restricted to bind to one atom of Hg through S, O chelating mode, as shown in Figure 4.19(a). Meanwhile the bridging binding mode of the chelated ligand may take place as the carboxylate group bridges to another Hg atom via two oxygen atoms, as shown in Figure 4.19(b). A fast removal rate of Hg is achieved due to the chelating and/or bridging effect of the ortho-positioned carboxylate group relative to the thiol functionality, from which a complex Hg-thiolate is formed.

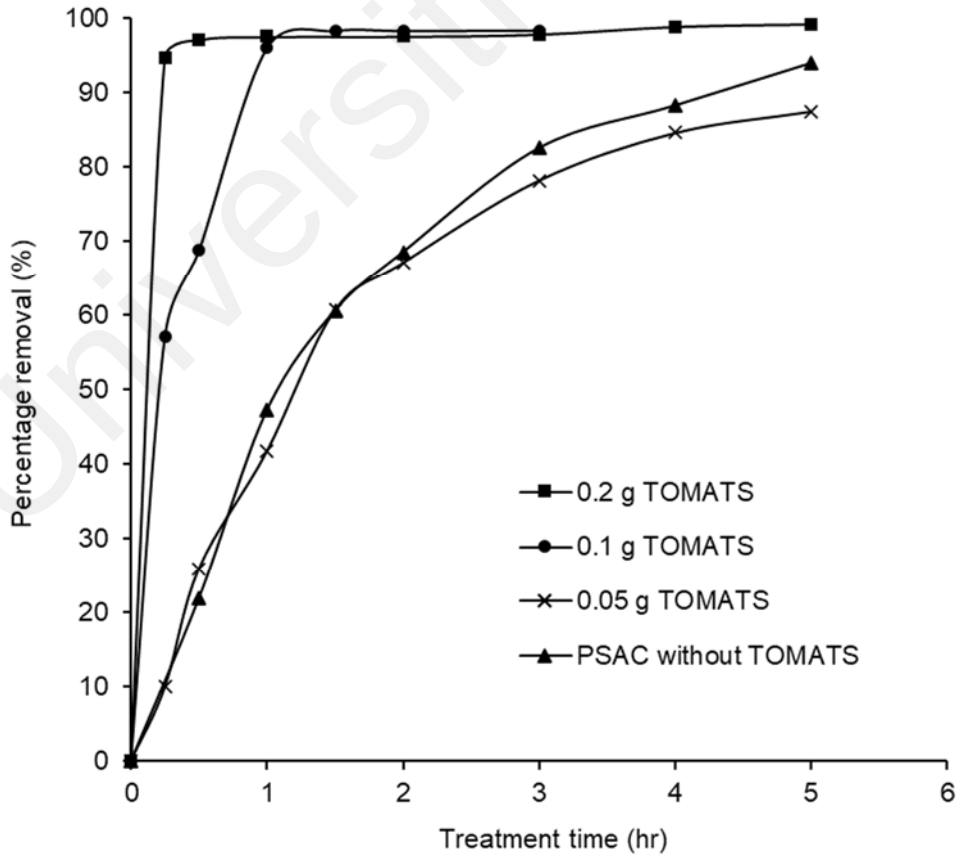

Figure 4.17: Effect of TSIL loading on the percentage removal of Hg

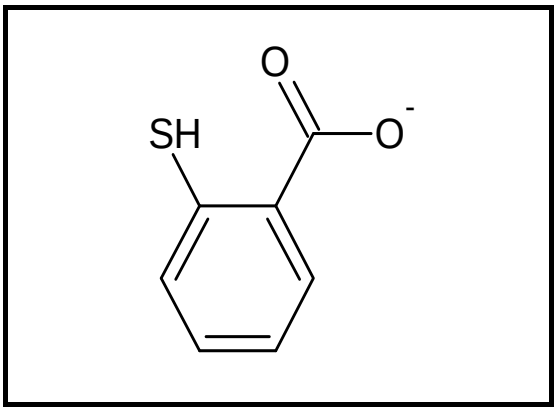

Figure 4.18: The anion of TOMATS having R−SH functional group

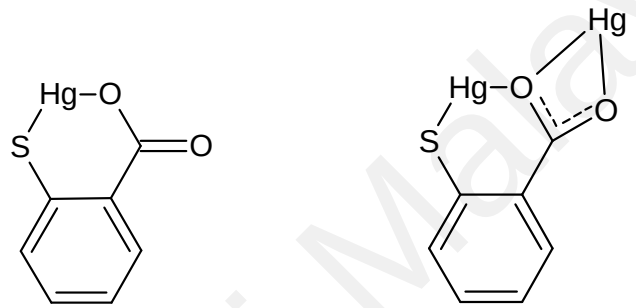

(a) (b)

Figure 4.19: Binding modes for thiosalicylate ligand: (a) chelating (b) bridging

By immobilizing 0.2 and 0.1 g of TOMATS onto the PSAC, a high percentage removal of Hg was achieved within a short treatment time. As listed in Table 4.6, the removal efficiency was 97.1 and 96.0% by immobilizing 0.2 and 0.1 g of TSIL, respectively for the optimum treatment time. Accordingly, it can be estimated that about 48 to 96 mg of Hg per g of TOMATS would be removed after an hour of electrochemical treatment time. Elsewhere, Kim and Lee (2017) reported that about 30 mg of Hg per gram of adsorbent (thiol-grafted porous polymer) was removed for the equivalent initial concentration of Hg, and this was attained after 2 hours of adsorption time. However, the removal efficiency by a TOMATS loading of 0.05 g on PSAC was apparently the slowest among the other PSAC-TOMATS electrodes. A TOMATS loading of 0.05 g resulted in the slowest removal rate, and this was further confirmed when after 6 hrs. of treatment time

only 91.1% Hg had been removed. In this case, it was shown that the TOMATS loading of 0.05 g was inadequate to improve the electrochemical removal of Hg by the PSAC-TOMATS electrode. In fact, it was observed that the percentage removal of Hg by this kind of electrode was slightly lower than that of the PSAC electrode without TOMATS for between three to six hours of electrochemical treatment time.

Table 4.6: Percentage removal of Hg, space-time yield, YST and energy consumption at an optimum treatment time using different TSIL loadings onto PSAC.

Mass of immobilised TSIL (g)	Mass ratio of TSIL to PSAC	Optimum treatment time (hrs)	Percentage removal at optimum treatment time (%)	Maximum current efficiency, CE (%)	Space-time yield, Y_{ST} ($kg/m^3 \cdot s$)	Energy consumption (kWh/m^3)
0	-	6	96.2	2.1	0.45	20.6
0.05	1:2	6	91.1	2.3	0.42	23.4
0.1	1:1	1	96.0	10.2	2.67	5.7
0.2	2:1	0.5	97.1	16.9	5.39	2.2

The BET analysis reveals that powdered PSAC is mainly made up of micropores (<20 A) with limited presences of meso (20 - 500 A) and macropores (>500 A). Thus, when a limited amount of TOMATS loading was applied (0.05 g), the electrochemical activity was expected to be mainly contributed by the electrosorption and electrodeposition of Hg on the PSAC surface area, with a negligible contribution from the thiol group, to extract the Hg ions from the aqueous solution. The limited presence of the thiol group on the PSAC was expected to partially occupy mainly the micropores of the PSAC and promote the electrosorption and electrodeposition of Hg on the unoccupied TSIL surface area. Thus, the presence of such an amount of TSIL contributed to the lower percentage removal and slower removal rate upon plateauing after a longer treatment time, as the treatment was prolonged to 6 hours.

It was observed that the Hg formed a whitish complex on the surface of the PSAC-TOMATS electrode after a short duration (about 10 minutes) of the electrochemical removal process. After a prolonged electrochemical process (more than 3 hours) with the aid of a stirring mode, the complex tended to leach out as a whitish precipitate in the solution. As TOMATS is hydrophobic in nature, a simple filtration was required to separate the produced complex from the solution. Although the TSIL to PSAC ratio of 2:1 provided the shortest electrochemical treatment time, the highest maximum current efficiency, the highest space-time yield, and the lowest energy consumption (as listed in Table 4.6), the removal efficiency (98.3%) was comparable to a TSIL to PSAC ratio of 1:1 for 90 minutes of electrochemical treatment time. Therefore, the TSIL to PSAC ratio of 1:1 was chosen for the subsequent experiment in order to minimize the amount of TOMATS used in the preparation of the electrode. Hence, in the subsequent experiment with a TSIL to PSAC loading ratio of 1:1, TSIL was assumed to be the limiting reactant.

The instantaneous current efficiency for various TSIL loadings was also determined to evaluate its trend throughout the reaction time, as shown in Figure 4.20. It can be seen that the instantaneous current efficiency for TSIL loadings of 0.1 and 0.2 g reached a substantial percentage of current efficiency for the first 15 minutes of reaction time as compared to a TSIL loading of 0.05 g with a PSAC electrode without TOMATS. The maximum current efficiencies calculated at 15 minutes of reaction time are listed in Table 4.6 for comparison. It can be seen from this table that a TOMATS loading of 0.05 g had very little or no apparent effect on the current efficiency values as compared to the PSAC without TOMATS. The current efficiency for the removal of Hg using a TOMATS loading of 0.05 g and PSAC without any TOMATS was 2.1 and 2.3%, respectively. Although the percentage removal of Hg at the optimum treatment time was increased by 5.1% using a TOMATS loading of 0.05 g, its maximum current efficiency can be considered as low compared to the TOMATS loadings of 0.1 and 0.2 g. Additionally, the

maximum current efficiency for a TOMATS loading of 0.2 g was increased by 6.7% as compared to a TOMATS loading of 0.1 g. However, the increase in the percentage removal was considered to be little, at only 1.1%. For this reason, a TOMATS loading of 0.1 g, which is equivalent to the 1:1 mass ratio of TOMATS to PSAC, was claimed to be the optimum loading and was chosen to be used for the subsequent experiment. By using this ratio, it was assumed that TOMATS was the limiting reactant.

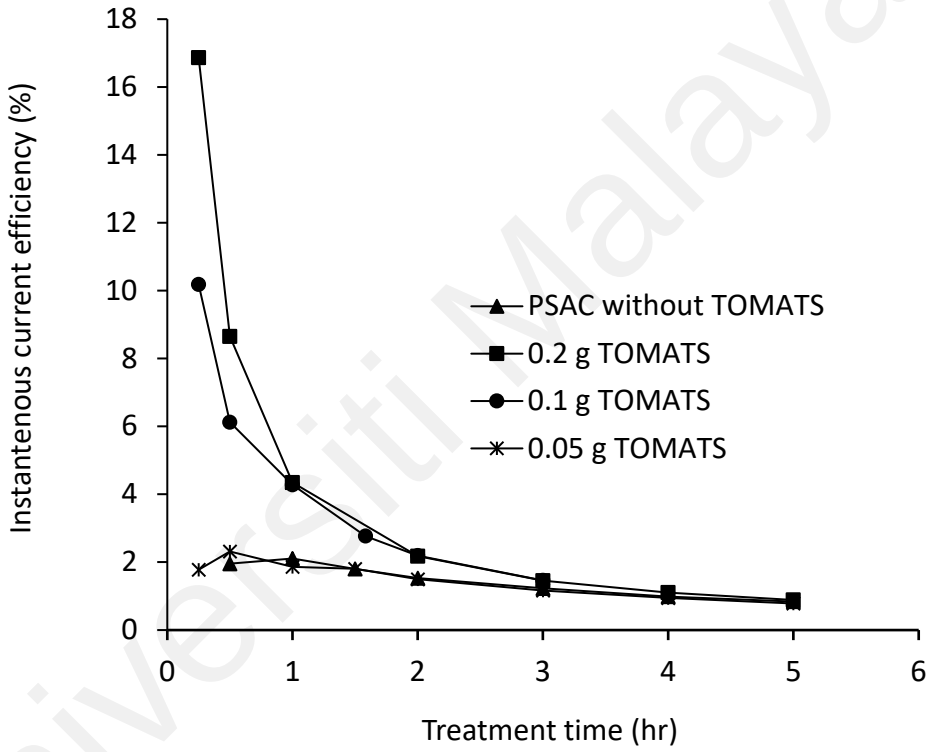

Figure 4.20: Instantaneous current efficiency at different TOMATS loadings.

4.3.1.1 FESEM & EDX analysis

The morphologies of the PSAC-TOMATS electrode were compared before and after the electrochemical removal of Hg. In both cases, the surface of the electrode was clearly heterogeneous under a magnification of 5k [Figure 4.21(a) and (c)]. Moreover, there was no noticeable difference in the morphologies of the electrode surface before [Figure 4.21(a)] and after [Figure 4.21(c)] the electrochemical removal of Hg. Additionally, under

a magnification of 25k, macropores (pores of more than 50 nm in size) were seen on the PSAC-TOMATS electrode. This finding confirmed that the amount of TSIL used (PSAC to TSIL ratio of 1:1) was not excessive to lead to total pore blockage. Such morphology is essential to allow the metal ions to enter the pores of the electrode, which functioned as a 3-dimensional electrode. Moreover, TOMATS was expected to be available at the surface of the pores beneath the opening to the macropores.

PSAC-TOMATS
(Before electrochemical removal of Hg)

PSAC-TOMATS
(After electrochemical removal of Hg)

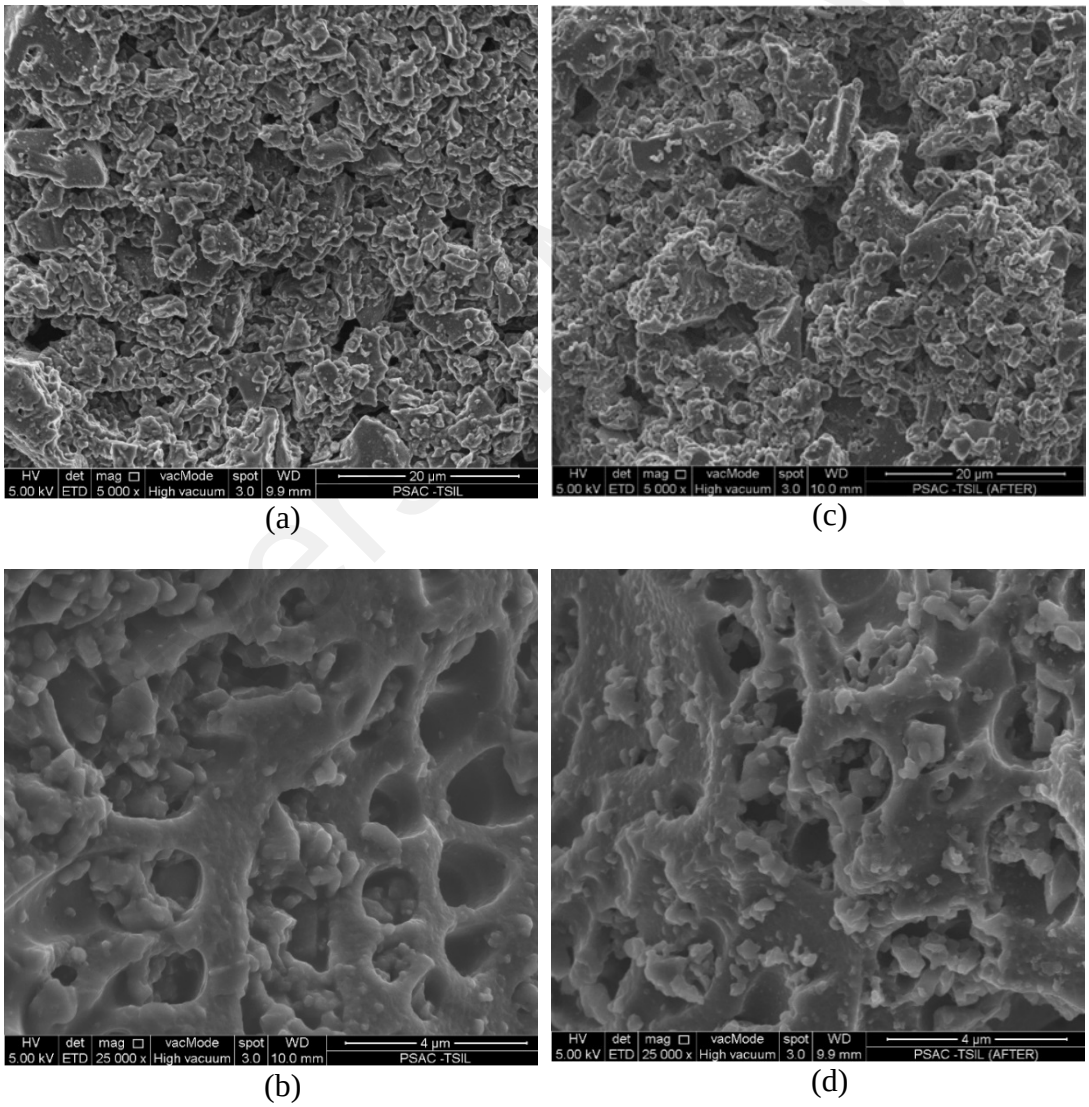

Figure 4.21: FESEM images of PSAC-TOMATS electrode before (a and b) and after (c and d) the electrochemical removal of Hg.

Additionally, an EDX analysis was performed to determine the elemental constituents on the surface of the electrode. The results are listed in Table 4.7. The presence of the thiolate group on the surface of the PSAC-TOMATS electrode before the electrochemical removal of Hg was evident from the detection of the S element, while the F element was contributed by the PTFE as the binder. As for the PSAC-TOMATS electrode after the electrochemical removal of Hg, a trace amount of Hg was detected on the surface of the electrode with a reduced amount of the S element. More Hg was expected to be found in the produced precipitate in the solution compared to the surface of the electrode.

Table 4.7: Elemental composition on the surface of the PSAC-TOMATS electrode before and after the electrochemical removal of Hg.

Element	Atomic (%)	
	PSAC-TOMATS (Before electrochemical removal of Hg)	**PSAC-TOMATS (After electrochemical removal of Hg)**
C	93.29	99.19
O	5.71	-
F	0.67	-
S	0.32	0.27
Hg	-	0.07
Total:	100.00	100.0

4.3.1.2 FTIR analysis

The FTIR spectra and the comparison of the IR data for the PSAC-TOMATS electrode before and after the electrochemical removal of Hg are shown in Figure 4.22. A C-H stretch was observed for both electrodes at 2921 and 2852 $cm^{-1,}$ while a C-H bending was observed at 1350 to 1500 cm^{-1}. These vibrations confirmed the presence of organic molecules, mainly contributed by the TOMATS cations immobilised on the surface of the PSAC. The S-H group band lay between the frequency range of 2550 to 2600. Generally, the S-H band is a weak band. Therefore, it was not clearly seen in both

electrodes. However, a weak band was observed at a frequency closer to 2560 cm^{-1} for the electrode, which was analysed after the electrochemical removal of Hg. The presence of this band suggested that the S-H group was available on the electrode surface even after the electrode had undergone the electrochemical process. Additionally, it was clearly seen that the C=O stretching gave a strong absorption at 1670 cm^{-1}. At the fingerprint region (1400 to 400 cm^{-1}), more functional groups with higher intensities were observed on the electrode after the electrochemical process. For instance, C-H, C-O and C-N stretching were observed at 705, 1045 and 1248 cm^{-1}, respectively. These functional groups are associated with the cations or anions of TOMATS, which facilitate the formation of metal-thiolate and/or metal-carboxylate complexes. The presence of hard and soft donor atoms by O and S, respectively, led to a wide range of coordination modes of metal-complexes (Wehr-Candler & Henderson, 2016).

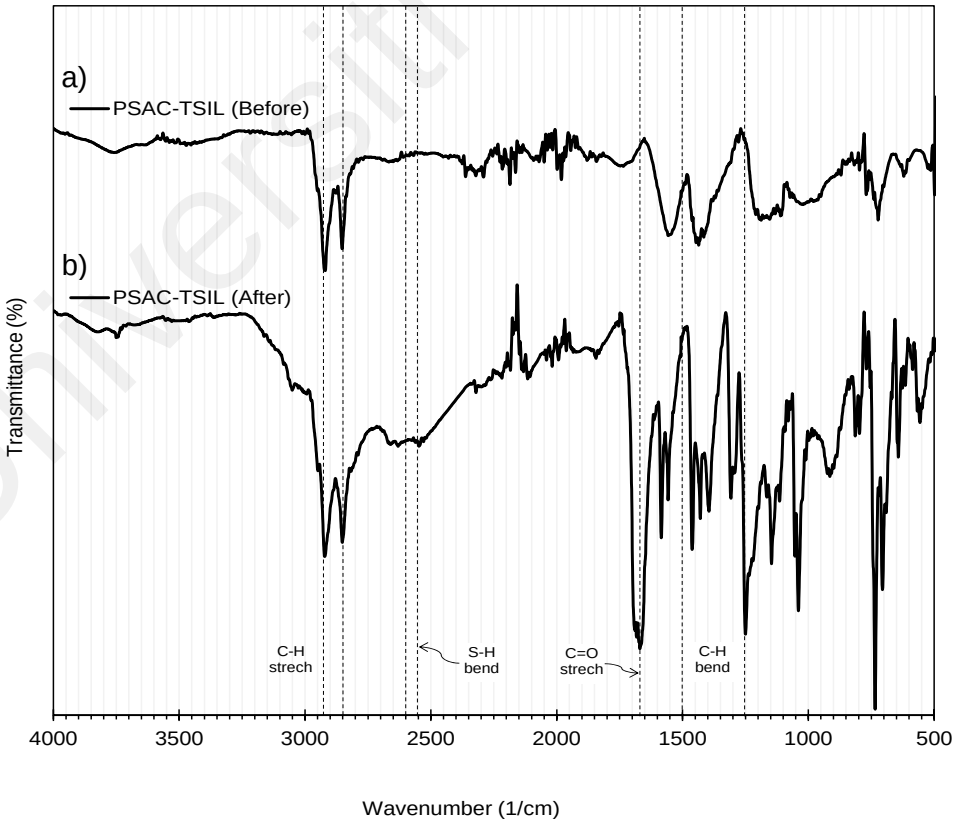

Figure 4.22: FTIR spectra of PSAC-TOMATS electrode (a) before and (b) after the electrochemical treatment of Hg from an aqueous solution.

4.3.2 Effect of pH

The effect of pH on the electrochemical removal of Hg depends on the characteristics of the electrode material and the nature of the solution. Mercury salt was diluted in three different supporting electrolytes, namely 0.01 M HCl, 0.01 M NaCl and 0.01 M NaOH, and the pH values of the solutions were 2, 6 and 12, respectively. The current density and the initial concentration of Hg were fixed at 6 mA/cm^2 and 100 mg/L, respectively. The current density and the initial concentration of Hg were fixed at 6 mA/cm^2 and 100 mg/L, respectively. Figure 4.23 shows the rate of percentage removal of Hg for three hours of treatment time using a PSAC-TOMATS electrode.

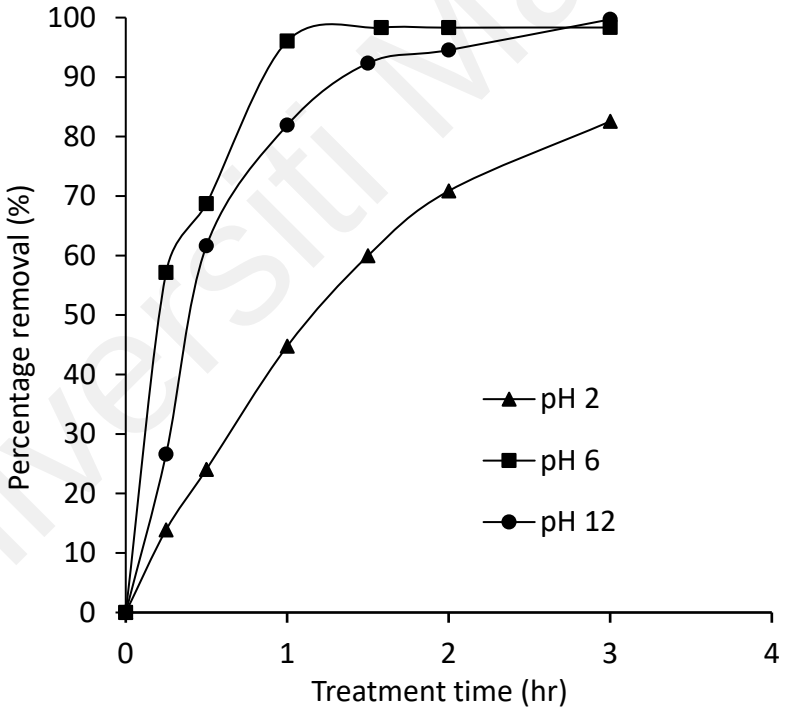

Figure 4.23: Percentage removal of Hg at pH 2, 6 and 12.

After an hour of electrochemical treatment, the highest percentage removal of Hg was achieved using 0.01 M NaCl (at pH 6). The least favourable removal efficiency of Hg at pH 2 was attributed to the competitive binding of protons (H+) to the ligands (Ismaiel et al., 2014b). After three hours of treatment time, a comparable percentage removal of Hg

was achieved at both pH 6 and 12. When 0.01 M NaOH was employed as the supporting electrolyte, the final pH (after three hours of electrochemical treatment) was decreased from 12 to 2. The decrease in the pH value was attributed to the consumption of hydroxyl anions and the predominant production of hydrogen ions (Su et al., 2009). The final pH for the electrochemical removal of Hg in 0.01 M NaCl also decreased from 6 to 2. When HCl was used as the supporting electrolyte, the final pH remained at around 2. A further approximate 10-fold increase in hydrogen ions is required to decrease the value of the pH to 1.

4.3.3 Effect of current density

Figure 4.24 shows the percentage removal of Hg at three different current densities. The trends indicate that a shorter electrochemical treatment time was required to remove up to 98% Hg as a higher current density was applied. It has been reported that the electrochemical removal of the targeted pollutant, particularly its percentage removal, was improved as the current density increased. Similar findings were reported by Akbal and Camcı (2011). Figure 4.25 gives a comparison of the cost of electricity between the three current density settings taken on the basis of RM22/kW for electricity charges as listed by the local authority for the industrial sector (non-peak hours). The average voltages of the system were 4.9, 5.4 and 5.9 V for current density settings of 2, 4 and 6 mA/cm^2, respectively. Accordingly, the energy consumption increased as the voltage increased. The system with the highest current density (6 mA/cm^2) had the highest energy consumption, and it only took 1.5 hours to reach 98.3% of Hg removal. Therefore, in this work, 6 mA/cm^2 was observed to be the optimum current density for the electrochemical removal of Hg. At this process setting, the highest space-time yield was achieved at a reasonable electricity cost.

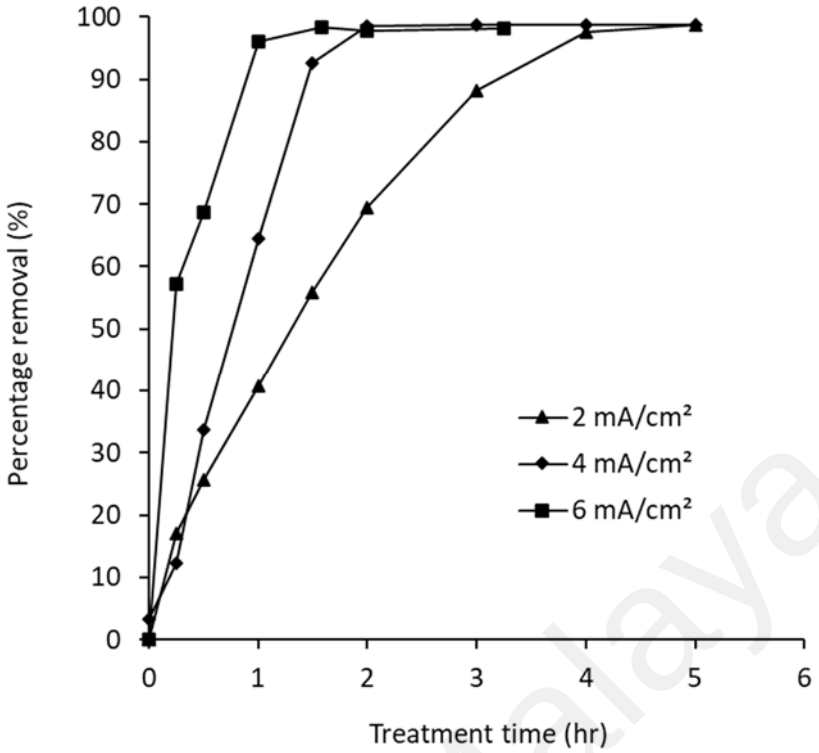

Figure 4.24: Effect of current density

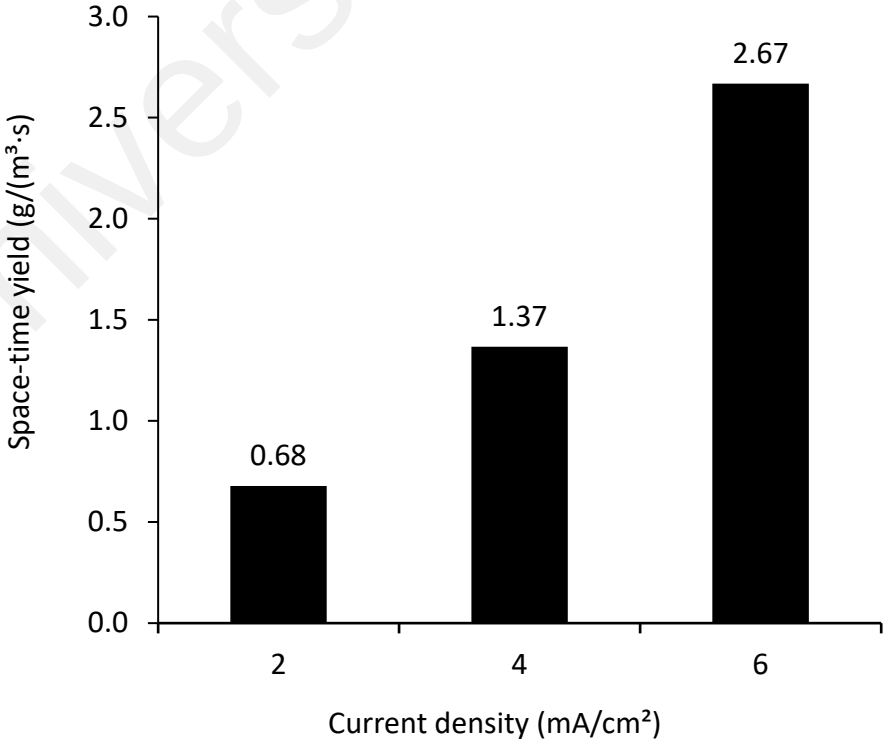

Figure 4.25: Effect of current density on space-time yield

Table 4.8: Process output at a different current density

Current density (mA/cm^2)	Treatment time (hrs)	Percentage removal (%)	Energy consumption (kWh/m^3)	Cost of electricity (RM/m^3)
2	4	97.6	3.9	85.80
4	2	98.5	4.3	94.60
6	1.5	98.3	5.3	116.82

4.3.4 Effect of initial concentration

The effect of the initial concentration of Hg was studied by comparing the removal efficiency at 10, 50 and 100 ppm. For each initial concentration experiment, the other prevailing conditions such as current density and initial pH of the solution were kept constant at 6 mA/cm^2 and pH 6, respectively. Figure 4.26 shows the removal efficiency that was obtained after 15 minutes of electrochemical treatment. A percentage removal of Hg of up to 99.8% was achieved for initial concentrations of 25 and 50 ppm. In comparison, only 57.1% removal was achieved for the initial concentration of 100 ppm. As expected, the lowest initial concentration (25 ppm) required a shorter time to achieve the total removal of the heavy metal compared to the higher initial concentration. The decrease in the concentration of Hg for all the initial concentrations studied exhibited an exponential decay. Therefore, first-order chemical reaction kinetics was employed to describe the reaction kinetics of the electrochemical removal of Hg using a PSAC-TOMATS electrode. The pseudo-first-order rate constant, k (min^{-1}) was determined by solving the nonlinear equation of the first-order chemical reaction given by Equation 4.4, where subscript A refers to the mercury. Equation 4.5 was derived upon integrating the mercury concentration with respect to time, t.

$$-r_A = -\frac{dC_A}{dt} = kC_A \qquad \text{Equation 4.4}$$

$$C_A = C_{Ao}e^{-kt} \qquad \text{Equation 4.5}$$

The first-order rate constant is 33.74 and 31.88 hr^{-1} for an initial concentration of 25 and 50 ppm, respectively. Although the data fitting to the first order is acceptable, as proven by the obtained $R^{2,}$ which is more than 0.95, the reaction is not a true first order as the reaction constant changes with changing of the initial concentration of mercury. The rate constant has been reduced to more than 10-fold for the initial concentration of 100 ppm. It seems that for 100 ppm initial concentration of Hg, TOMATS become the limiting reactant. Matthaiou et al. (2019) also reported a similar finding in their kinetic study of paraben degradation by activated persulfate, for which the rate constants decreased as the initial concentration of paraben was increased.

Elsewhere, Chen and Lim (2005) also claimed that the recovery of metal ions followed first-order reaction kinetics, where the rate constant was found to be 0.145 hr^{-1}, and the calculated half-life of the reaction obtained in their work was about 4 hours. As for the removal of Hg ions through the use of the PSAC-TOMATS electrode, the half-life for the reaction was faster as it was estimated to be about 1 minute for both Hg initial concentrations of 25 and 50 ppm. In comparison, it was about 15 minutes for the Hg initial concentration of 100 ppm.

Table 4.9: The reaction rate constants and R^2 for the first order reaction model using different initial concentrations of Hg.

Initial concentration of Hg (ppm)	C_{Ao} (ppm)	k (hr^{-1})	R^2
25	26.17	33.74	0.972
50	50.41	31.88	0.978
100	96.90	2.822	0.977

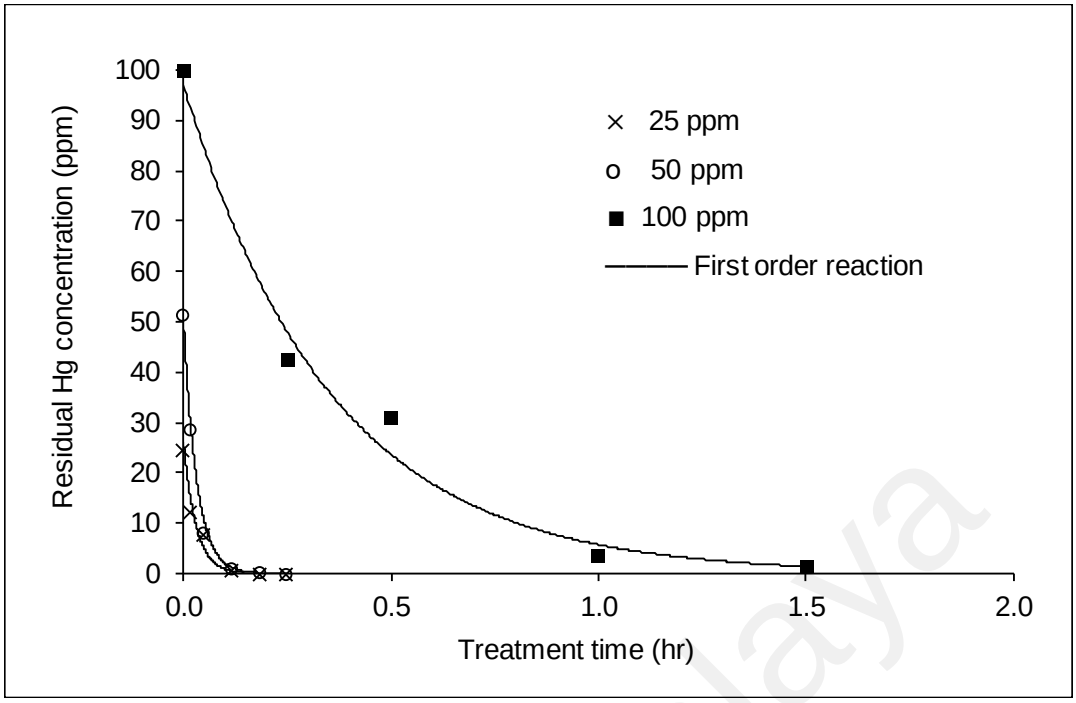

Figure 4.26: Percentage removal of Hg for electrochemical treatment time of 15 minutes for initial concentrations of 25, 50 and 100 ppm.

4.3.5 Electrode reusability

A study into the reusability of the electrode was carried out by recycling the same PSAC and PSAC-TOMATS electrodes for three cycles to remove Hg from a fresh concentration of 100 ppm. The experimental conditions were maintained at a current density of 6 mA/cm^2 for 100 mL of Hg solution in 0.01 M NaCl and at an agitation rate of 200 rpm. Figure 4.27 shows the percentage removal of Hg for each cycle. It was found that when the fresh PSAC-TOMATS electrode was used for the first, second and third cycles, 98.32, 83.32, and 81.36% of Hg, respectively were successfully removed after 1.5 hours of electrochemical treatment time. Meanwhile, when the PSAC electrode was used for the first, second and third cycles, 96.21, 94.69 and 93.84% of Hg, respectively were successfully removed after 6 hours of electrochemical treatment time. Hence, it can be said that the reduction efficiency of the PSAC-TOMATS electrode (15%) was higher than that of the PSAC electrode (2%) after the second cycle. However, with further analysis of its reusability, it was predicted that the PSAC-TOMATS electrode would eventually

reach the stage where there would be a very small change or a negligible percentage of reduction to its efficiency. Such a trend was observed after the third cycle, where the reduction in the efficiency of both electrodes was found to be between 1-2% only.

A higher reduction efficiency was observed for PSAC-TOMATS for the second cycle could be explained by the detachment of complexes thiosalicylate ligands from the surface of the PSAC-TOMATS electrode, which later leaving the electrode with limited active electrochemical surface area. However, it is expected that the percentage removal of Hg is higher if the electrochemical treatment time is prolonged to 6 hours. Elsewhere, Lan et al. (2016) reported the efficiency of an activated carbon fibre cathode had almost no influence on the reuse of the electrode for the degradation of glyphosate.

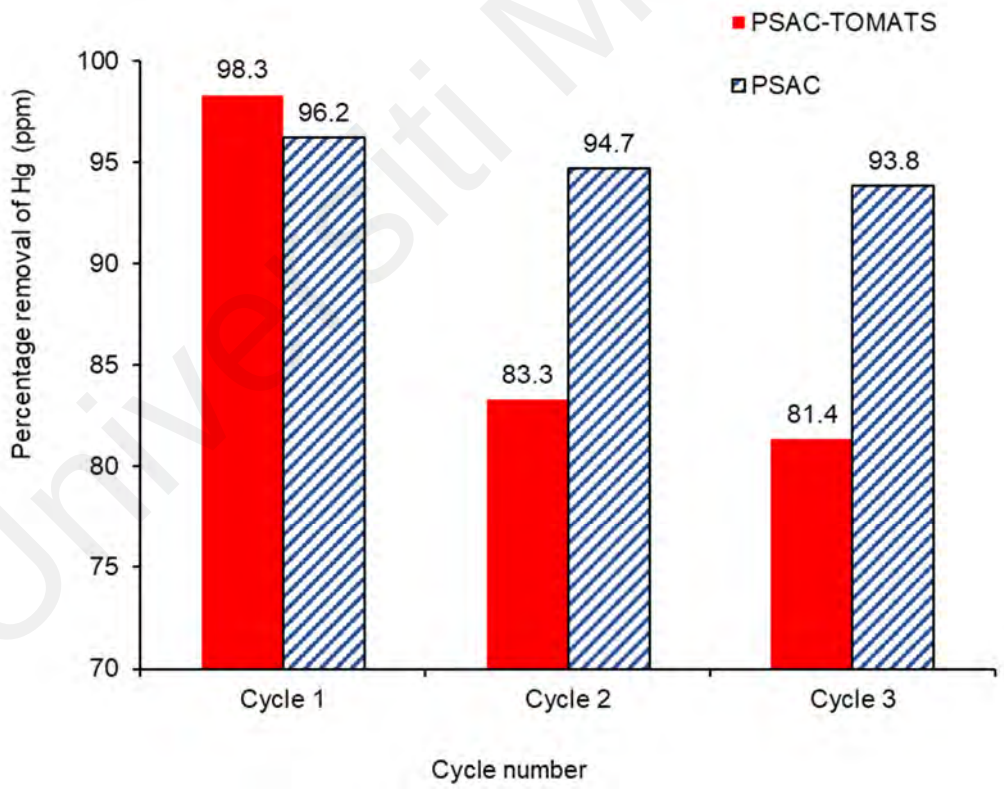

Figure 4.27: Percentage removal of Hg for fresh electrode, second and third cycles (condition: initial Hg concentration of 100 ppm, 100 mL solution at 27°C) using PSAC-TOMATS and PSAC electrodes after 1.5 and 6 hours of electrochemical treatment time, respectively.

4.3.6 Summary

The performance of the PSAC-TOMATS electrode for the electrochemical batch removal of Hg was evaluated at different TOMATS loadings, solution pH, current densities and initial concentrations of Hg solution. The higher the TOMATS loading, the shorter the time required to achieve the highest removal of Hg. A comparable percentage removal of Hg of 98.1 and 99.2% was achieved by a TOMATS loading of 0.1 and 0.2 g, respectively, after 1.5 hours of reaction time. Meanwhile, the highest removal of Hg was observed for the reaction that took place in a solution pH of 6. The removal rate of Hg was comparable at low initial Hg concentrations (25 and 50 ppm). However, the highest initial concentration studied (100 ppm) increased the removal rate by 10-fold compared to the low initial concentration of Hg. A higher initial concentration of Hg (100 ppm) resulted in a rise in the current efficiency and consequently, a fall in the specific energy consumption. Under the electrode reusability study, the PSAC-TOMATS electrode could remove between 81-83 % of Hg from an initial concentration of 100 ppm after the second and third cycles after 1.5 hours of electrochemical reaction time.

CHAPTER 5: CONCLUSION AND RECOMMENDATION

5.1 Conclusion

The virgin palm shell activated carbon (PSAC) electrode was satisfactorily prepared using the optimum amount of polytetrafluoroethylene (PTFE) as the binder. An amount of 20% binder was found to be the best for providing sufficient binding strength between PSAC and carbon black. It produced an acceptable reproducibility of voltammogram, and the double-layer capacitance properties of a PSAC-based electrode were clearly observed. Meanwhile, the EDX analysis revealed that the electrode consisted primarily of carbon. FESEM analysis proved the presence of a wide range of pore sizes, from micro to macropores. Additionally, the double-layer capacitance, C_E, and charge transfer resistance, R_{ct} was approximately comparable for all different amounts of binder (20, 30 and 40%).

For the electrode reversibility studies, sodium chloride (NaCl) was found to be the most suitable supporting electrolyte for the electrochemical characterization of the PSAC electrode. The PSAC electrode was observed to have a quasi-reversible electrode reaction for a common redox probe, $Fe(CN)_6^{4-}$/ $Fe(CN)_6^{3-}$. The Faradaic current and double-layer capacitance, as well as the electrode-electrolyte interfacial interaction, were ascertained. The electrode provided a low electron transfer resistance, R_{CT}, when 20 wt% of CB was used to improve its conductivity. It was revealed that the kinetic parameter, k^o, for the PSAC electrode was higher than that of several other reported carbon-based electrodes that used $Fe(CN)_6^{4-}$/ $Fe(CN)_6^{3-}$ as the redox couple.

PSAC immobilised with TOMATS was studied for the electrochemical batch removal of Hg at different TOMATS loadings, pH, current densities, and initial concentrations of Hg solution. The highest TOMATS loading required a shorter time to achieve the highest

removal of Hg. Almost an equivalent percentage removal of Hg of 98.1 and 99.2% was achieved by 0.1 and 0.2 g TOMATS loadings, respectively after 1.5 hours of reaction time. Meanwhile, the maximum removal of Hg was recorded for a reaction at a pH value of 6. The removal rate of Hg was comparable at low initial Hg concentrations (25 and 50 ppm). However, the highest initial concentration studied (100 ppm) increased the removal rate by 10-fold compared to the low initial concentrations studied. A relatively higher concentration of Hg led to a rise in the current efficiency and a decrease in energy consumption. For the electrode reusability study, the PSAC-TOMATS electrode was able to remove 83% of Hg from an initial 100 ppm concentration after the second cycle. There was a reduction of 15% in its efficiency. However, it was found that the efficiency of the PSAC-TOMATS electrode was reduced by only 2% after it had been used for the third cycle.

5.2 Recommendation

In the present work, PSAC and PSAC-TOMATS electrodes were prepared and analysed for the removal of mercury. The following are several recommendations for future research:

1. Immobilising an ionic liquid onto the PSAC offers a unique property to the electrode. Wet coating of an ionic liquid on the PSAC was employed in the present work. However, this method does not fully utilise the amount of PSAC. Practically, the electrode only required a thin layer of PSAC-TOMATS. The design of the cell system needs to be further explored, for instance, to immobilise the ionic liquid on the surface of the PSAC that coats the inner surface of a reactor. The reaction can take place in a cell that has been designed as a thin film catalytic reactor. The body of the reactor should function as a current collector. By having such a design, a series of reactor systems can be proposed, and the performance of the prepared electrode can be evaluated for a continuous process. Additionally, the electrodes might be arranged in a series and designed for the lab and on a pilot scale.
2. The task-specific ionic liquid (TSIL) used in the present work was TOMATS, which provided the chelating effect of the ortho-positioned carboxylate group relative to the thiol functionality. TOMATS is specifically designed to extract heavy metals. Therefore, it would be worthwhile to explore the feasibility of using the PSAC-TOMATS electrode to remove other heavy metals such as copper, cadmium, and lead. Among these heavy metals, copper is strongly suggested as the targeted pollutant. Although copper is not as harmful as cadmium and lead, many available works and findings in the open literature have focused on the removal of copper. Hence, the feasibility of PSAC-TOMATS can be compared with other electrodes, where a similar species is used as the pollutant.

3. The present work focused on the feasibility of the prepared electrode for a single species of pollutant, namely Hg. Further work to explore the performance of the electrode for the removal of synthetic multicomponent species would be useful to understand its reaction kinetics involving various species by taking as its basis a typical wastewater composition for a specific industry. The performance of the prepared electrode may later be verified for the removal of heavy metals from real wastewater.
4. It would be remarkable if the product of the electrochemical reaction could be evaluated at a molecular level. Such a study will provide insight into the possible reaction mechanisms and the presence of intermediate species produced on the surface of the electrode and in the electrolyte.

REFERENCES

Abbasi, Y. A., Shahida, S., Ali, A., & Khan, M. H. (2019). Liquid-liquid extraction of mercury(II) from aqueous solution using furosemide in benzyl alcohol. *Journal of Radioanalytical and Nuclear Chemistry, 319*(3), 1029-1036.

Abdel-Aziz, M. H., Nirdosh, I., & Sedahmed, G. H. (2013). Ion-exchange-assisted electrochemical removal of heavy metals from dilute solutions in a stirred-tank electrochemical reactor: A mass-transfer study. *Industrial & Engineering Chemistry Research, 52*(33), 11655-11662.

Abou-Shady, A., Peng, C., Bi, J., Xu, H., & Almeria O, J. (2012). Recovery of Pb (II) and removal of NO_3^- from aqueous solutions using integrated electrodialysis, electrolysis, and adsorption process. *Desalination, 286*, 304-315.

Adebisi, G. A., Chowdhury, Z. Z., & Alaba, P. A. (2017). Equilibrium, kinetic, and thermodynamic studies of lead ion and zinc ion adsorption from aqueous solution onto activated carbon prepared from palm oil mill effluent. *Journal of Cleaner Production, 148*, 958-968.

Agarwal, I. C., Rochon, A. M., Gesser, H. D., & Sparling, A. B. (1984). Electrodeposition of six heavy metals on reticulated vitreous carbon electrode. *Water Research, 18*(2), 227-232.

Ahmad, Z., Li, Y., Yang, J. J., Geng, N. B., Fan, Y., Gou, X. Y., Sun, Q. Y., & Chen, J. P. (2022). A Membrane-Supported Bifunctional Poly(amidoxime-ethyleneimine) Network for Enhanced Uranium Extraction from Seawater and Wastewater. *Journal of Hazardous Materials, 425*.

Ajeel, M. A., Aroua, M. K., & Daud, W. M. A. W. (2015a). Anodic Degradation of 2-Chlorophenol by Carbon Black Diamond and Activated Carbon Composite Electrodes. *Electrochimica Acta, 180*, 22-28.

Ajeel, M. A., Aroua, M. K., & Daud, W. M. A. W. (2015b). Preparation and characterization of carbon black diamond composite electrodes for anodic degradation of phenol. *Electrochimica Acta, 153*, 379-384.

Ajeel, M. A., Aroua, M. K. T., & Daud, W. (2016). Reactivity of carbon black diamond electrode during the electro-oxidation of Remazol Brilliant Blue R. *RSC Advances, 6*(5), 3690-3699.

Akbal, F., & Camcı, S. (2011). Copper, chromium and nickel removal from metal plating wastewater by electrocoagulation. *Desalination, 269*(1–3), 214-222.

Almazan-Ruiz, F. J., Caballero, F. V., Cruz-Diaz, M. R., Rivero, E. P., & Gonzalez, I. (2012). Scale-up of rotating cylinder electrode electrochemical reactor for Cu(II) recovery: Experimental and simulation study in turbulence regimen. *Electrochimica Acta, 77*, 262-271.

Almeida, L. C., Gasparotto, L. H. S., Bocchi, N., Rocha, R. C., & Biaggio, S. R. (2008). Galvanostatic Pb(II) removal from a simulated wastewater by using a stainless-

steel wool cathode in a flow-through cell: a factorial-design study. *Journal of Applied Electrochemistry, 38*(2), 167-173.

Amin, A., Latif, Z., Sarwar, A., Zeshan, B., & Saleem, M. A. (2021). Molecular Characterization of Mercury Resistant Bacteria Isolated from Tannery Wastewater. *Pakistan Journal of Zoology, 53*(1), 33-39.

Anson, F. C. (1964). Application of Potentiostatic Current Integration to the Study of the Adsorption of Cobalt(III)-(Ethylenedinitrilo(tetraacetate) on Mercury Electrodes. *Analytical Chemistry, 36*(4), 932-934.

Aoudj, S., Khelifa, A., Drouiche, N., Belkada, R., & Miroud, D. (2015). Simultaneous removal of chromium(VI) and fluoride by electrocoagulation–electroflotation: Application of a hybrid Fe-Al anode. *Chemical Engineering Journal, 267*, 153-162.

Armand, M., Endres, F., MacFarlane, D. R., Ohno, H., & Scrosati, B. (2009). Ionic-liquid materials for the electrochemical challenges of the future. *Nature Materials, 8*(8), 621-629.

Arredondo, J. L., Rivera, F. F., & Nava, J. L. (2014). Silver recovery from an effluent generated by plating industry using a rotating cylinder electrode (RCE). *Electrochimica Acta, 147*, 337-342.

Baghban, E., Mehrabani-Zeinabad, A., & Moheb, A. (2014). The effects of operational parameters on the electrochemical removal of cadmium ion from dilute aqueous solutions. *Hydrometallurgy, 149*, 97-105.

Bagheri, H., Afkhami, A., Khoshsafar, H., Rezaei, M., Sabounchei, S. J., & Sarlakifar, M. (2015). Simultaneous electrochemical sensing of thallium, lead and mercury using a novel ionic liquid/graphene modified electrode. *Analytica Chimica Acta, 870*, 56-66.

Barakat, M. A. (2011). New trends in removing heavy metals from industrial wastewater. *Arabian Journal of Chemistry, 4*(4), 361-377.

Bard, J. A., & Faulkner, L. R. (2001). *Electrochemical Methods: Fundamentals and Applications* (2nd ed.). New York: John Wiley & Sons, Inc.

Basha, C. A., Bhadrinarayana, N. S., Anantharaman, N., & Meera Sheriffa Begum, K. M. (2008). Heavy metal removal from copper smelting effluent using electrochemical cylindrical flow reactor. *Journal of Hazardous Materials, 152*(1), 71-78.

Basha, C. A., Somasundaram, M., Kannadasan, T., & Lee, C. W. (2011). Heavy metals removal from copper smelting effluent using electrochemical filter press cells. *Chemical Engineering Journal, 171*(2), 563-571.

Bebelis, S., Bouzek, K., Cornell, A., Ferreira, M. G. S., Kelsall, G. H., Lapicque, F., Ponce de León, C., Rodrigo, M. A., & Walsh, F. C. (2013). Highlights during the development of electrochemical engineering. *Chemical Engineering Research and Design, 91*(10), 1998-2020.

Bertazzoli, R., Widner, R. C., Lanza, M. R. V., Di Iglia, R. A., & Sousa, M. F. B. (1997). Electrolytic removal of metals using a flow-through cell with a reticulated vitreous carbon cathode. *Journal of the Brazilian Chemical Society*, *8*(5), 487-493.

Besenhard, J. O., & Fritz, H. P. (1983). The electrochemistry of black carbons. *Angewandte Chemie-International Edition in English, 22*(12), 950-975.

Bijad, M., Karimi-Maleh, H., & Khalilzadeh, M. A. (2013). Application of ZnO/CNTs nanocomposite ionic liquid paste electrode as a sensitive voltammetric sensor for determination of ascorbic acid in food samples. *Food Analytical Methods, 6*(6), 1639-1647.

Billinge, S. J. L., McKimmy, E. J., Shatnawi, M., Kim, H. J., Petkov, V., Wermeille, D., & Pinnavaia, T. J. (2005). Mercury binding sites in thiol-functionalized mesostructured silica. *Journal of the American Chemical Society*, *127*(23), 8492-8498.

Britto-Costa, P. H., & Ruotolo, L. A. M. (2011). Electrochemical removal of copper ions from aqueous solutions using a modulated current method. *Separation Science and Technology, 46*(7), 1205-1211.

Britto-Costa, P. H., & Ruotolo, L. A. M. (2013). Mass transfer study on the electrochemical removal of copper ions from synthetic effluents using reticulated vitreous carbon. *Environmental Technology, 34*(4), 437-444.

Britto-Costa, P. H., & Ruotolo, L. A. M. (2014). Optimization of copper electrowinning from synthetic copper sulfate solution using a pulsed bed electrode. *Hydrometallurgy, 150*, 52-60.

Britto-Costa, P. H., & Ruotolo, L. A. M. (2015). Copper electrowinning using a spouted-bed electrochemical reactor. *Quimica Nova, 38*(5), 657-662.

Brownson, D. A. C., & Banks, C. E. (2014). Interpreting Electrochemistry *The Handbook of Graphene Electrochemistry* (pp. 23-77). London: Springer London.

Candeago, R., Kim, K., Vapnik, H., Cotty, S., Aubin, M., Berensmeier, S., Kushima, A., & Su, X. (2020). Semiconducting Polymer Interfaces for Electrochemically Assisted Mercury Remediation. *Acs Applied Materials & Interfaces, 12*(44), 49713-49722.

Casasus, A. I., Hagan-Rogers, A. M., Rodriguez, R., & Mazyck, D. W. (2020). Novel photo-activated method for removal of mercury from industrial wastewater. *Journal of Water Process Engineering, 38*, 7.

Chan, M. Y., Tee, C. S., Chai, T. T., Sim, Y. L., & Beh, W. L. (2022). Evaluation of electro-assisted phytoremediation (EAPR) system for heavy metal removal from synthetic leachate using Pistia stratiotes. *International Journal of Phytoremediation*, Early Access.

Chang, J. J., Si, G. Z., Dong, J., Yang, Q. C., Shi, Y., Chen, Y. L., Zhou, K. X., & Chen, J. Q. (2021). Transcriptomic analyses reveal the pathways associated with the

volatilization and resistance of mercury(II) in the fungus Lecythophora sp. DC-F1. *Science of the Total Environment, 752*, 10.

Chellammal, S., Raghu, S., Kalaiselvi, P., & Subramanian, G. (2010). Electrolytic recovery of dilute copper from a mixed industrial effluent of high strength COD. *Journal of Hazardous Materials, 180*(1-3), 91-97.

Chen, G. (2004). Electrochemical technologies in wastewater treatment. *Separation and Purification Technology, 38*(1), 11-41.

Chen, J. P. (2012). *Decontamination of heavy metals: Processes, mechanisms, and applications*. Florida, USA: CRC Press.

Chen, J. P., & Lim, L. L. (2005). Recovery of precious metals by an electrochemical deposition method. *Chemosphere, 60*(10), 1384-1392.

Chen, L., Sharifzadeh, M., Mac Dowell, N., Welton, T., Shah, N., & Hallett, J. P. (2014). Inexpensive ionic liquids: HSO4 (-)-based solvent production at bulk scale. *Green Chemistry, 16*(6), 3098-3106.

Cheng, C. Y., Kelsall, G. H., & Pilone, D. (2005). Modelling potentials, concentrations and current densities in porous electrodes for metal recovery from dilute aqueous effluents. *Journal of Applied Electrochemistry, 35*(12), 1191-1202.

Cheng, S., & Wu, J. (2013). Air-cathode preparation with activated carbon as catalyst, PTFE as binder and nickel foam as current collector for microbial fuel cells. *Bioelectrochemistry, 92*, 22-26.

Choi, J. Y., & Choi, J. H. (2010). A carbon electrode fabricated using a poly(vinylidene fluoride) binder controlled the Faradaic reaction of carbon powder. *Journal of Industrial and Engineering Chemistry, 16*(3), 401-405.

Chong, L. G., Chen, P. A., Huang, J. Y., Huang, H. L., & Wang, H. P. (2018). Capacitive deionization of a RO brackish water by AC/graphene composite electrodes. *Chemosphere, 191*, 296-301.

Coeuret, F. (1980). The fluidized bed electrode for the continuous recovery of metals. *Journal of Applied Electrochemistry, 10*(6), 687-696.

Coeuret, F., & Paulin, M. (1988). Experiments on copper recovery in a pulsed granular fixed bed electrode. *Journal of Applied Electrochemistry, 18*(1), 162-165.

Colli, A. N., & Bisang, J. M. (2015). Comparison of the performance of flow-by three-dimensional cylindrical electrochemical reactors with inner or outer counter electrode under limiting current conditions. *Electrochimica Acta, 154*, 468-475.

Cyr, P. J., Suri, R. P. S., & Helmig, E. D. (2002). A pilot scale evaluation of removal of mercury from pharmaceutical wastewater using granular activated carbon. *Water Research, 36*(19), 4725-4734.

Czuprynski, P., Plotka, M., Glamowski, P., Zukowski, W., & Bajda, T. (2022). An assessment of an ion exchange resin system for the removal and recovery of Ni,

Hg, and Cr from wet flue gas desulphurization wastewater-a pilot study. *RSC Advances, 12*(9), 5145-5156.

Darwish, A. S., Zewail, T. M., Yousef, N. S., & El-Tawail, Y. A. (2015). Investigation of the performance of a batch air spouting bed in conducting ion exchange reactions involving heavy metal removal. *Journal of the Taiwan Institute of Chemical Engineers, 47*, 171-176.

Daud, W. M. A. W., & Houshamnd, A. H. (2010). Textural characteristics, surface chemistry and oxidation of activated carbon. *Journal of Natural Gas Chemistry, 19*(3), 267-279.

De Levie, R. (1965). The influence of surface roughness of solid electrodes on electrochemical measurements. *Electrochimica Acta, 10*(2), 113-130.

de Radigues, Q., Santoro, R., & Proost, J. (2010). Kinetic transitions during Ag and Cu electrorecovery on reticulated vitreous carbon electrodes in flow-by mode. *Chemical Engineering Journal, 162*(1), 273-277.

Dehkhoda, A. M., Ellis, N., & Gyenge, E. (2014). Electrosorption on activated biochar: effect of thermo-chemical activation treatment on the electric double layer capacitance. *Journal of Applied Electrochemistry, 44*(1), 141-157.

Dell'Era, A., Pasquali, M., Lupi, C., & Zaza, F. (2014). Purification of nickel or cobalt ion containing effluents by electrolysis on reticulated vitreous carbon cathode. *Hydrometallurgy, 150*, 1-8.

Dickinson, E. J. F., Limon-Petersen, J. G., Rees, N. V., & Compton, R. G. (2009). How much supporting electrolyte is required to make a cyclic voltammetry experiment quantitatively "diffusional"? A theoretical and experimental investigation. *Journal of Physical Chemistry C, 113*(25), 11157-11171.

Dong, H., Yu, H. B., & Wang, X. (2012a). Catalysis kinetics and porous analysis of rolling activated carbon-ptfe air-cathode in microbial fuel cells. *Environmental Science and Technology, 46*(23), 13009-13015.

Dong, H., Yu, H. B., Wang, X., Zhou, Q. X., & Feng, J. L. (2012b). A novel structure of scalable air-cathode without Nafion and Pt by rolling activated carbon and PTFE as catalyst layer in microbial fuel cells. *Water Research, 46*(17), 5777-5787.

Doulakas, L., Novy, K., Stucki, S., & Comninellis, C. (2000). Recovery of Cu, Pb, Cd and Zn from synthetic mixture by selective electrodeposition in chloride solution. *Electrochimica Acta, 46*(2–3), 349-356.

Du, X., Oturan, M. A., Zhou, M., Belkessa, N., Su, P., Cai, J., Trellu, C., & Mousset, E. (2021). Nanostructured electrodes for electrocatalytic advanced oxidation processes: From materials preparation to mechanisms understanding and wastewater treatment applications. *Applied Catalysis B: Environmental, 296*, 120332.

Du, Y., Yang, J., Liu, Y., Zhou, J., Cao, L., & Yang, J. (2022). Electrochemical reduction and kinetic analysis of oxidized mercury in wastewater by choosing titanium plate as cathode. *Separation and Purification Technology, 289*, 120808.

Duan, F., Li, Y., Cao, H., Wang, Y., Crittenden, J. C., & Zhang, Y. (2015). Activated carbon electrodes: Electrochemical oxidation coupled with desalination for wastewater treatment. *Chemosphere, 125*, 205-211.

Dutra, A. J. B., Espinola, A., & Borges, P. P. (2000). Cadmium removal from diluted aqueous solutions by electrowinning in a flow-by cell. *Minerals Engineering, 13*(10-11), 1139-1148.

Elias, G., Díez, S., & Fontàs, C. (2019). System for mercury preconcentration in natural waters based on a polymer inclusion membrane incorporating an ionic liquid. *Journal of Hazardous Materials, 371*, 316-322.

Elias, G., Díez, S., Zhang, H., & Fontàs, C. (2020). Development of a new binding phase for the diffusive gradients in thin films technique based on an ionic liquid for mercury determination. *Chemosphere, 245*, 125671.

Elias, G., Marguí, E., Díez, S., & Fontàs, C. (2018). Polymer Inclusion Membrane as an Effective Sorbent To Facilitate Mercury Storage and Detection by X-ray Fluorescence in Natural Waters. *Analytical Chemistry, 90*(7), 4756-4763.

Elyasi, M., Khalilzadeh, M. A., & Karimi-Maleh, H. (2013). High sensitive voltammetric sensor based on Pt/CNTs nanocomposite modified ionic liquid carbon paste electrode for determination of Sudan I in food samples. *Food Chemistry, 141*(4), 4311-4317.

Esmaeili, N., Rakhtshah, J., Kolvari, E., & Shirkhanloo, H. (2020). Ultrasound assisted-dispersive-modification solid-phase extraction using task-specific ionic liquid immobilized on multiwall carbon nanotubes for speciation and determination mercury in water samples. *Microchemical Journal, 154*, 104632.

Farma, R., Deraman, M., Awitdrus, A., Talib, I. A., Taer, E., Basri, N. H., Manjunatha, J. G., Ishak, M. M., Dollah, B. N. M., & Hashmi, S. A. (2013). Preparation of highly porous binderless activated carbon electrodes from fibres of oil palm empty fruit bunches for application in supercapacitors. *Bioresource Technology, 132*, 254-261.

Figueiredo, J. L., & Pereira, M. F. R. (2010). The role of surface chemistry in catalysis with carbons. *Catalysis Today, 150*(1–2), 2-7.

Fleischmann, M., & Kelsall, G. H. (1984). A feasibility study of mercury deposition in a lead fluidized-bed electrode. *Journal of Applied Electrochemistry, 14*(3), 277-284.

Foroutan, R., Peighambardoust, S. J., Ahmadi, A., Akbari, A., Farjadfard, S., & Ramavandi, B. (2021). Adsorption mercury, cobalt, and nickel with a reclaimable and magnetic composite of hydroxyapatite/Fe3O4/polydopamine. *Journal of Environmental Chemical Engineering, 9*(4).

Franklin, R. K., Martin, S. M., Strong, T. D., & Brown, R. B. (2008). 2.12 - Chemical Sensors. In Y. B. Gianchandani, O. Tabata, & H. Zappe (Eds.), *Comprehensive Microsystems* (pp. 433-461). Oxford: Elsevier.

Franklin, R. K., Martin, S. M., Strong, T. D., & Brown, R. B. (2016). Chemical and Biological Systems: Chemical Sensing Systems for Liquids *Reference Module in Materials Science and Materials Engineering*: Elsevier.

Friedrich, J. M., Ponce-De-Leon, C., Reade, G. W., & Walsh, F. C. (2004). Reticulated vitreous carbon as an electrode material. *Journal of Electroanalytical Chemistry, 561*, 203-217.

Fu, F., & Wang, Q. (2011). Removal of heavy metal ions from wastewaters: A review. *Journal of Environmental Management, 92*(3), 407-418.

Gambou-Bosca, A., & Belanger, D. (2015). Chemical mapping and electrochemical performance of manganese dioxide/activated carbon based composite electrode for asymmetric electrochemical capacitor. *Journal of the Electrochemical Society, 162*(5), A5115-A5123.

Georgiou, P., Walton, J., & Simitzis, J. (2010). Surface modification of pyrolyzed carbon fibres by cyclic voltammetry and their characterization with XPS and dye adsorption. *Electrochimica Acta, 55*(3), 1207-1216.

Ghafari, S., Hasan, M., & Aroua, M. K. (2009). Nitrate remediation in a novel upflow bio-electrochemical reactor (UBER) using palm shell activated carbon as cathode material. *Electrochimica Acta, 54*(17), 4164-4171.

Ghalehkhondabi, V., Fazlali, A., & Daneshpour, F. (2021). Electrochemical extraction of palladium from spent heterogeneous catalysts of a petrochemical unit using the leaching and flat plate graphite electrodes. *Separation and Purification Technology, 258*.

Goodridge, F., & Scott, K. (1995). Introduction to Electrochemical Engineering. In F. Goodridge & K. Scott (Eds.), *Electrochemical Process Engineering: A Guide to the Design of Electrolytic Plant* (pp. 1-16). New York: Springer.

Grimshaw, P., Calo, J. M., & Hradil, G. (2011a). III. Co-electrodeposition/removal of copper and nickel in a spouted electrochemical reactor. *Industrial & Engineering Chemistry Research, 50*(16), 9532-9538.

Grimshaw, P., Calo, J. M., Shirvanian, P. A., & Hradil, G. (2011b). II. Electrodeposition/removal of nickel in a spouted electrochemical reactor. *Industrial & Engineering Chemistry Research, 50*(16), 9525-9531.

Gu, Z. L., Song, W., Yang, Z. X., & Zhou, R. H. (2018). Metal-organic framework as an efficient filter for the removal of heavy metal cations in water. *Physical Chemistry Chemical Physics, 20*(48), 30384-30391.

Gupta, A., Vidyarthi, S. R., & Sankararamakrishnan, N. (2014). Enhanced sorption of mercury from compact fluorescent bulbs and contaminated water streams using

functionalized multiwalled carbon nanotubes. *Journal of Hazardous Materials, 274*, 132-144.

Hajeb, P., Jinap, S., Ismail, A., & Mahyudin, N. A. (2012). Mercury Pollution in Malaysia. In D. M. Whitacre (Ed.), *Reviews of Environmental Contamination and Toxicology, Vol 220* (Vol. 220, pp. 45-66). New York: Springer.

Harada, M. (1995). Minamata Disease: Methylmercury Poisoning in Japan Caused by Environmental Pollution. *Critical Reviews in Toxicology, 25*(1), 1-24.

Harris, D. C. (2010). *Quantitative Chemical Analysis* (8th ed.). New York, NY: W.H. Freeman and Co.

Hekmat, F., Sohrabi, B., Rahmanifar, M. S., & Jalali, A. (2015). Electrophoretic deposition of multi-walled carbon nanotubes on porous anodic aluminum oxide using ionic liquid as a dispersing agent. *Applied Surface Science, 341*, 109-119.

Henderson, W., & Nicholson, B. K. (2004). Synthesis and X-ray structures of triphenylphosphine-mercury(II) thiosalicylate complexes: novel aggregation processes. *Inorganica Chimica Acta, 357*(8), 2231-2236.

Hou, C. H., Huang, J. F., Lin, H. R., & Wang, B. Y. (2012). Preparation of activated carbon sheet electrode assisted electrosorption process. *Journal of the Taiwan Institute of Chemical Engineers, 43*(3), 473-479.

Hu, C., Liu, F., Lan, H., Liu, H., & Qu, J. (2015). Preparation of a manganese dioxide/carbon fiber electrode for electrosorptive removal of copper ions from water. *Journal of Colloid and Interface Science, 446*, 359-365.

Hu, X. L., Chen, C. H., Zhang, D. W., & Xue, Y. W. (2021). Kinetics, isotherm and chemical speciation analysis of Hg(II) adsorption over oxygen-containing MXene adsorbent. *Chemosphere, 278*.

Hua, K., Xu, X. L., Luo, Z. P., Fang, D., Bao, R., & Yi, J. H. (2020). Effective Removal of Mercury Ions in Aqueous Solutions: A Review. *Current Nanoscience, 16*(3), 363-375.

Huang, C. C., & He, J. C. (2013). Electrosorptive removal of copper ions from wastewater by using ordered mesoporous carbon electrodes. *Chemical Engineering Journal, 221*, 469-475.

Huang, S. Y., Fan, C. S., & Hou, C. H. (2014). Electro-enhanced removal of copper ions from aqueous solutions by capacitive deionization. *Journal of Hazardous Materials, 278*, 8-15.

Huang, Z., Lu, L., Cai, Z. X., & Ren, Z. J. (2016). Individual and competitive removal of heavy metals using capacitive deionization. *Journal of Hazardous Materials, 302*, 323-331.

Hussain, S. T., & Ali, S. A. K. (2021). Removal of Heavy Metal by Ion Exchange Using Bentonite Clay. *Journal of Ecological Engineering, 22*(1), 104-111.

Hussein, M. Z., Tarmizi, R. S. H., Zainal, Z., Ibrahim, R., & Badri, M. (1996). Preparation and characterization of active carbons from oil palm shells. *Carbon, 34*(11), 1447-1449.

Ismaiel, A. A. (2013). *Task Specific Ionic Liquids Mixed Palm Shell Activated Carbon as Ion Selective Electrodes for Cd(II) and Hg(II) Detection.* (Doctor of Philosophy Thesis), University of Malaya, Kuala Lumpur, Malaysia.

Ismaiel, A. A., Aroua, M. K., & Yusoff, R. (2014a). Cadmium (II)-selective electrode based on palm shell activated carbon modified with task-specific ionic liquid: kinetics and analytical applications. *International Journal of Environmental Science and Technology, 11*(4), 1115-1126.

Ismaiel, A. A., Aroua, M. K., & Yusoff, R. (2014b). A new electrochemical sensor based on task-specific ionic liquids-modified palm shell activated carbon for the determination of mercury in water samples. *Sensors, 14*(7), 13102-13113.

Issabayeva, G., Aroua, M. K., & Sulaiman, N. M. (2006). Electrodeposition of copper and lead on palm shell activated carbon in a flow-through electrolytic cell. *Desalination, 194*(1–3), 192-201.

Jamali, T., Karimi-Maleh, H., & Khalilzadeh, M. A. (2014). A novel nanosensor based on Pt:Co nanoalloy ionic liquid carbon paste electrode for voltammetric determination of vitamin B-9 in food samples. *Lwt-Food Science and Technology, 57*(2), 679-685.

Jaradat, A. Q., Telfah, D. B., & Ismail, R. (2021). Heavy metals removal from landfill leachate by coagulation/flocculation process combined with continuous adsorption using eggshell waste materials. *Water Science and Technology, 84*(12), 3817-3832.

Ji, H. X., Zhao, X., Qiao, Z. H., Jung, J., Zhu, Y. W., Lu, Y. L., Zhang, L. L., MacDonald, A. H., & Ruoff, R. S. (2014). Capacitance of carbon-based electrical double-layer capacitors. *Nature Communications, 5*.

Jia, K., Yi, Y. X., Ma, W. J., Cao, Y. J., Li, G. S., Liu, S. Q., Wang, T. J., & An, N. (2022). Ion flotation of heavy metal ions by using biodegradable biosurfactant as collector: Application and removal mechanism. *Minerals Engineering, 176*.

Kalb, R. S., & Kotschan, M. J. (2006). Trioctylmethylammonium thiosalicylate (TOMATS) *Aldrich ChemFiles* (Vol. 6, No. 9, pp. 13).

Kaminari, N. M. S., Schultz, D. R., Ponte, M. J. J. S., Ponte, H. A., Marino, C. E. B., & Neto, A. C. (2007). Heavy metals recovery from industrial wastewater using Taguchi method. *Chemical Engineering Journal, 126*(2–3), 139-146.

Kanani, N. (2004). Electrodeposition considered at the atomistic level. In N. Kanani (Ed.), *Electroplating* (pp. 141-177). Oxford: Elsevier.

KASA. (2021). Minamata Convention Initial Assessment Report Malaysia: Ministry of Environment and Water (KASA) Malaysia.

Kavitha, E., Poonguzhali, E., Nanditha, D., Kapoor, A., Arthanareeswaran, G., & Prabhakar, S. (2022). Current status and future prospects of membrane separation processes for value recovery from wastewater. *Chemosphere, 291*.

Keating, K. B., & Williams, J. M. (1976). The recovery of soluble copper from an industrial chemical waste. *Resource Recovery and Conservation, 2*(1), 39-55.

Khani, H., Rofouei, M. K., Arab, P., Gupta, V. K., & Vafaei, Z. (2010). Multi-walled carbon nanotubes-ionic liquid-carbon paste electrode as a super selectivity sensor: Application to potentiometric monitoring of mercury ion(II). *Journal of Hazardous Materials, 183*(1–3), 402-409.

Kim, H. H., & Lee, T. G. (2017). Removal of mercury ions in a simulated wastewater using functionalized poly(glycidyl methacrylate). *Journal of Industrial and Engineering Chemistry, 47*, 446-450.

Kim, J., Yoon, S., Choi, M., Min, K. J., Park, K. Y., Chon, K., & Bae, S. (2022). Metal ion recovery from electrodialysis-concentrated plating wastewater via pilot-scale sequential electrowinning/chemical precipitation. *Journal of Cleaner Production, 330*.

Kim, K., Candeago, R., Rim, G., Raymond, D., Park, A. H. A., & Su, X. (2021). Electrochemical approaches for selective recovery of critical elements in hydrometallurgical processes of complex feedstocks. *Iscience, 24*(5).

Koene, L., & Janssen, L. J. J. (2001). Removal of nickel from industrial process liquids. *Electrochimica Acta, 47*(5), 695-703.

Konopka, S. J., & McDuffie, B. (1970). Diffusion coefficients of ferri- and ferrocyanide ions in aqueous media, using twin-electrode thin-layer electrochemistry. *Analytical Chemistry, 42*(14), 1741-1746.

Kumar, V., & Dwivedi, S. K. (2021). A review on accessible techniques for removal of hexavalent Chromium and divalent Nickel from industrial wastewater: Recent research and future outlook. *Journal of Cleaner Production, 295*, 22.

Lan, H., He, W., Wang, A., Liu, R., Liu, H., Qu, J., & Huang, C. P. (2016). An activated carbon fiber cathode for the degradation of glyphosate in aqueous solutions by the Electro-Fenton mode: Optimal operational conditions and the deposition of iron on cathode on electrode reusability. *Water Research, 105*, 575-582.

Lavagnini, I., Antiochia, R., & Magno, F. (2004). An extended method for the practical evaluation of the standard rate constant from cyclic voltammetric data. *Electroanalysis, 16*(6), 505-506.

Lee, J. W., Kang, H., Kim, J. Y., & Kim, J. (2011). Electrode for electrochemical water treatment, method of manufacturing the same, method of treating water using the electrode, and device including the electrode for electrochemical water treatment. Retrieved 4th March 2015 https://www.google.com/patents/US20110198238

Li, J., Cassell, A., Delzeit, L., Han, J., & Meyyappan, M. (2002). Novel three-dimensional electrodes: Electrochemical properties of carbon nanotube ensembles. *Journal of Physical Chemistry B, 106*(36), 9299-9305.

Li, P., Feng, X. B., Qiu, G. L., Shang, L. H., & Li, Z. G. (2009). Mercury pollution in Asia: A review of the contaminated sites. *Journal of Hazardous Materials, 168*(2), 591-601.

Li, Q. G., Liu, G. H., Qi, L., Wang, H. C., Ye, Z. F., & Zhao, Q. L. (2022). Heavy metal-contained wastewater in China: Discharge, management and treatment. *Science of the Total Environment, 808*.

Li, S., Wei, Y., Kong, Y., Tao, Y., Yao, C., & Zhou, R. (2015). Electrochemical removal of lead ions using paper electrode of polyaniline/attapulgite composites. *Synthetic Metals, 199*, 45-50.

Li, Y. L., Yu, H., Liu, L. N., & Yu, H. B. (2021). Application of co-pyrolysis biochar for the adsorption and immobilization of heavy metals in contaminated environmental substrates. *Journal of Hazardous Materials, 420*.

Lin, R., Wang, H., & Zhu, Y. (2021). Optimizing the structural design of cathode catalyst layer for PEM fuel cells for improving mass-specific power density. *Energy, 221*, 10.

Lin, Y., Wang, S., Wu, Q., & Larssen, T. (2016). Material Flow for the Intentional Use of Mercury in China. *Environmental Science & Technology, 50*(5), 2337-2344.

Liu, X. J., & Wang, J. L. (2020). Electro-assisted adsorption of Cs(I) and Co(II) from aqueous solution by capacitive deionization with activated carbon cloth/graphene oxide composite electrode. *Science of the Total Environment, 749*.

Liu, X. M., Zhang, R., Zhan, L., Long, D. H., Qiao, W. M., Yang, J. H., & Ling, L. C. (2007). Impedance of carbon aerogel/activated carbon composites as electrodes of electrochemical capacitors in aprotic electrolyte. *New Carbon Materials, 22*(2), 153-158.

Liu, Y., Nie, C., Liu, X., Xu, X., Sun, Z., & Pan, L. (2015). Review on carbon-based composite materials for capacitive deionization. *RSC Advances, 5*(20), 15205-15225.

Liu, Y. X., Wu, X. Y., Yuan, D. X., & Yan, J. M. (2013a). Removal of nickel from aqueous solution using cathodic deposition of nickel hydroxide at a modified electrode. *Journal of Chemical Technology and Biotechnology, 88*(12), 2193-2200.

Liu, Y. X., Yan, J. M., Yuan, D. X., Li, Q. L., & Wu, X. Y. (2013b). The study of lead removal from aqueous solution using an electrochemical method with a stainless steel net electrode coated with single wall carbon nanotubes. *Chemical Engineering Journal, 218*, 81-88.

Liu, Y. X., Yuan, D. X., Yan, J. M., Li, Q. L., & Ouyang, T. (2011). Electrochemical removal of chromium from aqueous solutions using electrodes of stainless steel

nets coated with single wall carbon nanotubes. *Journal of Hazardous Materials, 186*(1), 473-480.

Loh, S. K. (2017). The potential of the Malaysian oil palm biomass as a renewable energy source. *Energy Conversion and Management, 141*, 285-298.

Low, C. T. J., de Leon, C. P., & Walsh, F. C. (2014). Electrodeposition of copper from mixed sulphate-chloride acidic electrolytes at a rotating disc electrode. *Transactions of the Institute of Metal Finishing, 92*(5), 282-288.

Lvovich, V. F. (2012). Equivalent-Circuit Elements and Modeling of the Impedance Phenomenon. In V. F. Lvovich (Ed.), *Impedance Spectroscopy* (pp. 37-47). New Jersey: John Wiley & Sons, Inc.

Macias-Garcia, A., Corzo, M. G., Dominguez, M. A., Franco, M. A., & Naharro, J. M. (2017). Study of the adsorption and electroadsorption process of Cu (II) ions within thermally and chemically modified activated carbon. *Journal of Hazardous Materials, 328*, 46-55.

Maleki, N., Safavi, A., & Tajabadi, F. (2006). High-performance carbon composite electrode based on an ionic liquid as a binder. *Analytical Chemistry, 78*(11), 3820-3826.

Martins, R., Britto-Costa, P. H., & Ruotolo, L. A. M. (2012). Removal of toxic metals from aqueous effluents by electrodeposition in a spouted bed electrochemical reactor. *Environmental Technology, 33*(10), 1123-1131.

Masinire, F., Adenuga, D. O., Tichapondwa, S. M., & Chirwa, E. M. N. (2021). Phytoremediation of Cr(VI) in wastewater using the vetiver grass (Chrysopogon zizanioides). *Minerals Engineering, 172*.

Matthaiou, V., Oulego, P., Frontistis, Z., Collado, S., Hela, D., Konstantinou, I. K., Diaz, M., & Mantzavinos, D. (2019). Valorization of steel slag towards a Fenton-like catalyst for the degradation of paraben by activated persulfate. *Chemical Engineering Journal, 360*, 728-739.

Misnon, I. I., Zain, N. K. M., Aziz, R. A., Vidyadharan, B., & Jose, R. (2015). Electrochemical properties of carbon from oil palm kernel shell for high performance supercapacitors. *Electrochimica Acta, 174*, 78-86.

Modestov, A. D., Evstefeeva, Y. E., Pleskov, Y. V., Mazin, V. M., Varnin, V. P., & Teremetskaya, I. G. (1997). Synthetic semiconductor diamond electrodes: kinetics of some redox reactions. *Journal of Electroanalytical Chemistry, 431*(2), 211-218.

Mohamadi, M., & Mostafavi, A. (2011). Flame Atomic Absorption Determination of Trace Amounts of Cadmium After Preconcentration Using a Thiol-Containing Task-Specific Ionic Liquid. *Journal of AOAC International, 94*(3), 959-967.

Mook, W. T., Aroua, M. K., & Szlachta, M. (2016). Palm Shell-based Activated Carbon for Removing Reactive Black 5 Dye: Equilibrium and Kinetics Studies. *Bioresources, 11*(1), 1432-1447.

Mook, W. T., Aroua, M. K. T., Chakrabarti, M. H., Noor, I. M., Irfan, M. F., & Low, C. T. J. (2013). A review on the effect of bio-electrodes on denitrification and organic matter removal processes in bio-electrochemical systems. *Journal of Industrial and Engineering Chemistry, 19*(1), 1-13.

MPOC. (2017). *Malaysia Palm Oil Council (MPOC) Annual Report 2017*. Retrieved from https://mpoc.org.my/wp-content/uploads/2019/05/Anual-Report-2017.pdf

Nadakatti, S., Tendulkar, M., & Kadam, M. (2011). Use of mesoporous conductive carbon black to enhance performance of activated carbon electrodes in capacitive deionization technology. *Desalination, 268*(1–3), 182-188.

Najafi, M., Khafilzadeh, M. A., & Karimi-Maleh, H. (2014). A new strategy for determination of bisphenol A in the presence of Sudan I using a ZnO/CNTs/ionic liquid paste electrode in food samples. *Food Chemistry, 158*, 125-131.

National Key Priority Area (NKPA) on Water. ASM Advisory Report 1/2015. (2015). https://issuu.com/asmpub/docs/a_national_key_priority_area__nkpa__on_water Academy of Sciences Malaysia (ASM)

Neto, B. A. D., Lapis, A. A. M., & Souza, R. Y. (2019). Task-Specific Ionic Liquids: Design, Properties and Applications. In S. Zhang (Ed.), *Encyclopedia of Ionic Liquids* (pp. 1-11). Singapore: Springer Singapore.

Nguyen, M. K., Tran, V. S., Pham, T. T., Pham, H. G., Hoang, B. L., Nguyen, T. H., Nguyen, T. H., Tran, T. H., & Ngo, H. H. (2021). Fenton/ozone-based oxidation and coagulation processes for removing metals (Cu, Ni)-EDTA from plating wastewater. *Journal of Water Process Engineering, 39*.

Nicholson, R. S. (1965). Theory and application of cyclic voltammetry for measurement of electrode reaction kinetics. *Analytical Chemistry, 37*(11), 1351-1355.

Nomanbhay, S. M., & Palanisamy, K. (2005). Removal of heavy metal from industrial wastewater using chitosan coated oil palm shell charcoal. *Electronic Journal of Biotechnology, 8*(1), 43-53.

Nugroho, A. P., Butar, E. S. B., Priantoro, E. A., Sriwuryandari, L., Pratiwi, Z. B., & Sembiring, T. (2021). Phytoremediation of electroplating wastewater by vetiver grass (Chrysopogon zizanoides L.). *Scientific Reports, 11*(1).

Obrist, D., Kirk, J. L., Zhang, L., Sunderland, E. M., Jiskra, M., & Selin, N. E. (2018). A review of global environmental mercury processes in response to human and natural perturbations: Changes of emissions, climate, and land use. *Ambio, 47*(2), 116-140.

Oda, H., & Nakagawa, Y. (2003). Removal of ionic substances from dilute solution using activated carbon electrodes. *Carbon, 41*(5), 1037-1047.

Opallo, M., & Lesniewski, A. (2011). A review on electrodes modified with ionic liquids. *Journal of Electroanalytical Chemistry, 656*(1–2), 2-16.

Ottewill, G. A., Reade, G. W., Campbell, S. A., de Leonb, C. P., & Walsh, F. C. (2005). Electrochemical removal of metal ions from aqueous solution: a student workshop. *Journal of Environmental Monitoring, 7*(10), 943-949.

Padamata, S. K., Yasinskiy, A. S., Polyakov, P. V., Pavlov, E. A., & Varyukhin, D. Y. (2020). Recovery of Noble Metals from Spent Catalysts: A Review. *Metallurgical and Materials Transactions B-Process Metallurgy and Materials Processing Science, 51*(5), 2413-2435.

Pakuła, M., Świątkowski, A., & Biniak, S. (1995). Electrochemical behaviour of modified activated carbons in aqueous and nonaqueous solutions. *Journal of Applied Electrochemistry, 25*(11), 1038-1044.

Pandolfo, A. G., & Hollenkamp, A. F. (2006). Carbon properties and their role in supercapacitors. *Journal of Power Sources, 157*(1), 11-27.

Park, K. K., Lee, J. B., Park, P. Y., Yoon, S. W., Moon, J. S., Eum, H. M., & Lee, C. W. (2007). Development of a carbon sheet electrode for electrosorption desalination. *Desalination, 206*(1–3), 86-91.

Peng, C., Jin, R., Li, G., Li, F., & Gu, Q. (2014). Recovery of nickel and water from wastewater with electrochemical combination process. *Separation and Purification Technology, 136*, 42-49.

Peterlevitz, A. C., May, P. W., Harniman, R. L., Jones, J. A., Ceragioli, H. J., & Zanin, H. (2016). Fast electron transfer kinetics on novel interconnected nanospheres of graphene layers electrodes. *Thin Solid Films, 616*, 698-702.

Pirkwieser, P., López-López, J. A., Kandioller, W., Keppler, B. K., Moreno, C., & Jirsa, F. (2018). Solvent Bar Micro-Extraction of Heavy Metals from Natural Water Samples Using 3-Hydroxy-2-Naphthoate-Based Ionic Liquids. *Molecules, 23*(11), 3011.

Pooja, G., Kumar, P. S., & Indraganti, S. (2022). Recent advancements in the removal/recovery of toxic metals from aquatic system using flotation techniques. *Chemosphere, 287*(2), 132231.

Porada, S., Zhao, R., van der Wal, A., Presser, V., & Biesheuvel, P. M. (2013). Review on the science and technology of water desalination by capacitive deionization. *Progress in Materials Science, 58*(8), 1388-1442.

Pospiech, B., & Kujawski, W. (2015). Ionic liquids as selective extractants and ion carriers of heavy metal ions from aqueous solutions utilized in extraction and membrane separation. *Reviews in Chemical Engineering, 31*(2), 179-191.

Punckt, C., Pope, M. A., & Aksay, I. A. (2013). On the electrochemical response of porous functionalized graphene electrodes. *Journal of Physical Chemistry C, 117*(31), 16076-16086.

Punia, P., Bharti, M. K., Dhar, R., Thakur, P., & Thakur, A. (2022). Recent Advances in Detection and Removal of Heavy Metals from Contaminated Water. *ChemBioEng Reviews,* Early Access.

Qasem, N. A. A., Mohammed, R. H., & Lawal, D. U. (2021). Removal of heavy metal ions from wastewater: a comprehensive and critical review. *Npj Clean Water, 4*(1).

Qian, A., Liao, P., Yuan, S., & Luo, M. (2014). Efficient reduction of Cr(VI) in groundwater by a hybrid electro-Pd process. *Water Research, 48,* 326-334.

Raffa, C. M., Chiampo, F., & Shanthakumar, S. (2021). Remediation of Metal/Metalloid-Polluted Soils: A Short Review. *Applied Sciences-Basel, 11*(9).

Rajumon, R., Aravind, S. P., Bhuvaneshwari, S., Ranjitha, J., & Mohanraj, P. (2020). Removal of cadmium heavy metal ions from wastewater by electrosorption using modified activated carbon felt electrodes. *Water Science and Technology, 82*(7), 1430-1444.

Ramalan, N. H. M., Karoonian, F. S., Etesami, M., Wen-Min, S., Hasnat, M. A., & Mohamed, N. (2012). Impulsive removal of Pb(II) at a 3-D reticulated vitreous carbon cathode. *Chemical Engineering Journal, 203,* 123-129.

Rasines, G., Lavela, P., Macías, C., Zafra, M. C., Tirado, J. L., Parra, J. B., & Ania, C. O. (2015). N-doped monolithic carbon aerogel electrodes with optimized features for the electrosorption of ions. *Carbon, 83*(0), 262-274.

Reade, G. W., Bond, P., de Leon, C. P., & Walsh, F. C. (2004a). The application of reticulated vitreous carbon rotating cylinder electrodes to the removal of cadmium and copper ions from solution. *Journal of Chemical Technology and Biotechnology, 79*(9), 946-953.

Reade, G. W., Nahle, A. H., Bond, P., Friedrich, J. M., & Walsh, F. C. (2004b). Removal of cupric ions from acidic sulfate solution using reticulated vitreous carbon rotating cylinder electrodes. *Journal of Chemical Technology and Biotechnology, 79*(9), 935-945.

Recéndiz, A., León, S., Nava, J. L., & Rivera, F. F. (2011). Mass transport studies at rotating cylinder electrode during zinc removal from dilute solutions. *Electrochimica Acta, 56*(3), 1455-1459.

Reyes Cruz, V., Oropeza, M. T., González, I., & Ponce-De-León, C. (2002). Electrochemical recovery of silver from cyanide leaching solutions. *Journal of Applied Electrochemistry, 32*(5), 473-479.

Rivero, E. P., Cruz-Diaz, M. R., Almazan-Ruiz, F. J., & Gonzalez, I. (2015). Modeling the effect of non-ideal flow pattern on tertiary current distribution in a filter-press-type electrochemical reactor for copper recovery. *Chemical Engineering Research & Design, 100*, 422-433.

Saljooqi, A., Shamspur, T., Mohamadi, M., Afzali, D., & Mostafavi, A. (2015). A microextraction procedure based on a task-specific ionic liquid for the separation and preconcentration of lead ions from red lipstick and pine leaves. *Journal of Separation Science, 38*(10), 1777-1783.

Sarkar, S., & Aquino, W. (2011). Electroneutrality and ionic interactions in the modeling of mass transport in dilute electrochemical systems. *Electrochimica Acta, 56*(24), 8969-8978.

Sato, T., Enokida, T., & Noguchi, Y. (2002). Liquid-liquid extraction of mercury(II) from hydrochloric acid solutions by tributyl phosphate. *Solvent Extraction Research and Development-Japan, 9*, 1-11.

Scott, K. (1993). Electrochemical Methods for the Treatment of Industrial Process Streams and Effluents: Part I: Cell Design and the Recovery of Dissolved Metals by Electrodeposition. *Developments in Chemical Engineering and Mineral Processing, 1*(4), 185-197.

Seeber, R., Zanardi, C., & Inzelt, G. (2016). The inherent coupling of charge transfer and mass transport processes: the curious electrochemical reversibility. *ChemTexts, 2*(2), 1-16.

Segundo, J., Salazar-Banda, G. R., Feitoza, A. C. O., Vilar, E. O., & Cavalcanti, E. B. (2012). Cadmium and lead removal from aqueous synthetic wastes utilizing Chemelec electrochemical reactor: Study of the operating conditions. *Separation and Purification Technology, 88*, 107-115.

Sharma, P., Pandey, A. K., Udayan, A., & Kumar, S. (2021). Role of microbial community and metal-binding proteins in phytoremediation of heavy metals from industrial wastewater. *Bioresource Technology, 326*, 10.

Shen, Y. Y., Wu, S. W., & Hou, C. H. (2021). Exploring the electrosorption selectivity and recovery of indium ions with capacitive deionization in acidic solution. *Journal of Colloid and Interface Science, 586*, 819-829.

Shirvanian, P. A., & Calo, J. M. (2005). Copper recovery in a spouted vessel electrolytic reactor (SBER). *Journal of Applied Electrochemistry, 35*(1), 101-111.

Song, Q. M., Liu, Y., Zhang, L. G., & Xu, Z. M. (2021). Selective electrochemical extraction of copper from multi-metal e-waste leaching solution and its enhanced recovery mechanism. *Journal of Hazardous Materials, 407*.

Spitzer, M., & Bertazzoli, R. (2004). Selective electrochemical recovery of gold and silver from cyanide aqueous effluents using titanium and vitreous carbon cathodes. *Hydrometallurgy, 74*(3-4), 233-242.

Stanisz, E., Werner, J., & Matusiewicz, H. (2013). Mercury species determination by task specific ionic liquid-based ultrasound-assisted dispersive liquid-liquid microextraction combined with cold vapour generation atomic absorption spectrometry. *Microchemical Journal, 110*, 28-35.

Strong, T. D. (2004). *Microfabricated voltammetric neuro-arrays for use in vitro* (Ph.D. thesis), University of Michigan, USA.

Su, Y. B., Li, Q. B., Wang, Y. P., Wang, H. T., Huang, J. L., & Yang, X. (2009). Electrochemical reclamation of silver from silver-plating wastewater using static

cylinder electrodes and a pulsed electric field. *Journal of Hazardous Materials, 170*(2-3), 1164-1172.

Sunderland, E. M., Krabbenhoft, D. P., Moreau, J. W., Strode, S. A., & Landing, W. M. (2009). Mercury sources, distribution, and bioavailability in the North Pacific Ocean: Insights from data and models. *Global Biogeochemical Cycles, 23*.

Suss, M. E., Porada, S., Sun, X., Biesheuvel, P. M., Yoon, J., & Presser, V. (2015). Water desalination via capacitive deionization: what is it and what can we expect from it? *Energy & Environmental Science, 8*(8), 2296-2319.

Swiatkowski, A., Pakula, M., Biniak, S., & Walczyk, M. (2004). Influence of the surface chemistry of modified activated carbon on its electrochemical behaviour in the presence of lead(II) ions. *Carbon, 42*(15), 3057-3069.

Tan, I. A. W., Ahmad, A. L., & Hameed, B. H. (2008). Adsorption of basic dye using activated carbon prepared from oil palm shell: batch and fixed bed studies. *Desalination, 225*(1-3), 13-28.

Tatapudi, P., & Fenton, J. M. (1995). Electrolytic Processes for Pollution Treatment and Pollution Prevention. In H. Gerischer & C. W. Tobias (Eds.), *Advances in Electrochemical Science and Engineering* (Vol. 4, pp. 362-417).

Teng, D. F., Xu, Y. Q., Zhao, T. N., Zhang, X. M., Li, Y., & Zeng, Y. C. (2022). Zein adsorbents with micro/nanofibrous membrane structure for removal of oils, organic dyes, and heavy metal ions in aqueous solution. *Journal of Hazardous Materials, 425*.

Terrazas-Rodriguez, J. E., Gutierrez-Granados, S., Alatorre-Ordaz, M. A., de Leon, C. P., & Walsh, F. C. (2011). A comparison of the electrochemical recovery of palladium using a parallel flat plate flow-by reactor and a rotating cylinder electrode reactor. *Electrochimica Acta, 56*(25), 9357-9363.

Tonini, G. A., Farinos, R. M., Prado, P. F. D., & Ruotolo, L. A. M. (2013). Box-Behnken factorial design study of the variables affecting metal electrodeposition in membraneless fluidized bed electrodes. *Journal of Chemical Technology and Biotechnology, 88*(5), 800-807.

Tran, N. A. T., Phuoc, N. M., Yoon, H., Jung, E., Lee, Y. W., Kang, B. G., Kang, H. S., Yoo, C. Y., & Cho, Y. (2020). Improved Desalination Performance of Flow- and Fixed-Capacitive Deionization using Redox-Active Quinone. *ACS Sustainable Chemistry & Engineering, 8*(44), 16701-16710.

Tran, T. K., Chiu, K. F., Lin, C. Y., & Leu, H. J. (2017). Electrochemical treatment of wastewater: Selectivity of the heavy metals removal process. *International Journal of Hydrogen Energy, 42*(45), 27741-27748.

Tunsu, C., & Wickman, B. (2018). Effective removal of mercury from aqueous streams via electrochemical alloy formation on platinum. *Nature Communications, 9*(1), 4876.

Turull, M., Elias, G., Fontas, C., & Diez, S. (2017). Exploring new DGT samplers containing a polymer inclusion membrane for mercury monitoring. *Environmental Science and Pollution Research, 24*(12), 10919-10928.

Vasudevan, S., Lakshmi, J., & Sozhan, G. (2011). Effects of alternating and direct current in electrocoagulation process on the removal of cadmium from water. *Journal of Hazardous Materials, 192*(1), 26-34.

Visser, A., Swatloski, R., Reichert, W., Davis, J., Rogers, R., Mayton, R., Sheff, S., & Wierzbicki, A. (2001). Task-Specific Ionic Liquids for the Extraction of Metal Ions from Aqueous Solutions. *Chemical Communications, 1*, 135-136.

Walsh, F. C., & Reade, G. W. (1994). Electrochemical Techniques for the Treatment of Dilute Metal-Ion Solutions. *Studies in Environmental Science, 59*, 3-44.

Wang, G., Qian, B., Dong, Q., Yang, J., Zhao, Z., & Qiu, J. (2013). Highly mesoporous activated carbon electrode for capacitive deionization. *Separation and Purification Technology, 103*, 216-221.

Wang, G. X., Guo, K., Wang, B. Z., Han, F. X., Guo, Z. L., Song, Z. R., Ji, J. W., & Tang, C. C. (2021). Mercury Adsorption on Thiol-Modified Porous Boron Nitride: A Combined Experimental and Theoretical Investigation. *Industrial & Engineering Chemistry Research, 60*(35), 12984-12998.

Wang, L., Liang, H., Huang, H., Wang, Q., Yang, Y., & Zheng, Q. (2022). Performance analysis of a half-batch multi-cell three-dimensional electrode reactor for drilling wastewater: COD removal, energy consumption and hydrodynamic characteristic. *Water Science and Technology*, Early Access.

Wang, Y., Laborda, E., Henstridge, M. C., Martinez-Ortiz, F., Molina, A., & Compton, R. G. (2012). The use of differential pulse voltammetries to discriminate between the Butler–Volmer and the simple Marcus–Hush models for heterogeneous electron transfer: The electro-reduction of europium (III) in aqueous solution. *Journal of Electroanalytical Chemistry, 668*, 7-12.

Wehr-Candler, T., & Henderson, W. (2016). Coordination chemistry of the thiosalicylate ligand. *Coordination Chemistry Reviews, 313*, 111-155.

Wei, Y., Liu, H., Jin, Y., Cai, K., Li, H., Liu, Y., Kang, Z., & Zhang, Q. (2013). Carbon nanoparticle ionic liquid functionalized activated carbon hybrid electrode for efficiency enhancement in supercapacitors. *New Journal of Chemistry, 37*(4), 886-889.

WHO. (2005). Mercury in Drinking-Water: Background Document for Development of WHO Guidelines for Drinking-Water Quality. World Health Organization: Geneva, Switzerland. Retrieved from https://apps.who.int/iris/bitstream/handle/10665/44584/9789241548151_eng.pdf

Widner, R. C., Sousa, M. F. B., & Bertazzoli, R. (1998). Electrolytic removal of lead using a flow-through cell with a reticulated vitreous carbon cathode. *Journal of Applied Electrochemistry, 28*(2), 201-207.

Wu, X., Li, H., Yang, X., Wang, X., Miao, Z., Zhou, P., Zhou, J., & Zhuo, S. (2021). Polytetrafluoroethylene-assisted removal of hard-template to prepare hierarchically porous carbon for high energy density supercapacitor with KI-additive electrolyte. *Electrochimica Acta, 368*, 137610.

Yang, K. L., Ying, T. Y., Yiacoumi, S., Tsouris, C., & Vittoratos, E. S. (2001). Electrosorption of ions from aqueous solutions by carbon aerogel: An electrical double-layer model. *Langmuir, 17*(6), 1961-1969.

Yang, L., Hu, W., Chang, Z., Liu, T., Fang, D., Shao, P., Shi, H., & Luo, X. (2021). Electrochemical recovery and high value-added reutilization of heavy metal ions from wastewater: Recent advances and future trends. *Environment International, 152*, 106512.

Yao, J., Lv, S., Wang, Z., Hu, L., & Chen, J. (2022). Variation of current density with time as a novel method for efficient electrochemical treatment of real dyeing wastewater with energy savings. *Environmental Science and Pollution Research*, Early Access.

Yasri, N. G., & Gunasekaran, S. (2017). Electrochemical Technologies for Environmental Remediation. In N. A. Anjum, S. S. Gill, & N. Tuteja (Eds.), *Enhancing Cleanup of Environmental Pollutants: Volume 2: Non-Biological Approaches* (pp. 5-73). Cham: Springer International Publishing.

Yek, P. N. Y., Liew, R. K., Osma, M. S., Lee, C. L., Chuah, J. H., Park, Y. K., & Lam, S. S. (2019). Microwave steam activation, an innovative pyrolysis approach to convert waste palm shell into highly microporous activated carbon. *Journal of Environmental Management, 236*, 245-253.

Yi, X. X., Qi, Y. P., Li, F. F., Shu, J. C., Sun, Z., Sun, S. H., Chen, M. J., & Pu, S. Y. (2019). Effect of electrolyte reuse on metal recovery from waste CPU slots by slurry electrolysis. *Waste Management, 95*, 370-376.

Yong, H. H., Lee, S. Y., Kim, S. K., & Ahn, S. H. (2008). US7316866. Google Patents.

Zhang, C., Jiang, Y., Li, Y., Hu, Z., Zhou, L., & Zhou, M. (2013). Three-dimensional electrochemical process for wastewater treatment: A general review. *Chemical Engineering Journal, 228*, 455-467.

Zhang, X. Y., Li, J. X., Sun, Y. K., Li, L. N., Pan, B. C., Zhang, W. M., & Guan, X. H. (2018). Aging of zerovalent iron in various coexisting solutes: Characteristics, reactivity toward selenite and rejuvenation by weak magnetic field. *Separation and Purification Technology, 191*, 94-100.

Zhang, X. Y., Xia, X., Ivanov, I., Huang, X., & Logan, B. E. (2014). Enhanced activated carbon cathode performance for microbial fuel cell by blending carbon black. *Environmental Science & Technology, 48*(3), 2075-2081.

Zhang, Y., & Duan, X. M. (2020). Chemical precipitation of heavy metals from wastewater by using the synthetical magnesium hydroxy carbonate. *Water Science and Technology, 81*(6), 1130-1136.

Zhang, Y. L., Zhao, Y. C., Xiong, Z., Gao, T., Gong, B. G., Liu, P. F., Liu, J., & Zhang, J. Y. (2021). Elemental mercury removal by I--doped Bi2WO6 with remarkable visible-light-driven photocatalytic oxidation. *Applied Catalysis B-Environmental, 282*, 11.

Zheng, T., Wang, J., Wang, Q., Meng, H., & Wang, L. (2015). Research trends in electrochemical technology for water and wastewater treatment. *Applied Water Science*, 1-18.

Zhou, M., Xu, Y., Zhong, R., & Wang, Y. R. (2021). Sensitive Electrochemical Detection of Caffeic Acid using a Carboxyl-Functionalized Reduced Graphene Oxide-Modified Glassy Carbon Electrode (ERGO-COOH/GCE). *International Journal of Electrochemical Science, 16*(7), 15.

Zhou, Y. H., Lei, J., Zhang, Y., Zhu, J., Lu, Y. N., Wu, X. F., & Fang, H. (2018). Determining Discharge Characteristics and Limits of Heavy Metals and Metalloids for Wastewater Treatment Plants (WWTPs) in China Based on Statistical Methods. *Water, 10*(9).

Zhu, Z. T., Tang, S. H., Yuan, J. W., Qin, X. L., Deng, Y. X., Qu, R. J., & Haarberg, G. M. (2016). Effects of various binders on supercapacitor performances. *International Journal of Electrochemical Science, 11*(10), 8270-8279.